A STUDY OF PHASE SEPARATION OF
SECONDARY DISPERSIONS

FAYEZ MAHMOUD SULEIMAN OTHMAN

A THESIS SUBMITTED TO
THE UNIVERSITY OF ASTON IN BIRMINGHAM
FOR THE DEGREE OF MASTER OF PHILOSOPHY

DEPARTMENT OF CHEMICAL ENGINEERING
THE UNIVERSITY OF ASTON IN BIRMINGHAM

APRIL   1986

" In the name of ALLAH

The most gracious

The most merciful "

THE UNIVERSITY OF ASTON IN BIRMINGHAM
S U M M A R Y
A STUDY OF PHASE SEPARATION OF SECONDARY DISPERSIONS
FAYEZ MAHMOUD SULEIMAN OTHMAN
M.Phil — April 1986

The literature pertaining to the formation and tech-
niques of separation of secondary liquid-liquid dispersions
has been critically reviewed. The different methods for
determination of drop size distribution were also reviewed.

The coalescence of a secondary dispersion of toluene in
water has been investigated using beds of fibrous material
made of glass wool. The variables studied were superficial
velocity, bed height, dispersed phase ratio and fibre
diameter. The inlet drop size,< 50 μm, was measured by a
Coulter Counter TAII, while the exit coalesced drops, >
10^{-3}m, were measured by photography. Effluent dispersed
phase concentration was also analysed by Horiba Oil
Analyzer.

Confirmation of a critical velocity of 1.5×10^{-2} m/s and
a critical bed height of 6×10^{-2} m was obtained. At these
conditions the separation efficiency was found to be 80%.

The experimental single phase pressure drop data were
found to be best presented by the Carman-Kozeny equation.
The two phase pressure drop was correlated by a modified
form of the Blake-Kozeny equation.

A theoretical comparison of drop capture mechanisms
revealed that interception and sedimentation were predomi-
nant. An equation describing the drop capture rate was for-
mulated. A combination of drop release mechanisms, i.e.
drip point, ballooning and jetting was observed and the exit
drop size was found to increase with increase of fibre size.

The saturation profiles were predicted, using the rela-
tive permeability correlations, and compared to those pre-
dicted from the pressure drop expression. Experimental
filter coefficients were compared with available models, and
found to vary over a magnitude of 800 for the same operating
conditions.

Key Words: Coalescence
                    Fibrous Beds
                    Secondary Dispersions

TO

MY PARENTS

AND

TO MY WIFE

ACKNOWLEDGEMENTS

CONTENTS   PAGE

LIST OF FIGURES   PAGE

LIST OF TABLES

CHAPTER 1

INTRODUCTION

CHAPTER ONE

INTRODUCTION

Liquid-liquid dispersions, such as oil-water dispersions, are commonly encountered in the chemical industry. These dispersions occur for example in liquid-liquid extraction, condensation or compression of vapor of immiscible liquids, direct contact heat transfer, caustic washing of light distillate, desalting and dewatering of crude oils and vacuum distillation using steam jets. In many cases it is desired to remove the dispersed liquid phase because of safety, ecological and economic considerations. In chemical processes incomplete separation of the dispersions may sometimes result in subsequent loss in efficiency of the equipment.

These dispersions are of two types. The first, a primary dispersion, contains droplets greater than 100 μm diameter and, unless stabilised e.g. by surfactants, separates readily in a few seconds or minutes by simple settling. A secondary dispersion contains large numbers of very small droplets, certainly less than 50 μm in mean diameter, and normally less than one micron.

Many techniques can be used to remove or separate a liquid dispersion. The final selection depends on the characteristics of the dispersion, particularly the drop

size distribution. Chemical methods can be used, which may change the solubility of the dispersed phase. Common physical methods include gravity settling (in the case of a primary dispersion), the use of surfaces (plates, baffles, grids, etc.) to promote coalescence, the use of packings and fibre beds, centrifugation and electrostatic separators.

Recently, fibrous bed coalescers have gained more attention as oil removal devices. Laboratory-scale studies indicate that greater than 95 per cent oil removal is possible. Thus, a fibrous bed coalescer may be incorporated with, or in lieu of conventional secondary de-oiling techniques. Micron sized droplets can thus be coalesced into millimeter sized or larger drops that can be readily separated in gravity settlers.

The practical design of a coalescer is largely a matter of trial and error since no standard design methods or selection criteria are available . The objectives of the present study were to investigate the performance of fibrous-bed coalescers for secondary dispersions under operating conditions, and to observe the mechanisms of droplet collection and release from beds, to minimize the need for empirical rules for design purposes. A mathematical model was developed to express the saturation profiles through the coalescer.

CHAPTER 2
FORMATION AND OCCURRENCE OF
SECONDARY DISPERSIONS

CHAPTER TWO

FORMATION AND OCCURRENCE OF SECONDARY DISPERSIONS

2.1. INTRODUCTION

Dispersions and emulsions both comprise droplets of one liquid (the dispersed phase) distributed in another (the continuous phase), the first liquid being immiscible or partly miscible with the second. The difference between a dispersion and an emulsion is that whilst dispersions are thermodynamically unstable emulsions are quasi-stable. The stability of the latter is normally due to reduced interdroplet coalescence, which is brought about by the presence, in trace form, of a third component which is surface active.

The mean drop size has been used to classify dispersions into primary dispersions, secondary dispersions and colloids or emulsions. Although there is no clear division between primary and secondary dispersions in terms of drop size, most previous investigators in the field have referred to a dispersion containing a mean droplet diameter less than 100 μm as a secondary dispersion. Such an arbitrary definition of a secondary dispersion is an over-simplification, especially when a theoretical description of the phenomenon of coalescence is attempted. This arises because, before coalescence, the dispersion

may behave as a colloidal system; during coalescence growth of the drops occurs by different mechanisms depending partly upon the coalescence medium selected. Finally as the larger drops leave the coalescence medium, they will behave as primary dispersions (1). The approximate ranges of the three types of dispersion are illustrated in Fig. 2.1.

2.2. THEORY OF FORMATION

Liquid-liquid dispersions, like all other dispersed systems, are usually thermodynamically unstable because the free energy associated with the large interfacial area between the two phases can decrease by aggregation or coalescence of the dispersed phase. Energetically then coalescence of a liquid dispersion would be expected, particularly in binary systems, until ultimately two liquid layers would be formed. However, it is the kinetics of this process which are of paramount importance in the design and operation of separation equipment (2).

The instability (or metastability) of colloids and dispersions is due to the existence of an energy barrier which has to be surmounted before the two particles can adhere. This energy is clearly a function of the distance of separation between the particles which decreases

Secondary

Colloidal   Primary

0.1 µm   1 µm   10 µm   100 µm
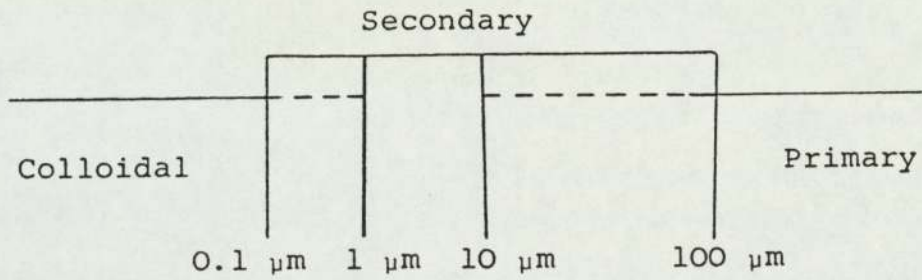
Fig. 2.1   Classification of Dispersions by
Drop size

P

P

I   Energy zero for infinite
separation of particles

II

M₂

M₁

Energy zero for infinite
III   separation

M₁

Energy zero for bulk phase

Distance between surfaces of particles
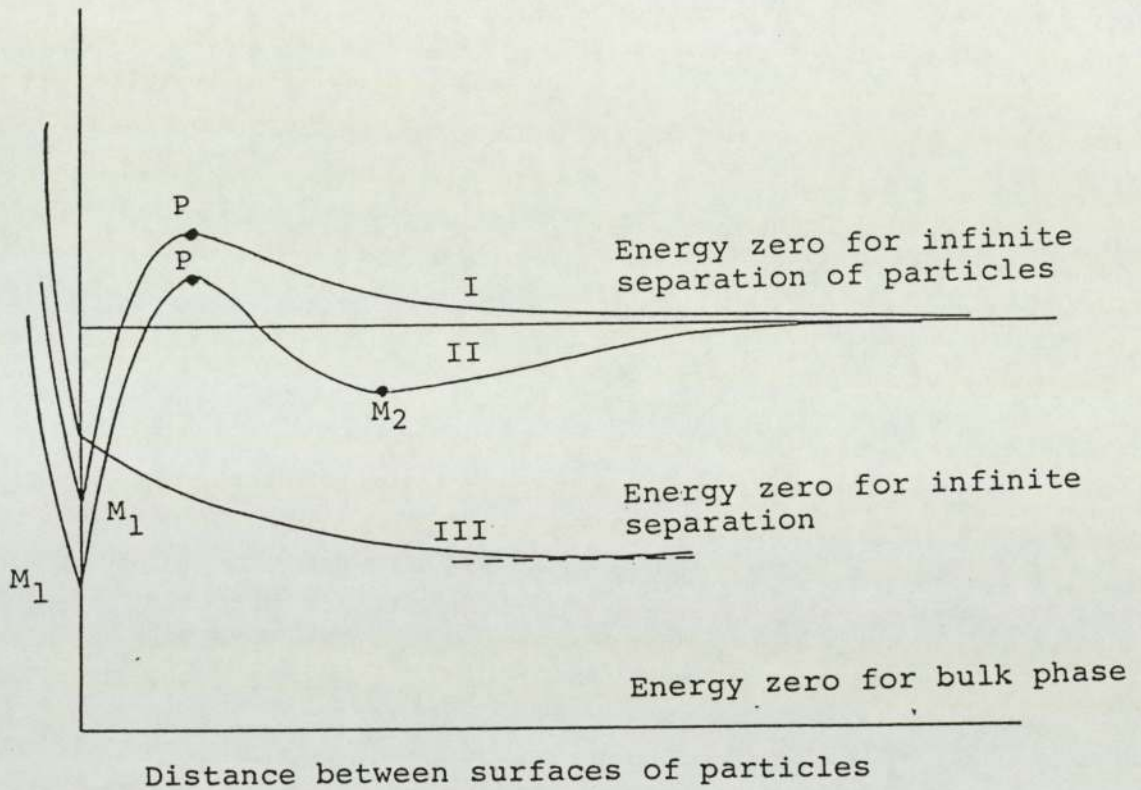
Fig. 2.2   Mutual potential energy of two colloidal
particles as a function of the distance
of separation between their surfaces:

(I)   Curve with primary maximum P and primary
minimum M_1

(II)   Curve with primary maximum P, primary minimum M_1
and secondary minimum M_2

(III) Curve for spontaneous (unactivated) dispersion

as the distance increases. In keeping with the usual
conventions, negative potential energies will be asso-
ciated with attraction and positive potential energies
with repulsion. This convention allows reference to the
"height" of energy "barriers" and the "depth" of energy
minima.

Fig. 2.2 is a qualitative sketch of potential energy
curves resultant from a repulsive and an attractive compo-
nent. Such curves may show a maximum and two minima,
although some of these features may be masked if one
contribution greatly exceeds the other. The height of the
maximum above Energy = 0 is called the height of the
energy barrier (P). The deeper minimum is called the
primary minimum (M_1); and the more shallow one, the
secondary minimum (M_2). Although attraction predomina-
tes at large distances-that is, the secondary minimum
is generally present- it may be quite shallow, especially
in view of the effects of retardation and the medium on
attraction.

The implication of the potential energy curves shown
in Fig. 2.2 can be qualitatively considered as follows:

In case I, if no barrier is present or the height
of the barrier is negligible compared to the thermal
kinetic energy associated with the collision, then the

net force of attraction will pull the droplets together
into the primary minimum, M_1, after which the two behave
as a single kinetic unit, i.e. flocculation has occurred.
If the height of the potential energy barrier is appreci-
able compared to the thermal kinetic energy, the particles
are prevented from flocculating in the primary minimum.
If the depth of the secondary minimum, M_2, is small
compared to thermal energy, then the particles will simply
diffuse apart; this system is flocculation-stable.

There may be situations in which the two droplets
may become associated as in case II; here, flocculation
occurs at the secondary minimum, but the flocs in this
case will clearly be much more easily disrupted than
those which form by flocculation at the primary minimum
and they may later either dissociate or pass over into
the primary minimum. Two droplets associated at the
primary minimum may remain so or may coalesce to form
a larger droplet with a lower surface energy as when
an emulsion breaks.

If the interaction curve between two droplets has
the form shown in case III, the dispersed state is
stable, at constant particle size, so that dispersion
of the particles occurs spontaneously.

Secondary dispersions may be formed by subdivision

of the bulk phase, by nucleation and growth, or by
spontaneous emulsification.

2.3. OCCURRENCE OF SECONDARY DISPERSIONS

Secondary dispersions are formed either by design
or accidently due to malfunction of process equipment.
Some of the areas in which dispersions can occur are shown
schematically in Table 2.1.

2.3.1 Pumping or Mixing Processes:

If mixing or pumping is too intense in systems of
low density difference, or low interfacial tension,
secondary dispersions can easily be formed, and in
equipment designed only for the separation of primary
dispersions (for example mixer settler units), entrainment
of both phases can occur. Mixing rates and pump speeds
must therefore be carefully controlled.

Liquid-liquid extraction is a method of separat-
ing multicomponent mixtures using a solvent which is
immiscible or partially miscible with a feed phase,
and transferring a desired component from one phase to
the other. The success of the operation hinges on
preferential solubility, but since two phases are mixed
separation problems may arise.

TABLE 2.1 : METHODS OF FORMATION OF DISPERSIONS AND EMULSIONS

IN DESIGNED PROCESSES		BY ACCIDENT OR MALFUNCTION
Deliberate formation of dispersions to increase the rate of a transfer process	Formation as a result of a physical or chemical change to material being processed	
1) Liquid-liquid extraction	1) Condensation of Vapours of immiscible liquids	1) Oil spillage on water
2) Liquid phase chemical reactions(e.g. alkylation)	2) Azeotropic distillation	2) Water contamination of oils
3) Direct contact heat transfer(e.g. conduction)	3) Steam stripping	3) Malfunction of designed apparatus
	4) Cooling (quenching) of oils	
	5) Gas compression	

There are two conflicting interests at this stage: better transfer rates are generally achieved by increasing the interfacial area between the phases, but, subsequent phase separation is slower and more difficult as the interfacial area increases. The compromise is to apply only sufficient energy to produce a primary dispersion which is relatively simple to separate. A suitable example occurs in the oil extraction field. The oils are washed with concentrated sulphuric acid to remove sulphur compounds, washed a second time with water to remove any excess sulphuric acid, and then a third time with a caustic solution for pH adjustment. Problems arise if aqueous sulphuric acid secondary dispersions are carried into the caustic wash stage, because the resulting sodium sulphonates act as stabilisers for emulsions. Hence good separation of dispersions is required at all stages but especially prior to caustic treatment.

Alkylation processes and the production of hydrogen peroxide are two examples of liquid phase chemical reactions where dispersion problems may arise.

In the alkylation process, a concentrated acid is used to catalyse the reaction between butane and isobutane for the formation of iso-octane, a petrol blend additive. Secondary dispersions are deliberately formed by passing the water/oil reaction mix through a

centrifugal pump. The subsequent dispersion requires
separation so that the iso-octane product can be collected
and the acid catalyst reused.

The hydrogen peroxide example involves a two stage
reaction:

    i)   hydrogen reduction of quinone in the
           presence of a catalyst.

   ii)   oxidation of hydroquinone produced in i)
           to give hydrogen peroxide and quinone.

These products are separated by solvent extraction and
dispersion separation problems may occur at this stage.

Direct contact heat transfer can be used for
immiscible liquids, and will yield an increase in heat
transfer coefficient over conventional equipment. The
interfacial area dependency again holds, and it is
imperative that the separation system used after heat
transfer can cope with the dispersion produced by the
mixing process.

2.3.2 Emulsification by Dispersion Methods

Mechanical dispersion involves breaking up the
liquid-liquid interface into fine ligaments and globules.
Under shear, a droplet undergoes distortion in a manner
characteristic of the system as a whole, and elongates

into thread like filaments. These cylindrical shapes, once formed became unstable as soon as the length exceeds the circumference and two spherical drops form. If the cylinder is extended far beyond its stability limit, it will have a tendency to break down into many droplets (35).

The droplet formation process can be achieved in practice by several methods and the effects of the system parameters on the process have been reviewed (36). It has also been noted (35,37, 38) that when long filaments were formed, at the removal of the shear the thread remained stationary, but after a short time, spontaneously broke up into droplets.

However, it is usually desirable to produce small droplets in a short time which necessitates the application of large velocity gradients. The variety of equipment to achieve this can be classified into simple mixers, colloid mills, homogenizers and ultrasonic devices. These are illustrated in Fig. 2.3.

The simple mixers may be of various types, ranging from high-powered propeller shaft stirrers immersed in a small tank or drum to large self-contained units with propeller or paddle systems and jacketed tanks through
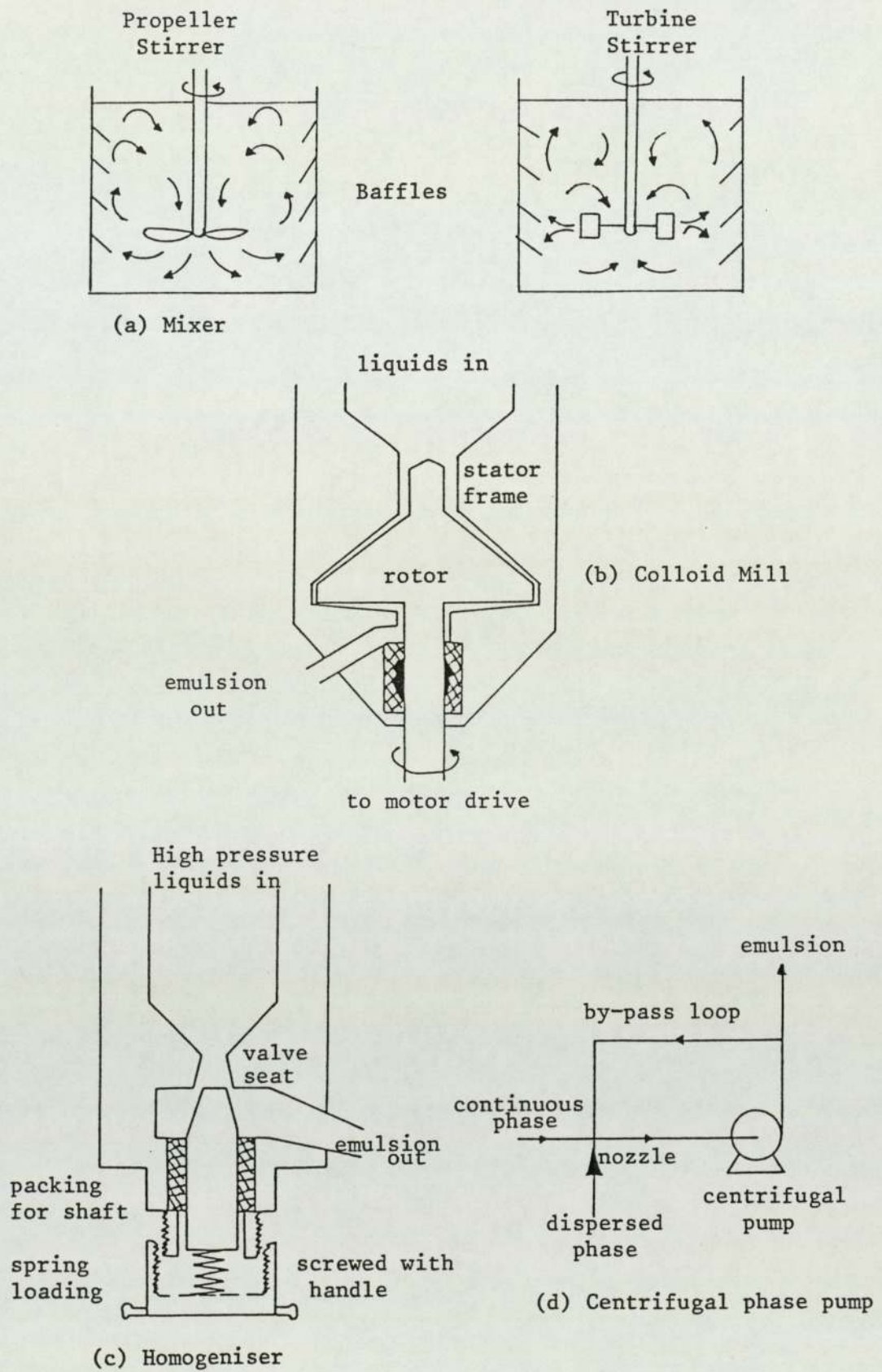
Fig. 2.3 Mechanical Methods of Emulsion Formation

which heating or cooling fluids may be circulated
(Fig. 2.3a). Careful design of the geometry and
materials of the mixer produces a homogeneous turbulent
flow field capable of reducing the drop diameter to
5 μm. The properties of the prepared dispersion also
depend upon the agitator speed and the physical properties
of the bulk phases (39).

Emulsification of the liquids is carried out in a
colloid mill or blender (Fig. 2.3b) under strong
shearing flow between a high speed rotor and a stator
surface. The emulsion passes between these two opposing
faces through a clearance which may be as small as
0.025 mm.

Deformation of drops in a homogenizer is achieved
by forcing the bulk phases through a small orifice
under pressures of approximately 350 bar as in Fig. (2.3c).
The adjustable orifice may be about 10^{-8} m^2 in area and
droplets of 1 μm can easily be produced. Alternatively
sub-micron droplets can be produced by repeated passes
of the dispersion through an orifice at a lower pressure
of approximately 2 bar (40) and larger drops may be
formed by a single pass through larger diameter capilla-
ries at low pressures (41).

One of the simplest and most effective methods of
producing secondary hazes continuously is to pass the

bulk phases through a centrifugal pump which is associated with a by-pass circuit (Fig. 2.3d). The characteristics of the dispersions formed in this manner have been investigated (1, 42, 43, 44); typically it produces a dispersion with a mean drop size of about 20μm.

Whilst the use of mixing and shearing devices represents a simple way of introducing the energy required for the formation of an emulsion, such mechanical methods are not the only ones to be employed.

2.3.3 Emulsification by Condensation

Vapor injection is a condensation method of emulsification which involves the injection of a supersaturated vapor of the dispersed phase using a jet orifice submerged in a continuous phase containing a suitable emulsifying agent. The supersaturated vapor condenses as micron-sized drops whose size is dependent on the pressure of the injected vapour, the diameter of the jet orifice, and the emulsifier added to the continuous phase (45). This procedure is illustrated in Fig. 2.4a.

'Freeze heat' is another condensation technique in which the temperature of an agitated mixture of organic and aqueous phases in a sealed system containing an emulsifier, is varied until condensation occurs.

To measurement and
control of pressure
and temperature.
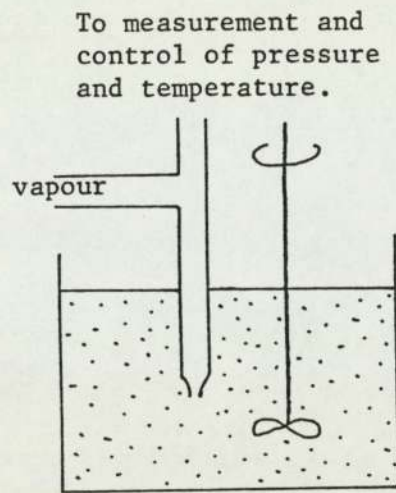
vapour

(a) Vapour injection

heating/cooling
jacket
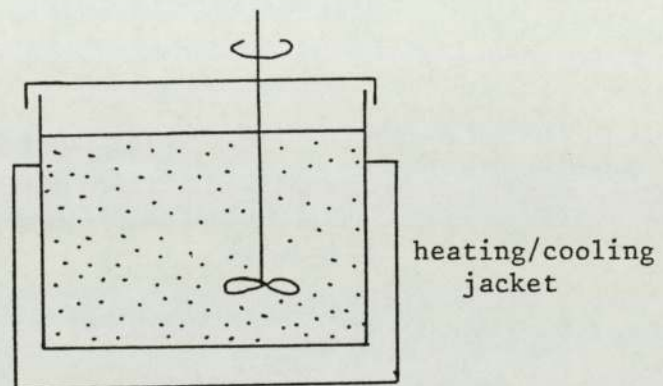
(b) Freeze-Heat Techniques

Fig. 2.4 Emulsification by Condensation

As it relies upon the temperature dependence of the mutual
solubility of the two liquid phases (46), this technique
is extremely sensitive to temperature changes and the
system may become heterodispersed once formed (47, 48).
Fig. 2.4b illustrates the arrangement.

Condensation methods are still limited to a laboratory
scale   because of the complexity of the equipment
required to adequately control the conditions of formation.

2.3.4 Emulsification Due to Chemical or Physical Change

In the process of steam distillation of organic
hydrocarbons, the condensation process does not usually
give two bulk phases from film condensation but rather
one phase as a dispersion in the other. The phase
continuity of the dispersion cannot be predicted with
confidence but it is thoughtthat droplet size, and
thus dispersion-type, is determined by the condensation
rate and the vapour loading. As these two parameters
increase, the mean drop size of the dispersion
decreases. Condensation of overhead vapours from
azeotropic distillation can also lead to dispersions if
the two liquid phases are immiscible.

A further process in which dispersions can be formed
is in packed column steam-stripping of oils where two

problems arise. Firstly, steam condensing on the lower part of the column can give water dispersions in the oil; and secondly, the more volatile oil components can vaporise and leave the top of the column with the steam.

Secondary dispersions also occur in cooling and quenching operations. If a hydrocarbon (oil) mixture is cooled, the solubility of water in the mixture decreases and any excess water comes out of solution to form a haze. Typical droplet sizes are between 0.5 and 5 microns in diameter, and generally the faster the cooling rate, the smaller the drop size.

Gas compression is also an operation in which secondary dispersions can occur. This mechanism is analogous to that of vapour condensation except that the change of state is forced. Compressing mixed vapours of a hydrocarbon and steam will probably lead to liquefaction of one component before the other, leading to dispersion formation.

2.3.5 Effluent From the Oil Industry

Wastewater from petroleum refineries and petrochemical plants may contain significant quantities of free and emulsified oils. Thus petroleum refineries are all involved in processes for removing small amounts of oil from effluents. As of January 1, 1974, a total of 247 refineries were processing about 15 million barrels per day

$(2.4 \times 10^6 \ m^3/d)$ of crude (3). Depending on the refining category, average refinery discharge is about 20 to 48 gallons of wastewater per barrel (426 to 1143 litres/m^3) of crude processed. Approximately 500 MGD ($1.9 \times 10^6 \ m^3/d$) of refinery wastewater must be treated.

One of the largest sources of oil-contaminated water are operations associated with the discharge of oil from oil tankers, which include for example the loading, and unloading of the crude oil, the cleaning operations and the use of clean ballast water in the fuel tanks, in order to compensate for the weight of fuel used in the journey and in order to load the ship. There are also inevitable spills and tanker accidents which in many cases pose the problem of massive oil pollution, as in the incident in the Arabian Gulf in Summer 1983. (123)

2.3.6 Other Sources

Undesirable effluents result from several industrial processes , such as the wool industry producing a waste oil-in-water dispersion from the process of scouring wool.

A similar effluent arises in the operation of steam engines where condensate from the cylinders is often found to form stable oil/water emulsions with the lubricating oil. Waste effluents also emanate from most

industrial operations which use oil as a lubricant or
process fluid.

Solvent extraction processes in the chemical industry
and some processes of the food industry also produce
contaminated effluents comprising dispersions.

CHAPTER 3

TECHNIQUES OF SEPARATION OF

SECONDARY DISPERSIONS

CHAPTER THREE

TECHNIQUES OF SEPARATION OF SECONDARY DISPERSIONS

3.1 INTRODUCTION

Separation techniques may depend on one or more of the following principles:

1. Gravitational forces
2. Centrifugal forces
3. Electrostatic fields
4. Use of packings and fibres

There are also chemical, biological, thermal and flotation treatments.

Selection between these techniques depends upon many factors; the cost, type of dispersion and the simplicity of each chosen technique.

3.2. TECHNIQUES OF SEPARATION
3.2.1 Gravity Settling

This is the simplest and most widely-used technique, and simply consists of allowing the dispersion sufficient time to separate by gravity. However its use is limited to primary dispersions because the time for settling for a secondary dispersion is very long. For example, on the basis of Stoke's law,

$$U = \frac{gd^2(\rho_1 - \rho_2)}{18\,\mu} \qquad\qquad (3.1)$$

Hence the settling velocity U is proportional to the square of the drop diameter so that a 10 μm drop settles 400 times slower than a 200 μm drop.

Whilst gravity settlers are effective in removing most of the free oil, soluble oil and a large portion of the emulsified oil will remain in the settler effluent.

3.2.2. Centrifugal Separation

This method is most efficient for separating two liquids of low density difference, high continuous phase viscosity or small drop size. Centrifuges are used in ordinary chemical processes only when low residence time is essential or when phase separation is difficult; examples therefore arise in pharamaceutical and radiological processes, or in military applications, such as the purification of aviation fuel.

3.2.3 Electrostatic Fields

Application of an electrostatic field is the most effective means of separating dispersions. The petroleum industry relies on electrostatic coalescers to purify crude petroleum of its connate sediments and corrosion-

inducing salts, and, thereby, reduce corrosion
and fouling of distillation equipment (5).

The basic requirements for the use of electrostatic
fields are that the disperse phase is an electrolyte and
the continuous phase is non-conducting. Sadek and
Hendricks (6), studied the electrical coalescence of
water droplets in low conductivity oils and concluded
that coalescence can be considered as a four-step mechanism.

a) When droplets are passed through an electrostatic
    field they assume a charge.

b) the charged droplets are propelled by the electrical
   force towards the oppositely - charged electrode of
   the field.

c) the droplets collide as they are being propelled.

d) coalescence occurs.

For dispersions containing uncharged drops, dipole
coalescence is the operative method (5) for high concen-
tration of the dispersed phase but the efficiency decre-
ases rapidly at concentrations below 0.1% due to a
decrease in the uncoalesced droplet population. The bulk
of research on electrically induced coalescence, has how-
ever focussed on water-oil systems, a reflection of the
importance of these emulsions to the oil industry,

where they occur during extraction of crude oil. High field strengths can be used in such systems because of the low conductivity of the continuous phase.

3.2.4 The Use of Packings and Fibres

In packed bed coalescers, coalescence occurs within the body of the packed section. Several prerequisities for successful operation have been proposed, viz.: the coalescer material should be preferentially wet by the dispersed phase; they should possess a large surface to volume ratio; the interstices should be small enough to cover the range of droplet sizes encountered; and they should cause as low a pressure drop as possible (7).

A wide variety of materials; including natural fibres such as cotton and wool, synthetic fibres such as glass, viscose and p.t.f.e., metal screens, steel wool, membranes and granular beds of gravel and conventional column packings such as Raschig rings and Berl saddles, have been used.

Recent workers on coalescence have used beds of fibrous materials (11, 12, 13), glass ballotini (14, 15), woven meshes (1) and building sand and steel mesh (16).

Beds of glass fibre were used as early as 1949 for the coalescence of emulsions in commercial processes, e.g.

in the desalting of crude oil (8). However Tuerk (9)
and Robertson (10) both indicate that fibrous bed
coalescers were initially developed for use on aircraft
fuels. Following a series of fatal jet plane crashes
in the early 1950's, investigation found the cause to be
water in the aircraft fuel and coalescers were urgently
developed to limit such contamination.

3.2.5 Disadvantages of Separation Techniques

All the existing techniques available for separating
dispersions suffer from certain disadvantages. Chemical
additions may cause contamination of the liquid system
and care is therefore needed in the choice of chemicals
and level of addition. Since additives may be surface
active, they may also reduce the interfacial tension
between the phases of the dispersion leading to the
formation of very small drops and also tend to form co-
atings on coalescer elements, thus preventing them from
functioning efficiently (34).

Flotation processes also suffer the disadvantage of
high cost and technical, and practical, limitations
in application. Results have been found to vary depend-
ent upon traces of impurities, degree of aeration and va-
riation in the type, and intensity, of agitation during
the flocculation stage.

Centrifugation also suffers from high capital and
operating costs. Consequently the use of centrifuges

has been restricted to military applications such as the purification of aviation fuel.

Electrostatic coalescers possess the disadvantage of high capital costs but are simple, simply adaptable to automatic operation, and problems from scaling-up seldom arise.

As most methods available for separating dispersions suffer from certain disadvantages, the trend for many duties is to use porous or fibrous bed coalescers as they are relatively inexpensive, compact and simple to operate. However problems may arise with them due to deposition of particulate matter .

3.3. COALESCENCE IN FIBROUS BEDS

3.3.1 Introduction

Media made from glass fibres are ideally-suited for use in coalescence operations because the fibres are smooth, circular, cylinders and are available with a wide selection of uniform diameters. Glass can be exposed to high temperatures for thermal treatment giving effective cleaning and mat formation. Fibrous materials can be used in various forms as:

- polyester felt, polypropylene felt and
  glass mats (4).

- membranes or small, randomly-packed fibres (17).

- fibre glass with polymer coating (18).

- Coarse/fine/coarse fibre glass beds compressed bet-
  ween a screen (21).

- Phenol-formaldehyde resin, treated, fibre glass,
  Teflon, Dacron and Nylon (22).

- Knitmesh packing composed of fibre glass and
  stainless steel (12).

In examining the operation of any type of fibrous bed
coalescer it is important to recognize that this is not
a filtration process (17, 23), and the design parameters
are therefore not necessarily the same as for filtration.

Fibrous bed coalescers are described under various
titles; viz cartridge coalescer (17), coalescer (4, 18,
21), packed bed coalescer (20), filter-separator (24) and
water-separator (25). There are analogous uses for glass
beads (19) or spheres (20).

3.3.2 Factors Affecting Coalescence

The separation efficiency of the coalescer may be
affected by numerous factors including,

1. the fibre diameter, surface roughness and wettability

2. bed voidage

3. packing depth

4. inlet drop size

5. flow rate

6. the effect of contaminants and additives

7. temperature

8. physical properties of the two phases

Each one of the above factors will be considered.

The fibre diameter is important in relation to
droplet collection efficiency. Sareen (26) reported
that a coalescer made up of small fibre elements
exhibits a high coalescence efficiency. For example,
a one micron fibre was found to be about 27 times more
effective than a 10 micron fibre in removing one micron
droplets of water from a fuel stream. However a
decrease in fibre diameter also reduces the size of the
enlarged droplets leaving the bed. Therefore in order
to increase the size of the released droplets it has been
recommended that the coalescer should be constructed with
the large fibres built into the downstream of the bed
and the fine fibres at the inlet. Many workers have
confirmed this design (17,24, 27, 28).

Surface roughness of the fibres can contribute further
to the above effect since a rough surface. has a larger
true surface area than a smooth surface. Thus from
a consideration of Van der Waals forces (29), the rougher
the surface the greater will be the unbalanced forces
of surface free energy available to attract a liquid droplet.

In a secondary dispersion the fibre wettability is less important than with a primary dispersion because the droplet sizes are very much less than the equilibrium drop size. The droplets in a secondary dispersion will, due to their size, be nearly spherical and will only make point contact with the surface without actually wetting the fibres.

Fibrous-bed voidage also affects the coalescence process. From a study of primary dispersions Johannesson (29) pointed out that voidages must be uniform in the bed otherwise some portions of the bed could be loaded more than others, resulting in 'channelling' which gives poor coalescence. The assumptions of constant voidage in a close packed fibre bed do not follow. Indeed Jeater (30) has established that the hold-up is not constant within a fibre bed but tends to be high at the inlet and outlet regions, presumably due to compression on assembly. Sherony and Kintner (31) pointed out that the degree of coalescence increased with increasing the hold-up. Spielman and Goren (32) reached similar conclusions.

Increasing the packing depth might be expected to allow the fibres to maintain a larger quantity of disperse phase and hence increase separation efficiency, but this does not occur. Sareen et. al (26) observed that coalescence performance improved with increase in bed depth but a practical limit to the maximum bed depth

was set by the pressure drop. Hazlett (33) showed that
fibres compressed from a free thickness of about ½ inch
down to a final thickness of 1/8 inch performed better
than a 1/16 inch bed thickness and that increasing the
thickness to 3/16 inch did not improve performance.
Sareen (26) demonstrated that varying the bed depth from
0.25 to 1.25 inch at increments of 0.25 inch increased
coalescence, but if the pressure drop was too high across
the bed, redispersion of the coalesced drops could occur
within the bed with the emergence of small drops from
the bed. Fahim and Akbar (12) applied micro photography
to study the outlet drop size, of kerosene in water
dispersions, and found that deeper beds of 0.2 m and 0.4 m
gave smaller drops than those produced using 0.1 m bed.
This raises the possibility of redispersion of kerosene
drops, or at least their splitting up within the down-
stream end of the bed which was less saturated.

Spielman and Goren (27) also confirmed that, as point-
ed out by Davies and Jeffreys (2,50) the bed depth for
the maximum throughput must be carefully selected and in
some systems, particularly low interfacial tension systems,
redispersion can take place in the bed. Langdon et.al.
(49) also stated that decreasing the density of coales-
ced layer resulted in poor oil removal efficiency.

With regard to the mean inlet drop size of a disper-
sion, the smaller the droplet size the more difficult
a dispersion is to coalesce.

The flow rate of dispersion must be kept below a
certain limiting value, since the force of adhesion
between the droplets and the fibres must be greater than
the local shear forces on the droplets otherwise the
retention time on the surface will be less than the time
required for coalescence. Sareen and Kintner (26)
used cotton and synthetic fibre beds and reported that
the maximum separation velocity initially increased with
bed depth up to a maximum value and then subsequently
decreased continuously. Spielman (27, 32, 51) also showed
that there is an optimum flow rate above which separation
efficiency decreases. Burtis and Kirkbride (52) found
that coalescence efficiency was improved by decreasing
superficial velocity in the range 0.66×10^{-2} to
0.027×10^{-2} m/s. This was also confirmed by Voyutskii
et. al (53) and Gudsen (54).

Gudsen separated petroleum fractions dispersed in :
water using a mixed fibrous bed of cotton and glass
wool and also identified a critical separation velocity
below which complete separation was possible. Sareen
et.al (26) observed visually the performance of single
fibres (cotton, polypropylene, glass and p.t.f.e)
and mixed fibres (cotton-glass fibre and cotton-dynel :
fibre) in coalescing several oil-in-water emulsions.
The superficial velocity was varied from 0.1×10^{-2} to
1.8×10^{-2} m/s and a critical separating velocity for
each fibre type was identified. Photomicrographs of

exit drops indicated that a drop would break away from
the fibre after attaining an equilibrium size; when the
superficial velocity was higher than the critical velo-
city a retained drop was carried away before attaining
the equilibrium size. These results were later confirmed
by Davies and Jeffreys (50).

Essentially 100% oil separation efficiency was
achieved by Langdon et.al (96) at a superficial velocity
of $1x10^{-2}$m/s using a coalescer made from phenol-formalde-
hyde coated glass fibre $3.2x10^{-6}$ m in diameter.

To simulate the flow through fibrous beds, Vinson and
Churchill (55) used photo-etched screens to separate a
0.05% oil-in-water emulsion with an average drop size
of $3x10^{-6}$ m. Coalescence efficiency decreased with
increase in superficial velocity, from $0.025x10^{-2}$ to
$2.08x10^{-2}$ m/s. A correlation developed for fractional
drop removal is discussed in more detail in section 9.3.

Generally, surface active agents can decrease coale-
scence rate, cause rupture of the dispersed film during
the passage process, and decrease the volume of the
released drops at the outlet.

Some theories have been presented as to how contamin-
ation and additives poison coalescer elements. The
presence of dirt tends to cause plugging of the porous
matrix of the fibres and hence to decrease the capacity

of the bed and also reduce efficiency by changing the conditions for droplet adhesion. Bartle (56) suggested that there was adsorption of the surfactants by the coalescer element which would cause re-dispersion of the dispersed phase present on the media. Osterman (34) suggested there was adherence of the surfactants to the media thus allowing the emulsion to pass through unaffected due to the change in fibre wettability. Lindenhofen (57) disproved the above theories experimentally and suggested that the surfactant film at the oil-water interface (water dispersed) may present a mechanical or electrical barrier to the coalescence of water droplets in the media. Flushing the coalescer with iso-propyl alcohol improved its coalescence performance and lowered its pressure drop. More recently (58) he suggested that commercial coalescers, which normally have a cotton outer wrapping or 'sock', malfunction due to the water wetted sock, causing a high surfactant concentration at the release point. By coating the sock with a fluorocarbon resin a hydrophobic surface was produced and this operated normally even if poisoning was attempted. These results supported the theory first presented by Hazlett (59) that poisoning is caused by interference with the detachment process at the point of release of the coalesced drop from the sock. Experimentally detachment was found to occur much more readily in fuel containing powerful sulfonate surfactants (25). Strong sulfonate surfactants lower the interfacial tension of fuel-water interfaces below 10 dynes/cm and degrade coalescer performance

significantly. Bitten (22) studied the effect of
addition of 5 mg/litre of sodium sulfonate on coalescence
during experiments including photography of droplet growth
or coalescence on plastic fibres. JP-5 fuel emulsions
were formed containing 100 and 1000 ppm of free water
respectively. It was found that an emulsion of 100 ppm
free water containing 5 ppm of surfactant would not
coalesce or form droplets upon Dacron, nylon or Teflon
fibres. An emulsion of 1000 ppm free water with no sur-
factant would form large droplets on Dacron, nylon and
Teflon fibres. The addition of 5 ppm of sodium sulfonate
to the system caused the droplet growth to stop. Over
a 20 min. period, all the small drops were released from
the fibres, and most of the big drops disappeared from
the Teflon fibres. All signs of chain formation on the
nylon fibres had also disappeared.

Although increasing the temperature of the dispersion
feed may not appear practicable from an economic view,
it may be useful in some cases where a high separation
efficiency is required. Langdon et.al. (49) observed
that the pressure drop across a bed increased almost
linearly with time but the rate of increase was lower
at higher temperatures. Lowering the influent temperature
lowered the bed capacity at a fixed pressure drop and
influent concentration. Sareen and Kintner (26) noted
that high temperatures improved operation. Hazlett (24)
explained that the efficiencies of interception,
diffusion and inertial impaction are all decreased by

lowering the temperature. The latter mechanism is the most sensitive to temperature reduction since inertial impaction decreases with a decrease in density difference and with an increase in continuous phase viscosity. The diffusion process is affected by temperature in a complex way, because it is related to the diffusion coefficient and the continuous phase viscosity. Temperature change has a slight influence on the interception mechanism since the change in continuous phase viscosity and density with temperature affects only the Reynolds number.

The physical properties of the dispersion are also of significance. Davies and Jeffreys (50) demonstrated that separation efficiency was higher with high interfacial tension, high density difference systems confirming the results of Kintner et.al. (26) . System interfacial tension is important in the operation of a coalescer; generally, the higher the interfacial tension, the easier the separation. Systems with interfacial tensions as low as 20×10^{-3} N/m can be separated satisfactorily, but below this value separation becomes increasingly difficult (56). Rose (61) confirmed this from a study of nine different water-organic dispersions for the separation of oil in water emulsions. Sareen et.al (26) found that, for an interfacial tension value of 20×10^{3} N/m there was incomplete coalescence for water soluble surfactants whilst coalescence was complete with oil soluble surfactants for values as low as 3.52×10^{-3} N/m.

CHAPTER 4

COALESCENCE MECHANISMS OF

DISPERSIONS IN FIBROUS BEDS

CHAPTER FOUR

COALESCENCE MECHANISMS OF DISPERSIONS IN FIBROUS BEDS

4.1. INTRODUCTION

Numerous workers have attempted to analyse quantitati-
vely the coalescence in fibrous bed coalescers (11, 17,
23, 24). Until now, however the complex events occuring
in a coalescer are not adequately understood. The co-
existence of a secondary and a primary dispersion in a
fibrous bed, results in the distribution between them
being ill-defined.

The separation phenomena in a fibrous bed may be consid-
ered as the sum of several steps (24, 59). In this study
the major three steps to be discussed are:

1. Capture of drops by the fibrous bed.
2. Coalescence and passage of collected dispersed phase
   through the bed.
3. Release of coalesced drops.

4.2. DROP CAPTURE MECHANISMS

Capture of a drop in a flowing continuous phase may
in theory be accomplished by one or more of the follow-
ing processes:
   (a) Collision with an adjacent drop suspended
       in the dispersion.

(b) Collision with an obstruction in the packing structure.

(c) Collision with a drop that has already been captured and is attached to the packing.

Sareen et. al (26) investigated drop capture photographically and found that coalescence between freely-moving drops was negligible.

Collision with the packing fibres and with drops attached to the fibres was found to be important by Sareen (26) and Bitten (22). Direct collision with the fibres is obviously important during start-up of the equipment but steady-state operation of the coalescer will also be dependent on drop attachment to drops already captured. A number of authors (24, 26, 61) have defined the mechanisms by which particles from the stream collide with those attached to the fibres.

The effect of the degree of saturation of the dispersed phase on the packing in assisting drop capture has been incorporated into models describing droplet capture. Sherony and Kintner (31) considered the size distribution of retained drops which act as potential collectors and this was extended by Rosenfeld and Wasan (105) by inclusion of an 'effective fibre diameter'. Spielman and Goren (106) assumed that the dispersed phase consisted entirely of discrete spherical drops and evaluated the capture rate from an analysis of the trajectory of a drop approaching a spherical particle. This method permitted independent evaluation of drop capture by packing fibres and of capture by drops attached to the fibres.

The numerous possible droplet-fibre capture mechanisms are summarised in Fig. 4.1. These are to be independently examined to ascertain their relative contributions to the overall capture efficiency.

4.2.1 Interception

In laminar flow, a fluid passing a submerged cylinder, such as a glass fibre, will follow flow streamlines such as those in Fig. 4.2 (a) where F is the cross section of a fibre. A dispersed phase droplet, W_1, will follow these flow lines. The droplet shown on streamline S_4 will be intercepted by the fibre when it reaches position W_2. A droplet of somewhat smaller size W_3, following streamline S_2, which is equidistant with S_4 from the centre line, will pass the fibre without opportunity for interception, even at closest approach, W_4. Such a smaller droplet will be intercepted, however, if it follows a streamline closer to the center line of the fibre. In evaluating the interception mechanism, the equation developed by Langmuir (108) is useful:

$$\eta_I = \frac{1}{2(2-\ln N_{Re})} \left(2(1+N_R) \ln (1+N_R) - (1+N_R) + \frac{1}{(1+N_R)}\right) \quad (4.1)$$

The Reynolds number includes the velocity term and uses fibre diameter as the characteristic dimension. The need for inclusion of the Reynolds number arises from
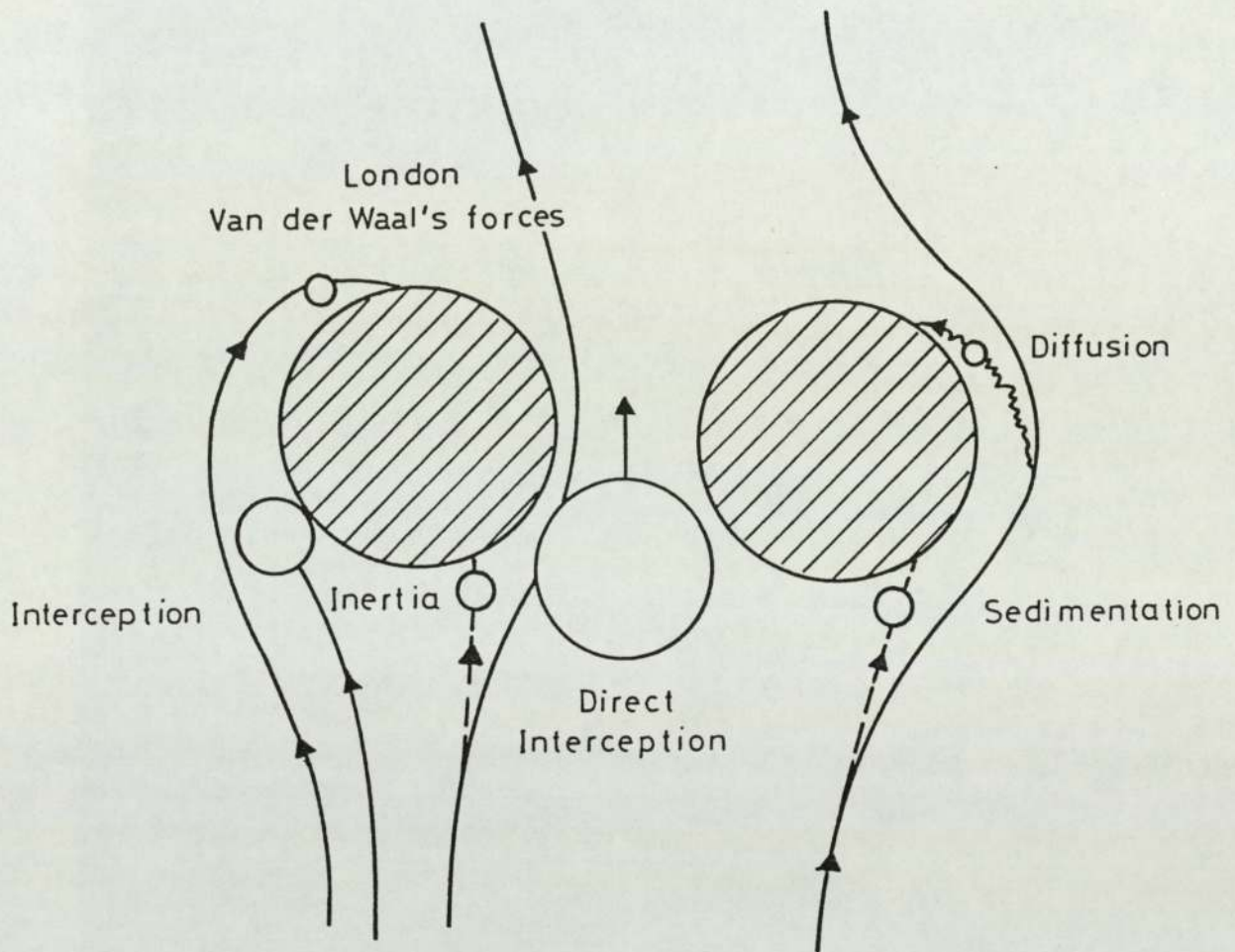
Fig. 4.1   Depiction of Drop Capture Mechanisms
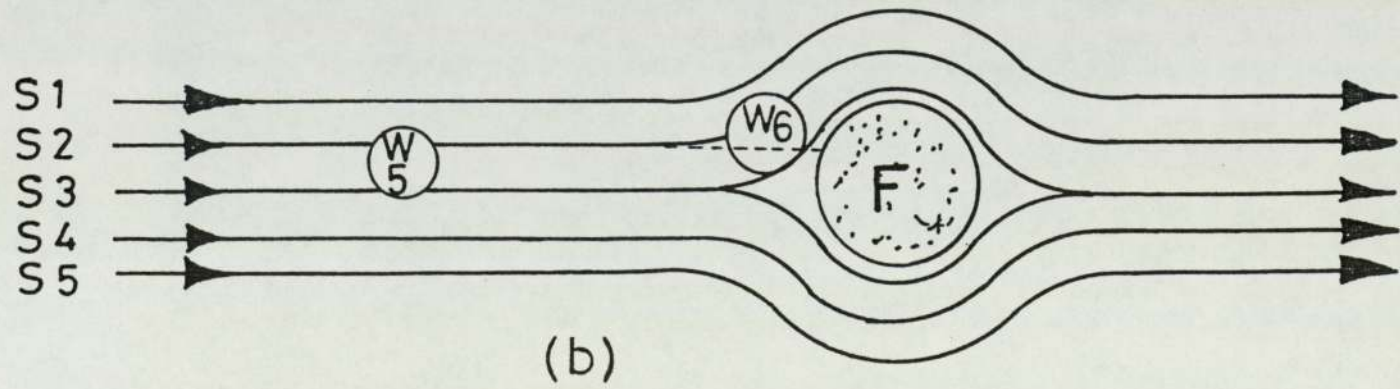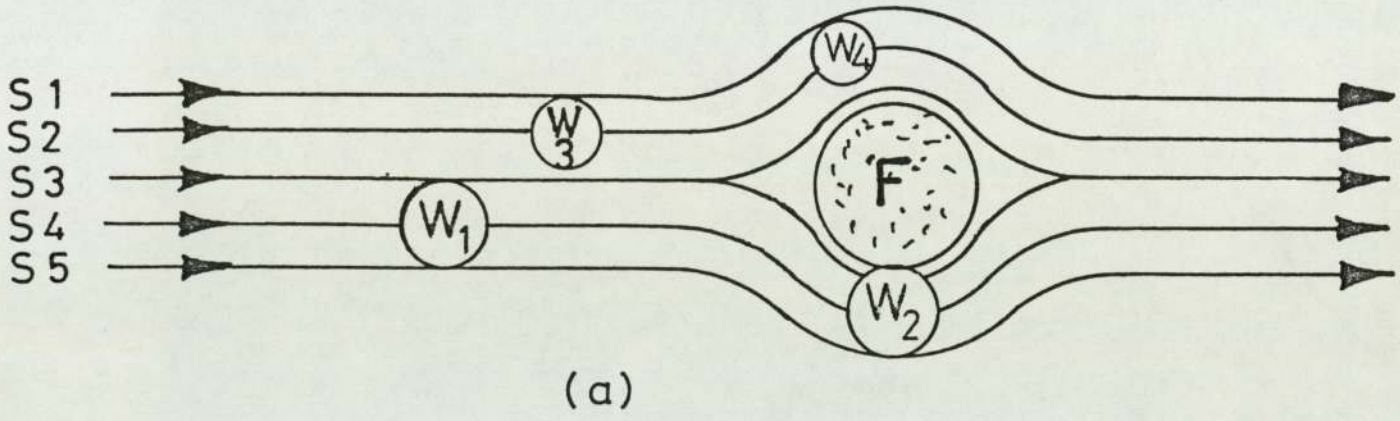
Fig.4.2 Flow patterns for Interception and
Inertial Impaction Mechanisms

the fact that the streamlines are influenced by it, being

affected at a greater distance upstream from the fibre

and displaced further from the fibre laterally as the

Reynolds number (or velocity for a fixed particles diam-

eter) decreases (24).

4.2.2 Direct Interception

Interception by pore catchment occurs when an approa-

ching drop is arrested by a pore through which it cannot

pass (see Fig. 4.1). Bartle (56) suggested that other

drops would then be captured and coalesced with a retained

drop. This mechanism predominates in the coalescence of

primary dispersions since it is well-known that when the

drop diameter is less than the equivalent diameter of the

packing interstice, the coalescence rate is very low,

even when the dispersed phase wets the packing (20).

Direct interception of drops, with subsequent mechanical

retention by the packing may be characterised by a second

interception number, $N_{Rd} = \dfrac{d_p}{d_a}$. Inspection of N_{Rd} shows

that pore catchment will contribute significantly to the

capture rate either when drop diameter is increased by

coalescence, or when the equivalent diameter of the

interstices, d_a is decreased. The latter occurs when drops

captured and retained by the collectors reduce the effec-

tive area of the apertures available for flow of the

dispersion. The capture efficiency by direct interception

may be mathematically expressed as follows:

$$\eta_D = 1 \quad ; \quad N_{Rd} \geq 1$$

$$(4.2)$$

$$\eta_D = 0 \quad ; \quad N_{Rd} < 1$$

4.2.3 Inertial Impaction

A particle with a density different from that of a fluid with which it is flowing will deviate from the flow streamlines. A more dense particle tends to move in a line less curved than that of the streamline. A possible path for a more dense particle is illustrated in Fig. 4.2(b), where the broken line indicates the departure from streamline S_2. Particle W_5, in deviating from the streamline, approaches close enough to the fibre to be captured when it reaches position W_6. Thus the greater the density a particle has with respect to the continuous phase, the higher the probability that the particle will be captured. This approach mechanism has been termed the 'inertial impaction process'.

Inertial impaction is a significant mechanism for particle removal in aerosol filtration. Because of the low viscosity and density of air, inertial impaction is the most important mechanism at high flow velocities (24).

Sherony (31) suggested this mechanism as being relevant to coalescence in fibrous beds and characterised its contribution by the magnitude of the Stoke's number:

$$N_{Stk} = \frac{d_p^2 \, \rho_c \, u}{9 \, \mu_c \, d_f} \qquad (4.3)$$

Impaction becomes significant when N_{stk} exceeds a critical value which depends on the Reynold's number. For viscous flow, values of N_{stk} of between 0.1 and 0.9 have been proposed. For potential flow conditions, Langmuir (108) determined the value of 0.063 to be the critical value of N_{stk}. Referring to Table 4.1, the majority of studies in coalescence appear to have been conducted under conditions where N_{stk} is less than the critical value. Notable exceptions are the investigations of Sherony (31), Shalhoub (43) and Austin (1), but of these, only the work of Sherony involved a situation where the density of the dispersed phase was greater than that of the continuous phase. The other studies were therefore completed under conditions which preclude any contribution to capture by impaction. Landahl (107) proposed an empirical expression relating capture efficiency by inertial impaction to the Stoke's number.

$$\eta_{II} = \frac{N_{Stk}^3}{N_{Stk}^3 + 0.77 \, N_{Stk}^2 + 0.22} \qquad (4.4)$$

for $N_{Re} \leq 10$; $N_{Stk} \geq N_{Stk}$ (critical)

It has been concluded that inertial impaction contributes very little to the coalescence of liquid dispersions.

Investigator	Dimensionless Groups Characterising Mechanisms							Predominant Mechanisms Proposed for Drop Capture
	N_{Re}	N_R	N_{Rd}	N_{Stk}	N_G	N_{Ad}	$N_{Re} N_{Pe}$ [a]	
Hazlett (59)	1	0.1	-	10^{-4}	10^{-6}	10^{-6}	10^{-4}	Interception/Inertial Impaction/Diffusion
Rajagopalan (109)	10	10^{-4}	-	10^{-6}	0.1	10^{-9}	10^6	Interception/London/Diffusion/Sedimentation
Sareen (26)	1	0.1	-	10^{-4}	-10^{-4}	10^{-6}	10^5	Interception/Inertial Impaction/Diffusion
Shalhoub (43)	1	10	-	0.1	-10^{-6}	10^{-6}	10^5	Interception
Sherony (31)	1	1	-	0.1	10^{-4}	10^{-5}	10^6	Interception/Inertial Impaction/Diffusion
Spielman (51)	0.1	1	-	10^{-2}	10^{-7}	10^{-2}	10^3	London Forces
Vinson (55)	10^{-2}	0.1	0.1	10^{-3}	-10^{-3}	-	10^4	Interception/Inertia Impaction
Austin (1)	10	0.1	0.1	0.1	-10^{-2}	10^{-5}	10^5	Interception/London/Sedimentation
Pole (14)	10	1	2	10^{-3}	-10^{-5}	10^{-2}	10^8	Interception/London/Diffusion
This study	0.5	0.8	-	0.03	0.002	10^{-7}	10^5	Interception/London/Sedimentation[b]

a. Minimum values of the Peclet number are stated, since N_{Pe} decreases, the contribution by diffusion to drop capture increases

b. See section 9.2

Table 4.1 Maximum values of Dimensionless Groups Encountered in Coalescence Studies.

4.2.4 Diffusion

A particle moving with a fluid will tend to depart
from the flow streamline. The most important mechanism
effecting this departure is the random transverse motion
due to diffusion. Capture of particles by the diffusion
mechanism is important at lower flow velocities in aerosol
filtration (31). The higher viscosity of liquids would
lower the efficiency, while the generally lower flow
velocities used in liquid coalescence would raise the
efficiency by this mechanism. The viscosity of the fluid
is incorporated in the formula for the diffusion coeffi-
cient along with the temperature and particle size. This
formula is known as the Stokes-Einstein equation,

$$Dif = \frac{k' \, T}{3 \, \pi \, \mu_c \, d_p} \tag{4.5}$$

where k' is the Boltzman constant and T is the
absolute temperature.

Langmuir (108) related the efficiency of the diffusion
mechanism for a single, isolated fibre to the diffusion
coefficient at low flow velocities by

$$\eta_D = 2.16 \left(\frac{1}{2(2-LnN_R)} \right)^{\frac{1}{3}} \left(\frac{Dif}{u \, d_f} \right)^{\frac{2}{3}} \tag{4.6}$$

The efficiency decreases with an increase in flow velocity,
drop size, or fibre size. At a flow velocity of 0.9 cm

per second, diffusion would be important only for droplets
less than 1 micron in diameter, and only then if the fibre
diameter were less than 1 micron.

The Peclet number, $N_{pe} = \dfrac{d_c u}{D_{if}}$ is often used to
characterise diffusion and is a measure of the ratio of
transport by convective forces to transport by molecular
diffusion. The Sherwood number, $N_{Sh} = \dfrac{I}{\pi d_c \, Dif \, C}$
is employed as a measure of the mass transfer or deposition
rate. For a cylindrical collector, the Sherwood number
is related to capture efficiency by the relationship

$$N_{Sh} = \eta_D N_{pe} \tag{4.7}$$

For a spherical collector, the relationship is,

$$\eta_D = 4.04 \, N_{Pe}^{-\frac{2}{3}} \tag{4.8}$$

4.2.5 Sedimentation

Buoyancy forces, as a result of density difference
between the dispersed and continuous phases; also cause
the drops to deviate from the fluid streamlines. Defin-
ing the gravity number; $N_G = d_p^2 \dfrac{(\rho_d - \rho_c) g}{18 \, \mu_c \, u}$,
which is the ratio of the drop terminal velocity, assuming
viscous flow conditions, to the superficial velocity
of the dispersion flowing through the bed; the magnitude
of sedimentation would be characterised.

Rajagopalan and Tien (109) showed that the capture efficiency is equal to the value of the Gravity number,

$$\eta_G = N_G \quad ; \quad N_G > 10^{-3} \tag{4.9}$$

The condition associated with this equation is not restrictive since the contribution due to sedimentation is negligible for $N_G < 10^{-3}$.

4.2.6 London-Van der Waals' Forces

Spielman and Goren (106) recognised that the long range attractive forces between a drop and collector may contribute to drop capture. These London, or dispersion, forces increase rapidly as the drop approaches the collector to overcome the hydrodynamic retardation effects. Dispersion forces arise due to the polarization of one molecule caused by fluctuations in the charge distribution within an adjacent molecule and vice-versa.

Hamaker (110) derived an expression from which the London attractive forces between a sphere and a plane surface may be evaluated,

$$F_{Ad} = \frac{-2}{3} \frac{Q}{a_p} \frac{1}{(H+2)^2 H^2} \tag{4.10}$$

Where a_p : the sphere radius

H : the dimensionless separation between the sphere and plane surface,

$$H = \frac{h}{a_p}$$

Q : Hamaker constant

Since the London forces depend on separation, knowledge
of the motion of a drop in the vicinity of a collector
is required to determine the capture efficiency.

Spielman and Goren (106) considered a force balance
on a drop and derived an equation to describe the critic-
al trajectory. The capture efficiency may then be deduced
since approaching drops, whose paths lie within the
flow area associated with the critical trajectory, will
contact the collector. The London force term given by
Equation (4.10) was modified using a more rigorous
expression developed by Rosenfeld (111) to describe the
attraction between a sphere and cylinder.

An adhesion number:

$$N_{Ad} = \frac{4Q}{9 \pi N_R^2} \left[\frac{1}{\mu_c u d_p^2} \right]$$

represents a measure of the dispersion forces and Spielman
solved the trajectory equation analytically for small
Interception numbers and large Adhesion numbers to give
the capture efficiency in terms of this dimensionless
parameter,

$$\eta_L = \frac{N_R^2}{A} \; (\frac{3 \pi A}{2} N_{Ad})^{1/3} \qquad (4.11)$$

This section concludes the description of drop
capture mechanisms known to feature in secondary disper-
sion coalescence. Their relative contribution to the over-
all capture efficiency are considered quantitatively in

Chapter 9.

4.3 <u>COALESCENCE AND PASSAGE OF CAPTURED DROPS</u>

Following capture, either by retained drops or by fibres of the packing, the drops coalesce until the hydrodynamic forces cause detachment from the fibre. The possible coalescence mechanisms have been reviewed by Austin (1) and are illustrated in Fig. 4.3.

When the drops are small compared with the collector and aperture diameters, coalescence may take place between adjacent drops located on the collector surface (Fig. 4.3 a) . Bitten (22) found that this is a slow process for the coalescence of drops on single fibres compared to growth by acquisition of the dispersed phase from the packing (Fig. 4.3 b).

Coalescence of a drop into a liquid film, which either adheres to the collector surface or occupies the packing void, has been proposed by Davies and Jeffreys (112) as the predominant mechanism for primary dispersions when the dispersed phase wets the packing (Figs. 4.3 c and 4.3 d). Coalescence may occur between two freely-moving drops (Fig. 4.3 e) which may be important for primary dispersions but experimental observations refute this possibility for secondary dispersion coalescence (26, 31). Drops captured by direct interception and retained by the collectors, may then trap other approach-

50

(a) Adjacent Drops (both in contact with collector)

Small Drop:Collector Diameter Ratio

(b) Adjacent Drops (drop 2 captured by and coalesced with 1)

Wetted Packings

(c) Coalescence with film of dispersed phase adhering to collector

(d) Coalescence with dispersed phase retained in packing void

Non-Wetted Packings

(e) Interdrop coalescence between freely moving drops

(f) Interdrop coalescence between one moving and another retained by collectors

(g) Deformation as drops jostle for position which causes drainage of the intervening film causing coalescence

(h) Coalescence after one drop has gained priority

(i) Coalescence of a locally formed dispersion band upstream of a blocked pore

FIG.4.3 Coalescence Mechanisms in a Packed Bed

ing drops and subsequently coalesce with them (Fig. 4.3 f).

Various mechanisms for the passage of drops through
the packing voids have been proposed by Wilkinson
(113) as illustrated in Fig. 4.4.

Dispersed phase collected by a fibrous bed is not
released immediately. It has been found that a fibrous
coalescer accumulates a considerable amount of dispersed
phase and attains an equilibrium concentration which de-
pends upon the input concentration, flow velocity and
surfactant content. The dispersed phase is not equally
distributed throughout the bed, rather the forepart
retains most of the dispersed phase.When the equilibrium
content for a particular set of flow conditions is exce-
eded, dispersed phase moves into flow channels and passes
through the remainder of the bed. As a result, the
drops of the dispersed phase will tend to concentrate
in relatively few channels where they queue in a localised
'dispersion band' type formation until coalescence
occurs with adjacent drops and the drop which blocks
the pore. As more flow paths become blocked, eventually
the increasing pressure gradient will be sufficient
to force coalesced drops through the pores. The passage
of drops through the pores will meet with less resistance,
due to capillary action, as they coalesce directly
with a flowing continum of the dispersed phase. This
behaviour would imply a lower pressure drop for beds in
which the dispersed phase wets the packing compared to
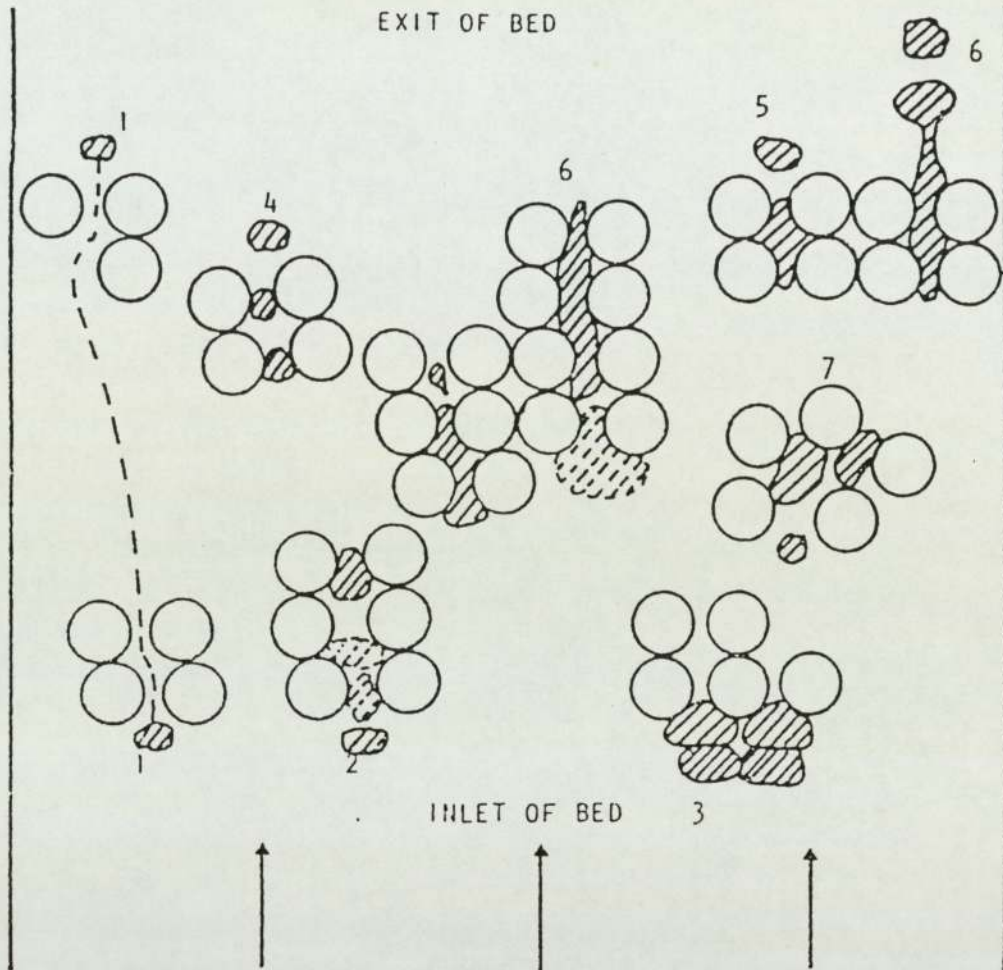
1. Unrestricted drop passage
2. Restricted drop passage (penetration due to kinetic forces)
3. Inlet drop restriction
4. Retention – impact – release
5. Unrestricted drop release
6. Restricted drop release
7. Preferential flow-path

FIG. 4.4 Proposed Droplet Hydrodynamics in a
Non-Wetted Packing of Equal-Sized Spheres.

those in which it does not. Lower pressure gradients,
due to easier drop removal from the coalescence site,
may, however, lower deformation of drops in the local
'dispersion bands' with a possible lowering of coalescence efficiency.

4.4. EXIT DROP RELEASE MECHANISMS

When a dispersion is passed through a fibrous bed,
there is a tendency for the micron size droplets of
the dispersed phase to be forced together as they move
through the passages and then film thinning would occur.
At the upstream face of the fibre bed, the dispersed phase
is released as individual drops. Three factors which
affect the size of the droplets released are the flow
velocity, the surfactant content, and the fibre size.
Single fibre studies have shown that detachment occurred
more readily from small than from large diameter fibres.
As would be expected, operation at a higher velocity
removed smaller drops. The nature of the material had
little effect on the detachment flow velocity but additives
in the fuel usually encouraged detachment.

Beatty (114) suggested that the hydrodynamic force
acting on a drop must overcome the adhesive force between
the droplet and fibre before release can occur.

The following discussion examines four possible mechanisms for release based upon rupture of a thread of

dispersed phase : drop-volume rupture (ballooning),
drop-elongation rupture (graping), jet rupture (jetting)
and point rupture. These are illustrated in Fig. 4.5.

4.4.1 Ballooning

The detaching force for a dispersed phase droplet in
a moving fluid, is found by equating the drag exerted
on the droplet with the restraining force of the interfa-
cial tension (24).:

$$C \, \rho_c \, (\Delta U)^2 \, \pi \, (\tfrac{1}{4} \, d_p^2 - d_a^2 \,) = 2 \, \pi \, d_a \gamma \qquad (4.12)$$

Where   C = drag coefficient

   d_a = orifice radius, cm

   γ = interfacial tension, dynes per cm

   U = difference between fluid and droplet
      velocity, cm per second

The drag coefficient of interest here is in the
Reynolds number range (0.3 to 1000) between the Stoke's
law region and the Newton's law region (115) where:

$$C = \frac{18.5}{N_R^{0.6}} = 18.5 \, (\frac{\mu_c}{d_p \, \rho_c \Delta u})^{0.6} \qquad (4.13)$$

Hazlett (24) derived an expression to predict the
size of released drops,

$$d_{pe} = \frac{0.55 \ d_a^{0.71} \ \gamma^{0.71}}{\Delta U \ \rho_c^{0.29} \ \mu_c^{0.43}}$$
(4.14)

With this mechanism the balloon-shaped drop grows until
the hydrodynamic forces are enough to cause a rupture
at the neck of the drop, as illustrated in Fig. 4.5.
The drop size released depends upon the flow velocity
and interfacial tension.

4.4.2 Graping

This mechanism produces bubbles of the continuous
phase enclosed by a film of the dispersed phase. After
release, the bubbles frequently agglomerate in clusters
and may eventually burst to produce a large number of
very small drops.

The mechanism can be explained as the elongation of
freely suspended drops and rupture of the threads so
formed. The ratio of the viscosity of the drop to that
of the continuous phase controls the stretching phenomena.
For a viscosity ratio in the range 0.5 to 1.0, the
elongation at small distortions is proportional to a di-
mensionless number, F.

$$F = \frac{2G \ \rho_c \ (\frac{1}{2} \ d_p)}{\gamma}$$
(4.15

Where G is the shear rate, in S^{-1}.
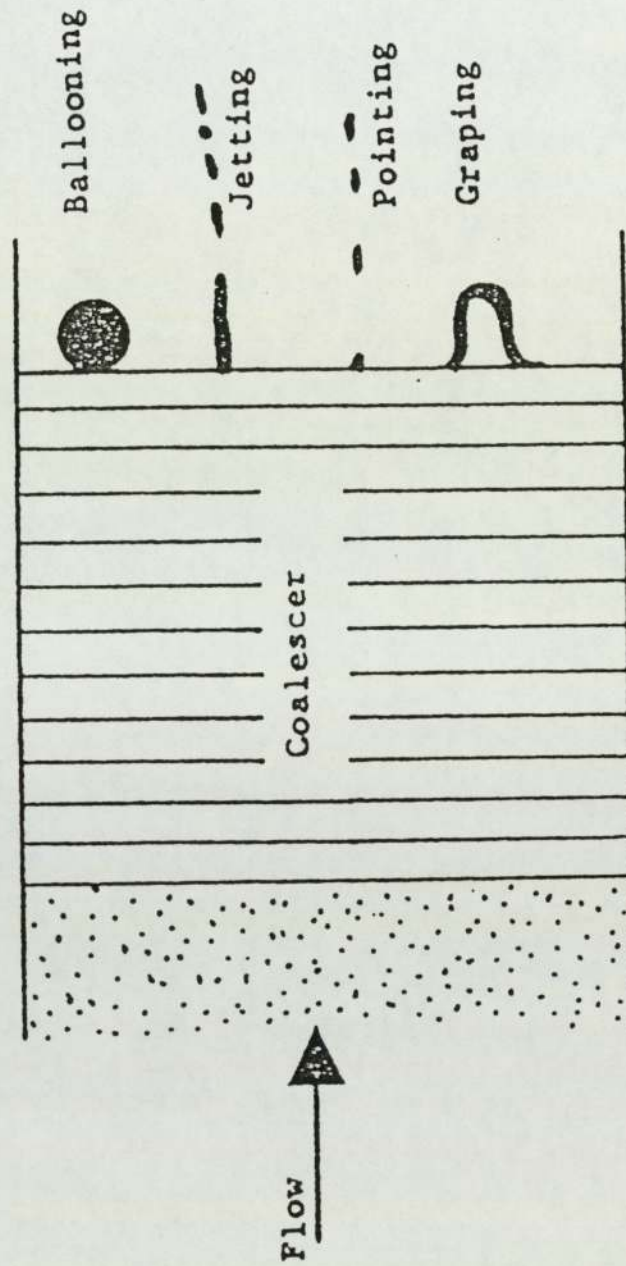
Fig. 4.5 Exit Drop Release Mechanisms

The elongation becomes more sensitive to an increase
in F at distortions near those where rupture takes place.
The control of elongation by the interfacial tension is
apparent in Equation (4.15). A reduction of γ would in-
crease F and ,under certain circumstances, could shift
the thread from a stable but extended equilibrium
configuration to a condition of instability with respect
to rupture. The graping release mechanism is directly
proportional to the shear rate and hence the velocity
difference between the dispersed and continuous phases.

4.4.3 Jetting

When surfactants are present in the liquid system,
an extended thread or jet of the dispersed phase ruptures
by Rayleigh instability to form a series of small drops
of uniform diameter. The drop size is governed by inter-
facial tension and nozzle size. Many correlations,
reviewed by Wilkinson (113), are available for prediction
of drop sizes by jetting and other mechanisms but they
strictly only apply when the continuous phase is stationary.

4.4.4 Pointing

In this mechanism, 'fingers' of collected drops
project beyond the exit face. These 'fingers' taper
to a point, vibrate and kick small drops from the tip.

In the present study, it was observed that drop release

from the exit face of the coalescer took place by a
combination of all the mechanisms described above since
the bed consisted of random fibres. Large drops were
produced by formation via ballooning or by the drip
point mechanism; in general therefore these mechanisms
are desirable. Further details are given in Chapter 7.

CHAPTER 5

EXPERIMENTAL INVESTIGATION

CHAPTER FIVE

EXPERIMENTAL INVESTIGATION

Previous investigators of the coalescence of secon-
dary dispersions in fibrous beds have recommended the
use of chemically inert, mechanically-strong, materials
through out the equipment.

Different types of fibrous glass packing were used
in the present study. They were inserted into a specially-
designed, packing holder which was in turn placed in
a glass holder. Equipment was constructed to generate
and supply a secondary dispersion of known drop size
and dispersed phase concentration at a specified flow
rate to the coalescence section.

The experimental investigation involved:

(i) Preparation of a coalescer cell
(ii) Preparation of oil-in-water secondary
dispersions.
(iii) Recording and collection of experimental data.
(iv) Analysis of the results using computer facilities.

5.1 MATERIALS OF CONSTRUCTION

To minimize contamination to the liquid-liquid system,

the materials of construction were restricted to QVF
glass, stainless steel, p.t.f.e., and a very small
amount of Viton rubber for pump tubing.

Pipelines and apparatus were incorporated to faci-
litate recycling of the liquid during single phase
pressure drop measurements, and for wetting of the fibrous
beds with the dispersed phase during coalescence exper-
iments. The coalescer design, which was modified
several times, is described in the following sections.

5.2 EQUIPMENT DESIGN

The flow diagram of the apparatus is shown in
Fig. 5.1 and the general arrangement in Fig. 5.2.

The continuous phase was produced by distillation
of tap water using an electrically heated boiler.
Water leaving the still was allowed to cool to ambient
temperature in a storage tank of Plexiglass construction
which was designed to control the level inside the tank.
It was essential to cover the storage tank, otherwise
the partially de-aerated water would have absorbed
air during cooling, which would subsequently be evolved
at many points throughout the equipment. A gravity-fed
Corning Glass, centrifugal pump with Viton seals was
used to transfer the water through the flow metering
equipment, coalescence device, and to a gravity settling
vessel, Fig. 5.3. Flow rates were monitored using two
glass rotameters with stainless steel floats which
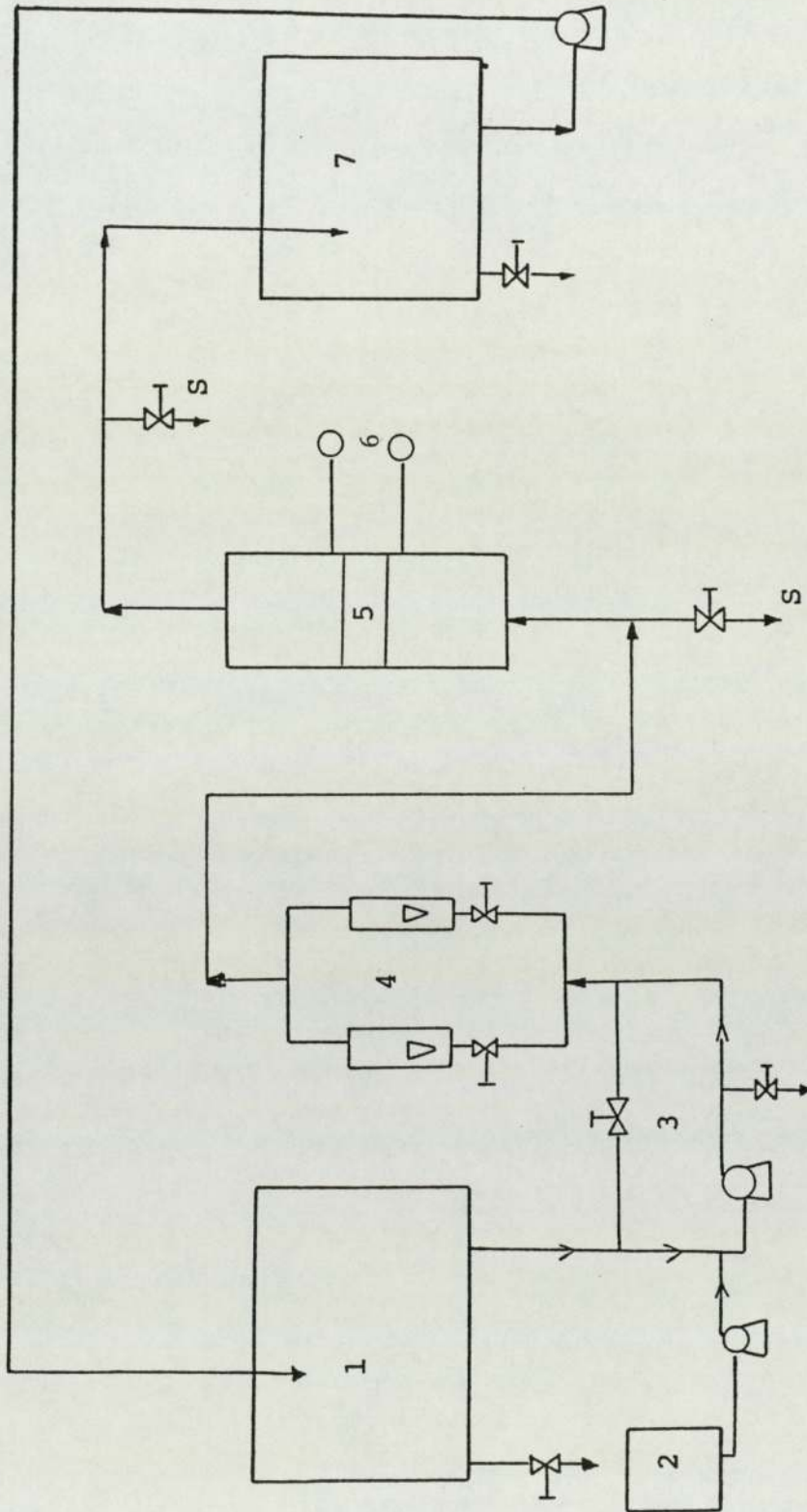
Fig. 5.1 Flow Diagram of the Apparatus

1	=	Continuous Phase Tank	2	=	Dispersed Phase Tank
3	=	Emulsification Loop	4	=	Flow meters
5	=	Coalescence Cell	6	=	Pressure transducers
7	=	Settler	S	=	Sample points
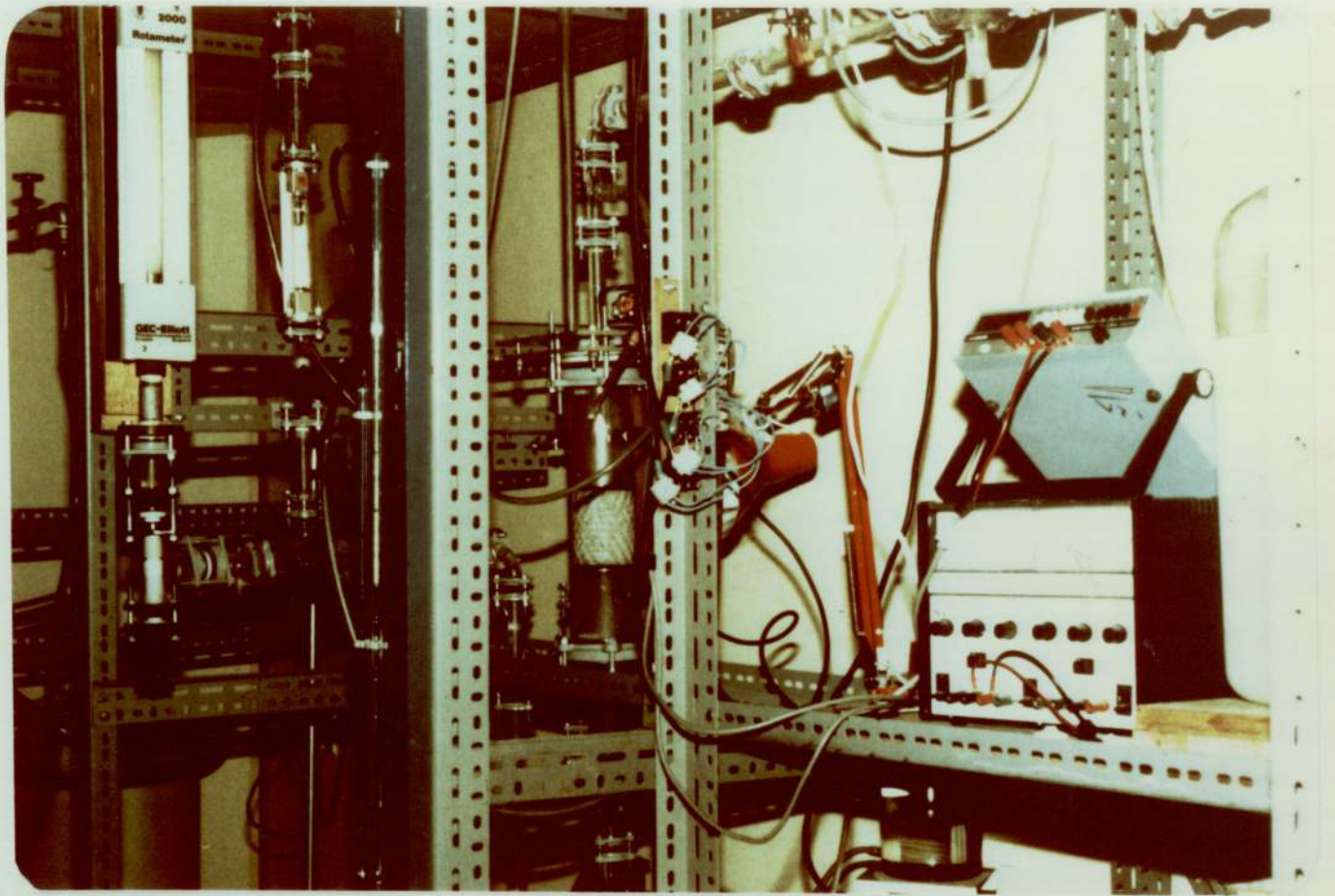
Fig. 5.2 : General Arrangement of Equipment
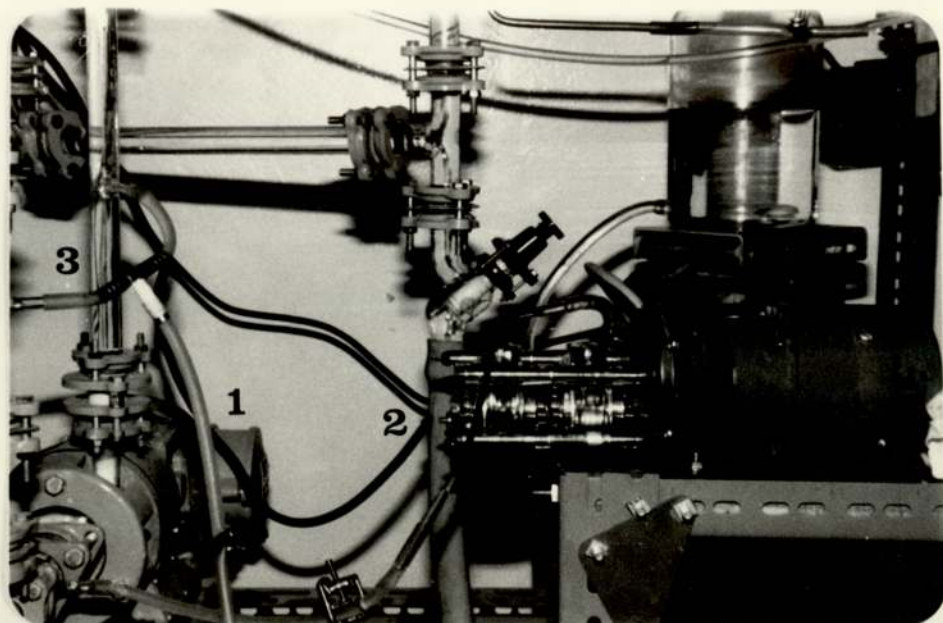
FIGURE 5.3 CONTINUOUS PHASE PUMP (1), DISPERSED PHASE PUMP (2) AND EMULSIFICATION LOOP (3)

metered for a range of superficial velocity from 0 to
5×10^{-2} m/s within the coalescer, Fig. 5.4. QVF
glass pipelines 18 mm bore, connected via p.t.f.e.
gasket rings were used throughout the construction to
permit visual detection of possible air ingress, whilst
facilitating easy cleaning and avoiding contamination
of the liquid systems. Stainless steel was employed
in the fabrication of non-standard components such as
reducing flanges and vessel covers.

From the storage vessel, the dispersed phase was
gravity fed through Viton tubing to a peristaltic tubing
pump, Fig. 5.3.

The mixing and emulsification techniques available
for production of a secondary dispersion are described
in Chapter 2. A glass centrifugal pump with a recycle
loop was selected for its inexpensive, simple construct-
ion: and ease of operation and control. Previous work
(1, 14, 42, 43) showed that for a given throughput and
pump design, the angular velocity of the impeller
determined the mean drop size produced. The dispersed
phase was injected through a 2 mm bore Viton rubber
tube into the suction line of the pump causing immediate
break up of the organic phase forming a secondary
dispersion. No separation of the dispersion within the
recycle loop was observed even after considerable op-
erating periods,i.e 3 hours.
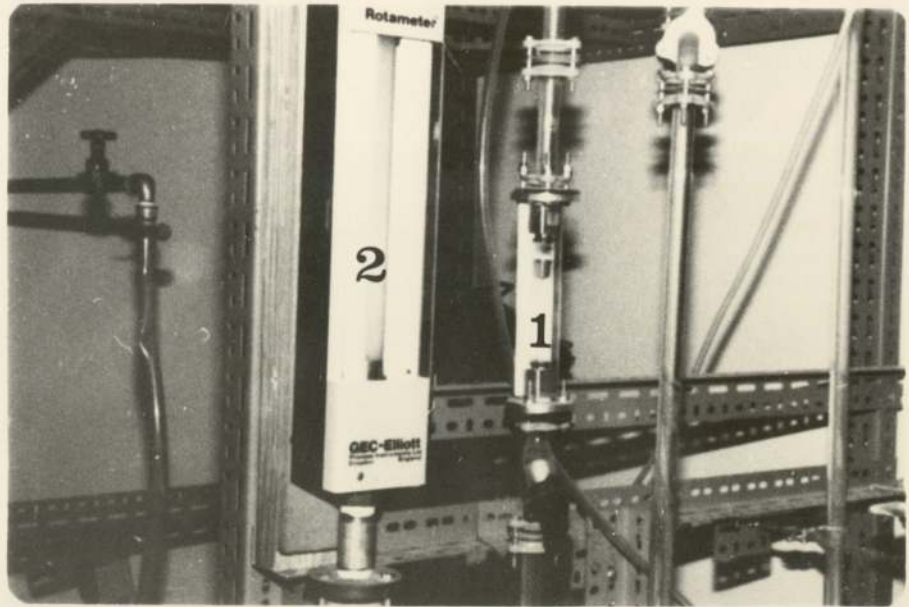
FIGURE 5.4   LOW RANGE (1) AND HIGH RANGE (2)

FLOW METERS

After passing through the coalescer, the primary
dispersion produced was recovered in a Plexiglass
plastic settler placed after the bed. After filtration
through a sintered glass disc, the continuous phase was pu-
mped to a storage tank using a glass centrifugal pump.
Sample points and valves were provided where necessary.

5.3 COALESCER DESIGN

The coalescer column was a 3-inch bore and 20 inch
length QVF glass section which allowed for different
bed depths to be tested. Two pressure transducers and
two connections to a manometer were provided on one
side of the section, Fig. 5.5.

The coalescer holders were of polypropylene,
supplied by G.H. Bloore Ltd., (97), and were manufactured
of different heights to hold the various fibrous beds.
They were made to fit the 3-inch diameter QVF section.
Two stainless steel supporters and p.t.f.e. rings
were used to hold the coalescer holders one of which is
shown in Fig. 5.6.

5.4. SELECTION OF FIBROUS PACKING AND PREPARATION

Coalescence of secondary dispersions using fibrous
beds has been studied by many investigators (4, 12, 17,
51, 59, 98, 99). Glass is favoured as a raw material
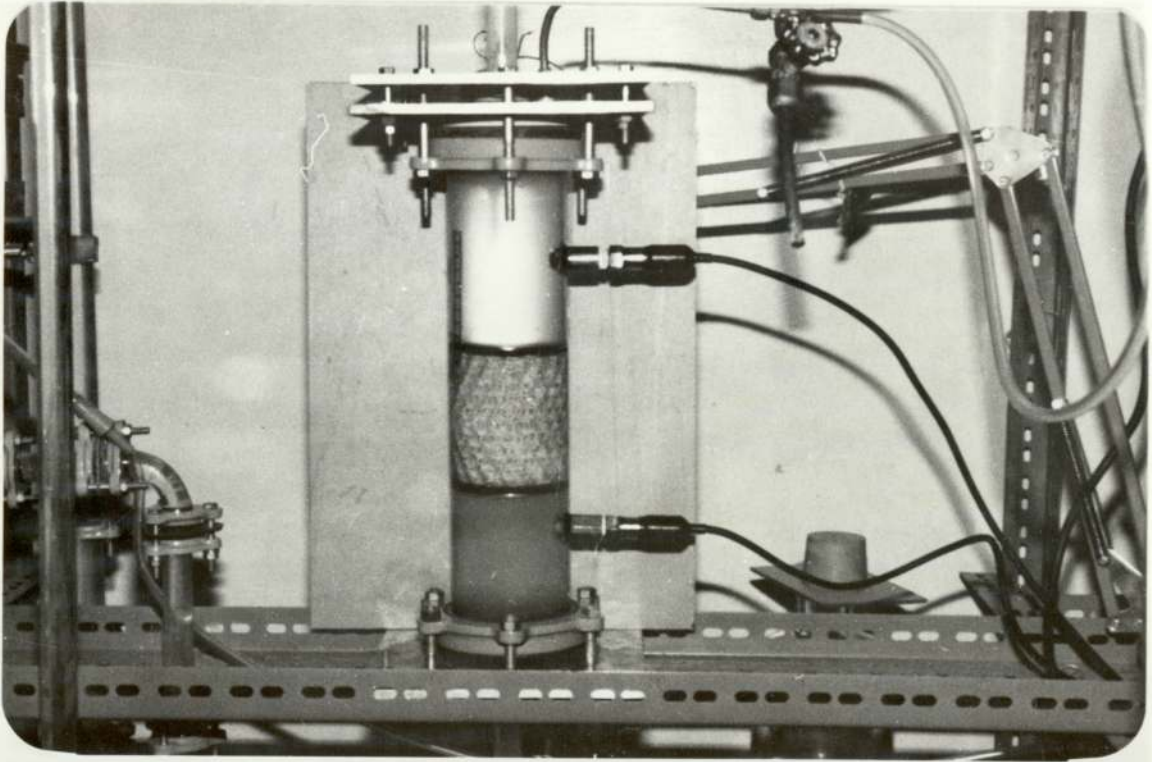
FIGURE **5.5** PRESSURE DROP MEASUREMENT
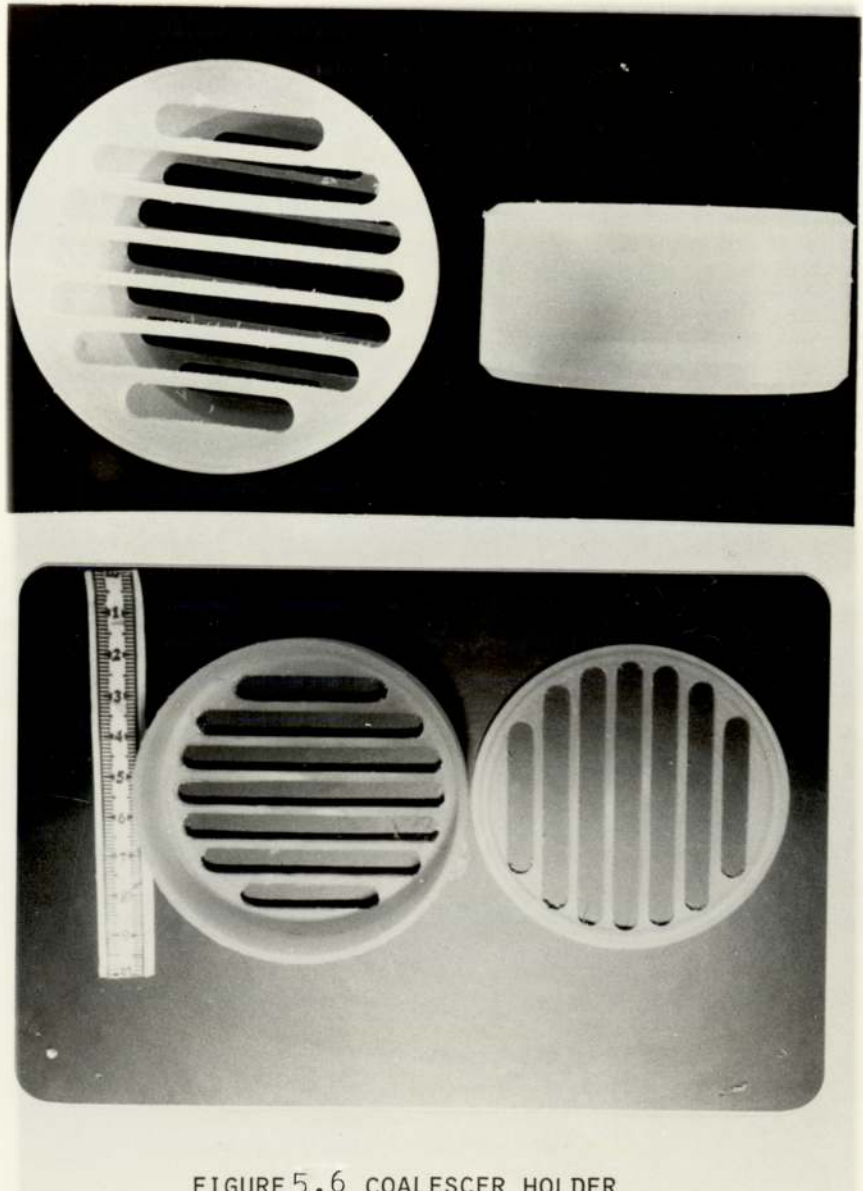
FIGURE 5.6 COALESCER HOLDER

for these fibrous beds, because it is relatively inexpe-
nsive, is resistant to the extreme thermal and chemical
environment commonly used in cleaning procedures, and
its wetting properties may be modified by the attachment
of silicon groups to the surface of the fibres (100).

Simple compression of a quantity of fibrous
material to the required voidage fraction produces
an acceptable structure, but frequently the glass fibres
used have a distribution of diameters and the above pack-
ing technique produces a bed with a pore size distribu-
tion and where the fibre orientations are unknown. This
lack of an accurate geometrical description of the bed
has sometimes favoured investigations where the coalescer
packing consisted of layers of fine woven meshes, where
the fibre diameter and mesh apertures were constant,
the fibre orientation known and different packing
characteristics could be expressed mathematically in
terms of these known factors.

Fibrous media, can be made to have both a higher
porosity and a higher specific surface than granular media,
and have been observed to give more complete phase
separation for the same bed depth and operating conditions.
Hence fibrous media appear more attractive from the stand-
point of space requirements.

Different types of fibrous material were tested
to observe their performance in coalescence experiments.
Table 5.1 lists the Specifications of these materials
which are illustrated in Fig. 5.7. Microscopic examina-
tion of the fibres confirmed that the relevant dimensions
were both consistent and accurate to the manufacturers'
specifications. Inspection of the nature of the fibre
surfaces using Stereoscan electron-micro photography
for several types, as shown in Fig. 5.8 with magnifica-
tions in the range 500 to 25 times, revealed the smooth-
ness and regular arrangement of the fibres for all
materials. A quantitative analysis of surface roughness
was not attempted.

Circular pieces of fibrous material, 70 mm in
diameter were prepared from the supplied sheets using
a specially-designed punch which was manufactured from
high carbon steel. Only the glass wool/stainless steel
packing material was used as a layer of 0.1 m height.

Due to accumulation of small quantities of foreign
material after long operating periods, new packing
material was employed for each run.

5.5. LIQUID SYSTEM DESCRIPTION

The equipment was designed for coalescence of
secondary dispersions of an organic liquid dispersed

Type No	Material	Supplier	Fibre diam. Micron	Weight gm/m^2
1	Hyperfine untreated glass fibre	Knit-Mesh Ltd., U.K	6	150
2	Needlemat Type M (A)	Woven Glass products, ltd., U.K.	11	600
3	Needlemat Type M (B)	"	16	1030
4	Random loose glass fibre	Local market Kuwait	18	135
5	Plain cloths Type TG11	Scandura ltd., U.K	9	950
6	Disks of Polyester fibre	Knit-Mesh ltd., U.K.	25	250

Table 5.1 Specifications of the types of fibrous materials

used

FIG 5.7 TOP-VIEW OF FIBROUS MATERIALS USED
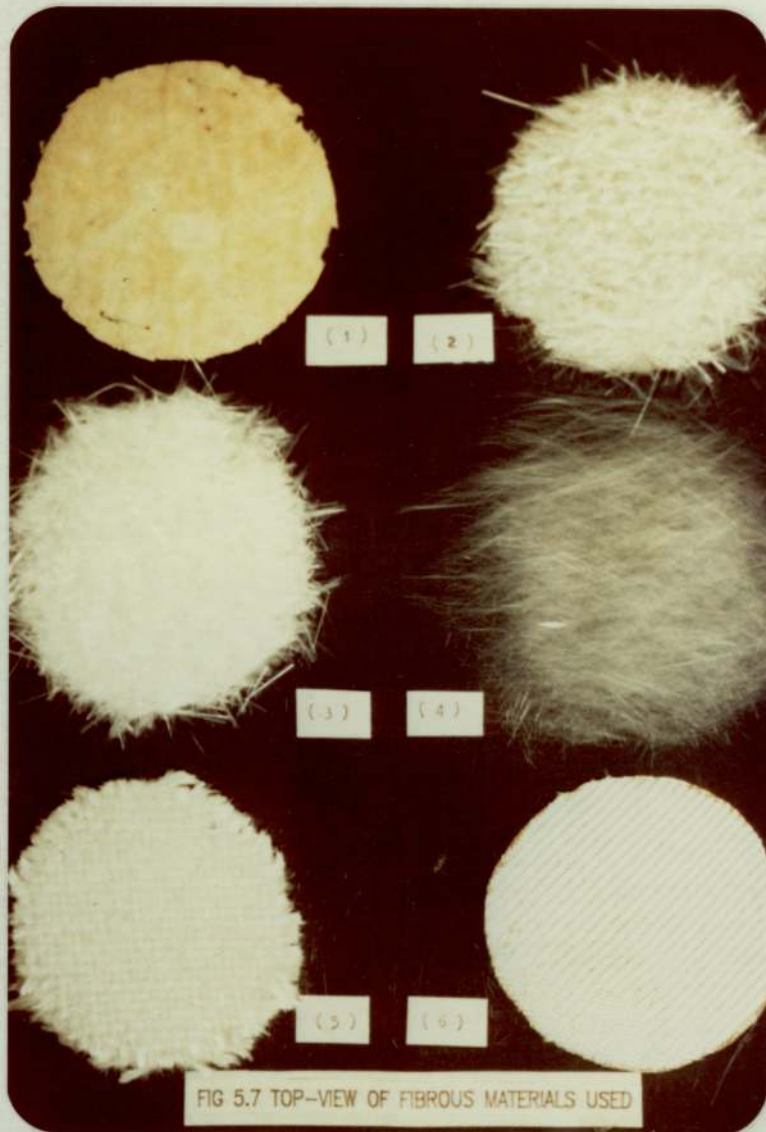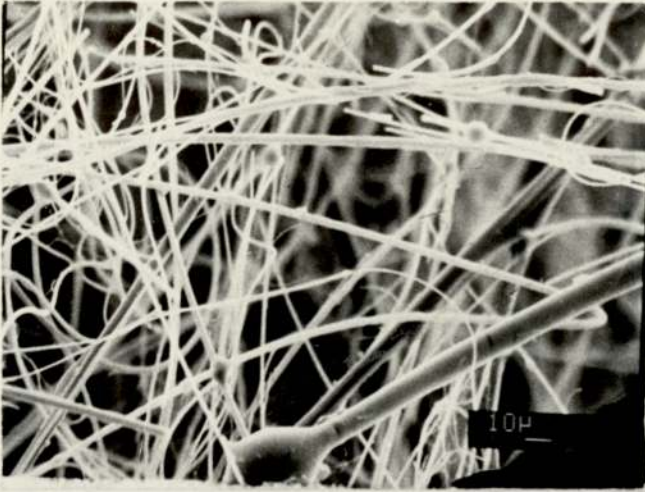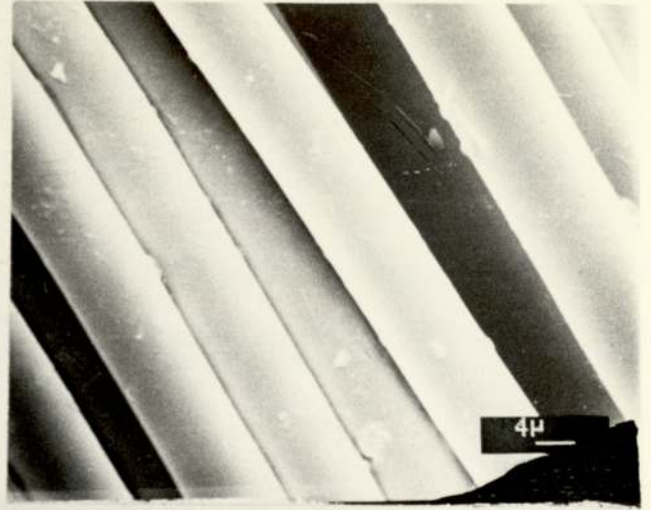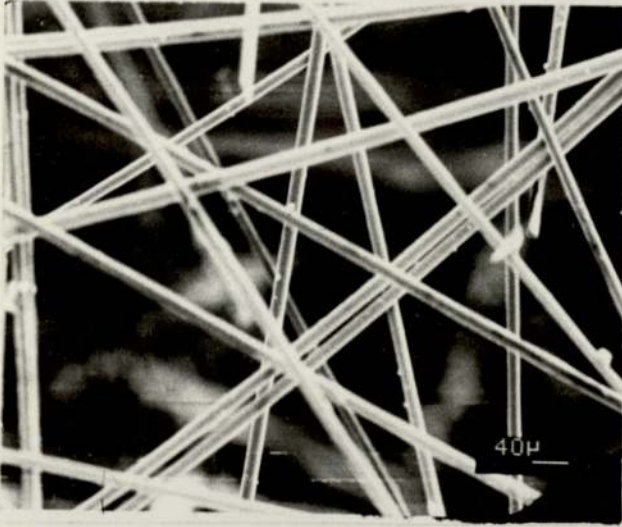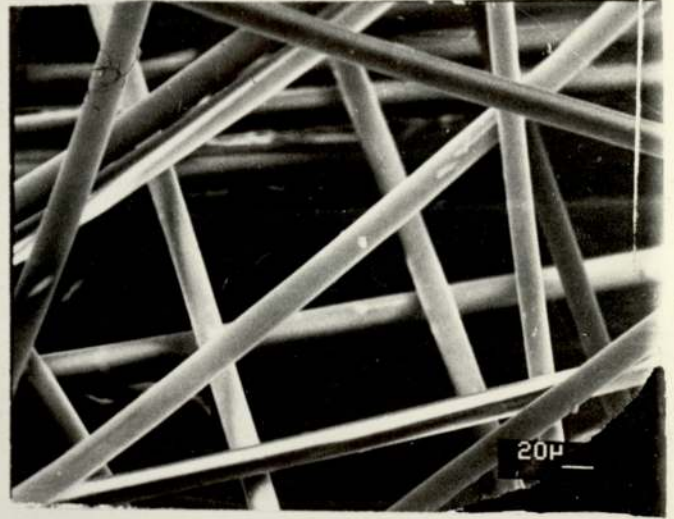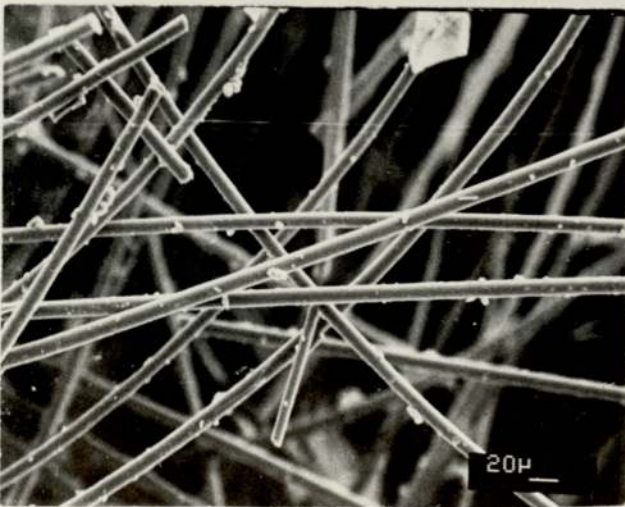
FIG. 5.8 STEREOSCAN PHOTOGRAPHS OF
FIBROUS MATERIALS

in distilled water. In this study, toluene was selected
as the dispersed phase since it is relatively non-toxic,
non-corrosive and inexpensive. Analar grade toluene was
distilled to within $\pm 1^{\circ}$K of its boiling point and
stored in clean, dark glass bottles to prevent exposure
to sun light which has been reported to cause degradation
(101).

Any effects due to the mutual solubility of the
dispersed phase and water were minimized by allowing
the two phases to attain mutual saturation by contact
for over 24 hours before use. The properties of the
dispersed phase are given in Appendix A.

The temperature was controlled at 20°C through
out each run. The continuous phase rotameters were
calibrated experimentally at 20°C and the calibration
curve is given in Appendix C.

5.6 PRESSURE DROP MEASUREMENT

The pressure drop across the bed was measured by
two methods. A 'U-tube' manometer, filled with mercury,
was used to indicate the pressure drop across the
coalescer. It was connected in parallel to pressure
taps upstream and downstream of the coalescer by tubes
containing distilled water.

The second method involved the use of pressure transducers as shown in Fig. 5.9. The output voltage was selected via a switch and read from a digital voltmeter.

The two methods are used to check the pressure drop for either single phase or two phase flows.

5.7. CLEANING PROCEDURE

Before each set of experiments the equipment was thoroughly cleaned by flushing with distilled water. A solution of 2% Decon 90 in distilled water was then allowed to recirculate through the equipment. This solution was left inside the equipment for 24 hours. The next step was to flush the equipment again with distilled water several times to remove any residual surface-active compounds. It was then drained and fresh distilled water was introduced.

5.8. OPERATING PROCEDUCE

The first step in the operating procedure was to recirculate continuous phase at a high velocity, e.g. 3.5×10^{-2} m/s, for 30 minutes to remove any air trapped in the coalescer. The continuous phase flow rate was then regulated incrementally and single phase pressure drop across the bed was recorded.
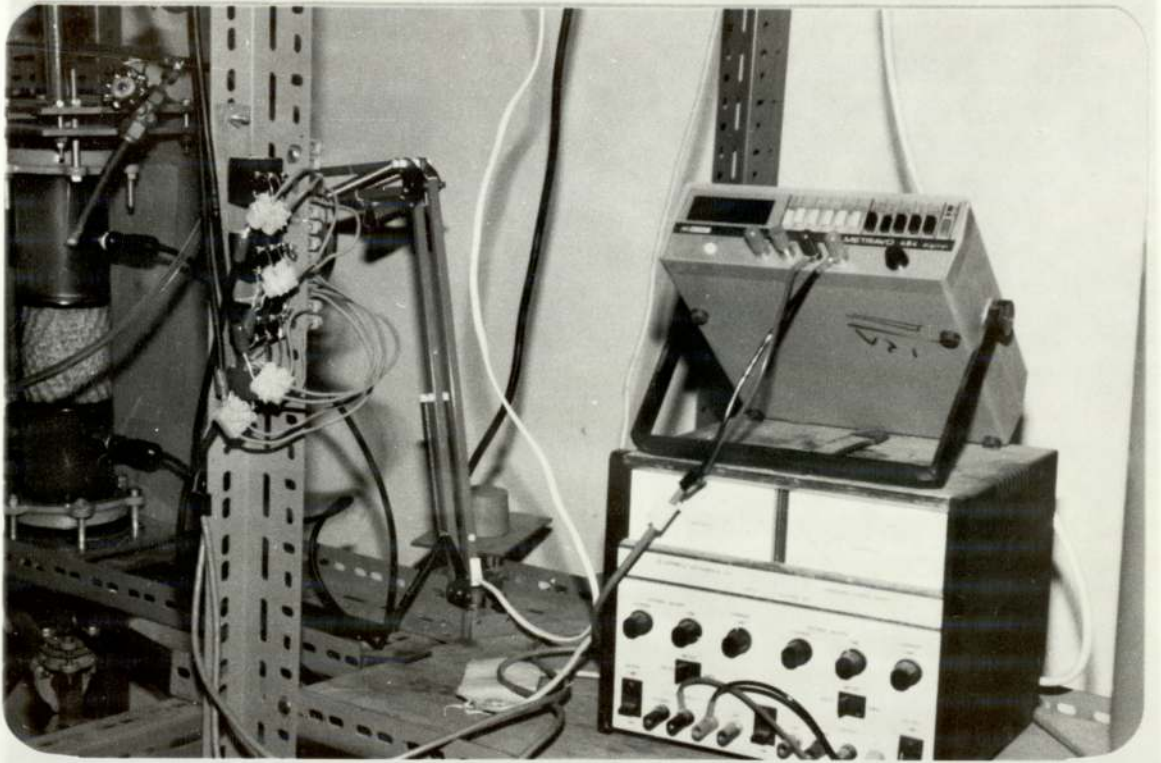
FIGURE 5.9 PRESSURE TRANSDUCERS ARRANGEMENT

The flow was then regulated to the desired value
and the dispersed phase flow was metered at a rate
sufficient to give the desired phase ratio in the range
200 to 1000 ppm. The mixture passed into the emulsifi-
cation loop through the centrifugal pump. After the
appearance of a milky haze in the loop, characteristic
of a secondary dispersion, pressure drop data were
recorded at regular intervals. Steady-state was deduced to
have been achieved when pressure drop remained constant.
Both the continuous and dispersed phase flow rates were
then varied to give the same phase ratio at a combination
of different velocities and, when steady-state had been
re-established, new data were collected.

Samples were taken at the inlet and outlet positions
of the glass section. Oil content of these samples
was measured using a HORIBA OIL ANALYZER. The particle
size distribution of the inlet stream, containing very
fine dispersed phase drops, was measured by COULTER
COUNTER MODEL TA II. The outlet stream from the coale-
scer, containing relatively large drops, was photographed
and the drop size determined using an OPTON SIZE ANALYZER.

5.9. EXPERIMENTAL DESIGN

The factors which affect the coalescence process
may be classified into 4 main categories:

A)   System parameters:

    1. oil/water or water/oil dispersion

    2. interfacial tension

    3. densities of dispersed and continuous
       phases.

    4. viscosities of dispersed and continuous
       phases.

    5. mutual solubility

B)   Fibrous bed parameters:

    1. fibre diameter

    2. aperture diameter

    3. bed arrangement/material

    4. bed voidage

    5. bed thickness

C)   Measured parameters:

    1. single-phase and two-phase pressure drop

    2. coalesced drop size

    3. effluent drop size

    4. time to steady state

    5. mechanism of coalescence

    6. filter coefficient

    7. separation efficiency

    8. exit oil concentration

D.   Operating parameters:

1. velocity

2. phase ratio

3. inlet drop size distribution

In view of the complex interactions between the
operating parameters listed above, it was necessary to
design experiments carefully. The scope of this rese-
arch was to compare different types of fibrous materials
under different operating conditions. It was concluded
from the preliminary experiments and previous workers
(1, 14) that decreasing the fibre size increased the
pressure drop, decreased the exit drop size and lowered
the superficial velocity at which drop redispersion
occurred. A set of experiments was devised whereby ch-
anges in fibre size, bed depth, superficial velocity
and dispersed phase concentration were measured as
changes in the pressure drop, exit drop size, effluent
drop size and separation efficiency. The experimental
program is presented in Table 5.2.

Velocity $U \times 10^{-3}$ m/s	Bed Height, $\times 10^{-2}$ m		
	2.4	4	6
1.5	6 9	6 9 25	6
3.0	6 9	6 9 25	6
6.5	6 9	6 9 25	6
10	6 9	6 9 25	6
13	6 9	6 9 25	6

Table 5.2 Experimental Design

The numbers in the grid refer to the fibre sizes used(μm).

All experiments were carried out for dispersed phase

concentrations in the range : 200-1000 ppm.

CHAPTER 6

DETERMINATION OF DROP SIZE

DISTRIBUTION

CHAPTER SIX

DETERMINATION OF DROP SIZE DISTRIBUTION

6.1. INTRODUCTION

The secondary dispersion produced in this study, by
the use of a centrifugal pump, was a polydispersion which
is a desirable feature. To characterize this dispersion,
a knowledge of the drop size distribution and the mean
drop size was necessary. Furthermore since the capture
efficiency of drops flowing through a fibrous bed depends
upon their diameters, and as the mechanisms of coalescence
were being investigated, the sole use of a mean drop diameter
could have been misleading.

not in research but in practical

The dispersion produced was analysed at regular inte-
rvals during an experiment to ascertain the drop size
distribution and to check that the feed to the coalescer
was consistent. Coalesced drops were also monitored to
measure coalescence efficiency. Preliminary experiments
revealed that operation at velocities greater than 2×10^{-2}
m/s caused break through of the secondary dispersion
which flowed from the exit face of the bed cocurrently
with the primary dispersion produced by coalescence.

Different methods have been proposed to analyse
the drop diameter, including

a) Optical methods such as microscopy,

   using manual or automatic scanning (65).

b) Light reflectance (66).

c) Light Scattering (67).

d) Ultrasonics (68).

e) The Coulter-Counter (71).

f) Lasers (69) to produce holograms (1)

   or direct measurements (70).

g) Photography.

6.2. MICROSCOPY

This technique involves diluting the sample in the
well of a glass slide and examining it under the microscope.
The various size ranges are then determined by matching
against a calibrated graticule situated in the eye piece
of the microscope. This is efficient in the range 0.25 μm
to 20 μm . The lower limit is imposed by the resolving
power of the microscope; the upper limit is determined
by the diameter of the drop in relation to the depth
of field of the optical system. Also long periods may
result in settling of the drops or loss by evaporation
and it is recommended that 300 drops should be counted
per sample to obtain statistically valid results for
a polydispersion (72). This method was clearly unsuitable
for frequent sampling of the inlet dispersion.

6.3. LIGHT REFLECTANCE

This technique uses a linear relationship between the reflectance of a coloured emulsion and droplet size data determined microscopically (66); the droplet size range is from 1 μm to 30 μm . This technique gives only an average particle size and special equipment is required (73, 74, 75).

6.4. LIGHT SCATTERING

This technique, first described by Tyndall in 1871, involves passing a coherent beam of light through the emulsion and measuring the intensity of the scattered light as a function of the scattering angle from the direction of the incident beam. If the emulsion is sufficiently dilute, the total scattered light is simply the sum of light scattered from individual drops. The light scattered from a drop depends on the area intercepting the beam, and thus on the square of the effective radius of the drop.

Light scattering can be divided into three classes dependent upon the size of the droplet relative to the wave length of the incident light and its refractive index to that of the continuum (67): Rayleigh scattering, Debye scattering and Mie scattering.

This technique depends upon a complex theory of light
scattering and is only valid for monodispersed systems
or for determining an average drop size for a narrow dis-
tribution.

6.5. ULTRASONICS

This technique depends upon the difference in ela-
stic properties between the continuous and dispersed liquid
phases and upon the consequent difference in the velocities
of transmission of longitudinal acoustic waves (76).
The composition of the mixture can be deduced by measuring
the acoustic velocity of the mixture provided the acoustic
velocity can be measured by finding the wave length at
a fixed frequency. A variance in composition dependent upon
the sizes of the droplets of the dispersed liquid is
obtained when drops of dispersed liquid enter and leave
the sample volume. Measurement of this composition variance
allows the average drop volume to be calculated. Further
details of this technique are to be found in Attarzadeh's
Dissertation (68).

6.6. THE COULTER COUNTER

The Coulter Counter Model TA II is a sixteen channel
particle size analyzer which employs the basic Coulter
patented principle for its operation (71).

Shalhoub (43) concluded that use of a Coulter Counter

is preferable for the analysis of secondary dispersions
since it produces reliable results in a short time.
The instrument was used by many previous workers (1, 14,
15, 16, 43).

The Coulter Counter determines the number and size
of particles suspended in an electrically conductive
liquid. This is done by forcing the suspension to flow
through a small aperture having an immersed electrode
on either side. As a particle passes through the aperture,
it changes the resistance between the electrodes. This
produces a voltage pulse of short duration having a
magnitude proportional to particle size. The series of
pulses is then electronically scaled and counted. The
voltage pulses are amplified and fed to a threshold circuit
having an adjustable threshold level. If this level is
reached or exceeded by a pulse, the pulse is counted.
The threshold level is indicated on an oscilloscope screen
by a brightening of the pulse segments above the threshold
,facilitating the selection of appropriate counting levels.

By taking a series of counts at selected threshold
levels, data are obtained directly for plotting cumulative
frequency (larger than stated size) versus particle size.
Integration of all, or part of, the resultant curve
provides a measure of the particle content of the suspension.
The principle does not permit significant discretion of
particle shape, and results are expressed in spherical
equivalents. This proves to be valid, as sufficiently high

numbers of particles are counted to assure an averaging
of orientations of particles traversing the aperture.
Fig. 6.1 is a schematic diagram illustrating the Coulter
principle.

In this study, a sample of the dispersion was taken,
stabilized with a surfactant (Hyamine 2389), and diluted
in an electrolyte (0.9 % w/w sodium chloride). The sample
was then withdrawn through an aperture whose diameter
was accurately known and which was positioned between two
electrodes.

The sized particle pulses were routed to:

1) The digital address card, which produces
   digital identification signals that are
   routed to the Population Accessory to increment
   one of 16 counters. The count is then made
   available to the TA II for display, plotting
   and printing.

2) Their respective integrators where they are
   converted to a voltage representative of the
   volume of particles in each of the sixteen size
   ranges.

From plotting the cumulative frequency against
drop size, a mean drop size is obtained. This
is shown in Fig. 6.2 which is a cumulative plot
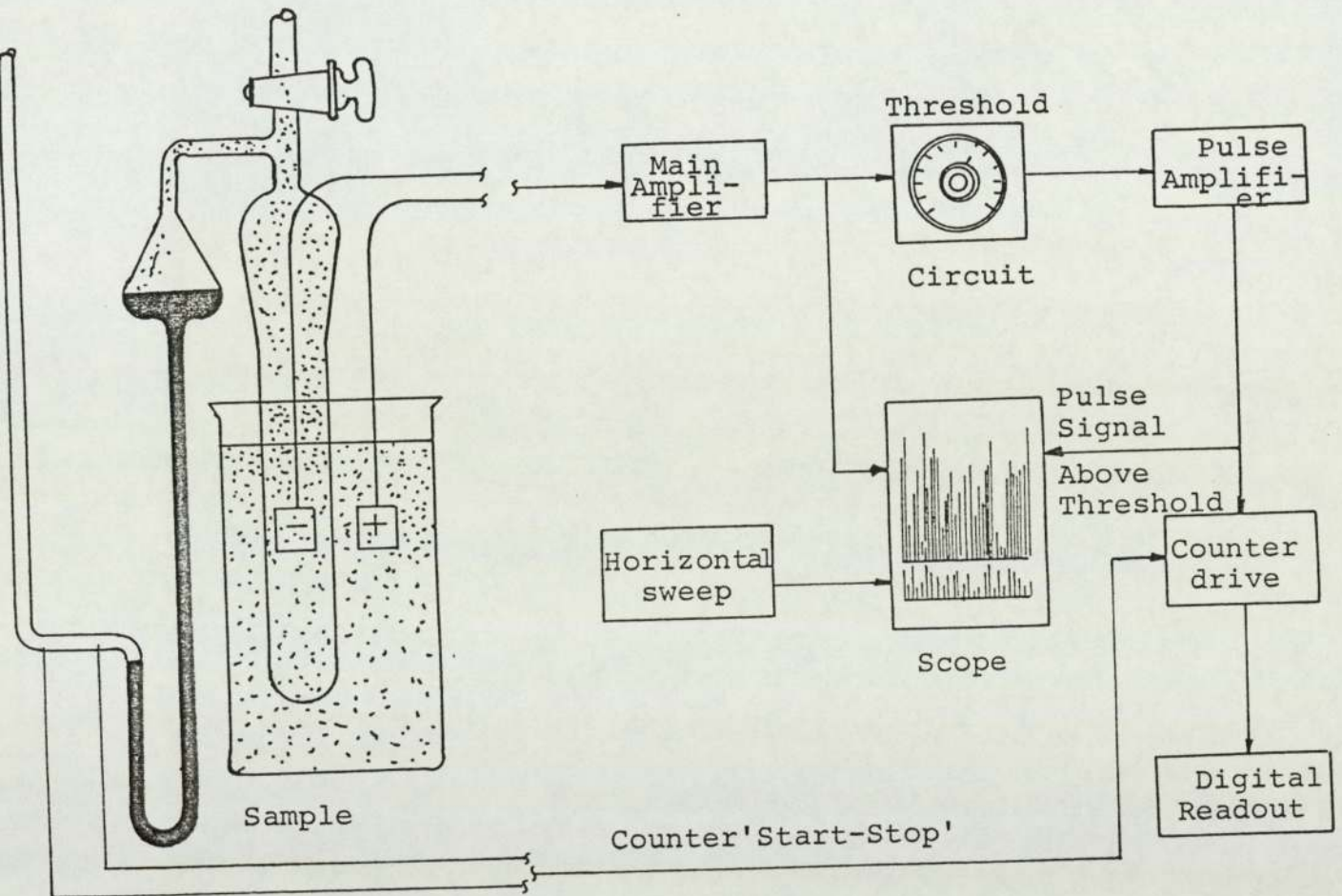
Fig. 6.1   Schematic Diagram of Coulter Principle
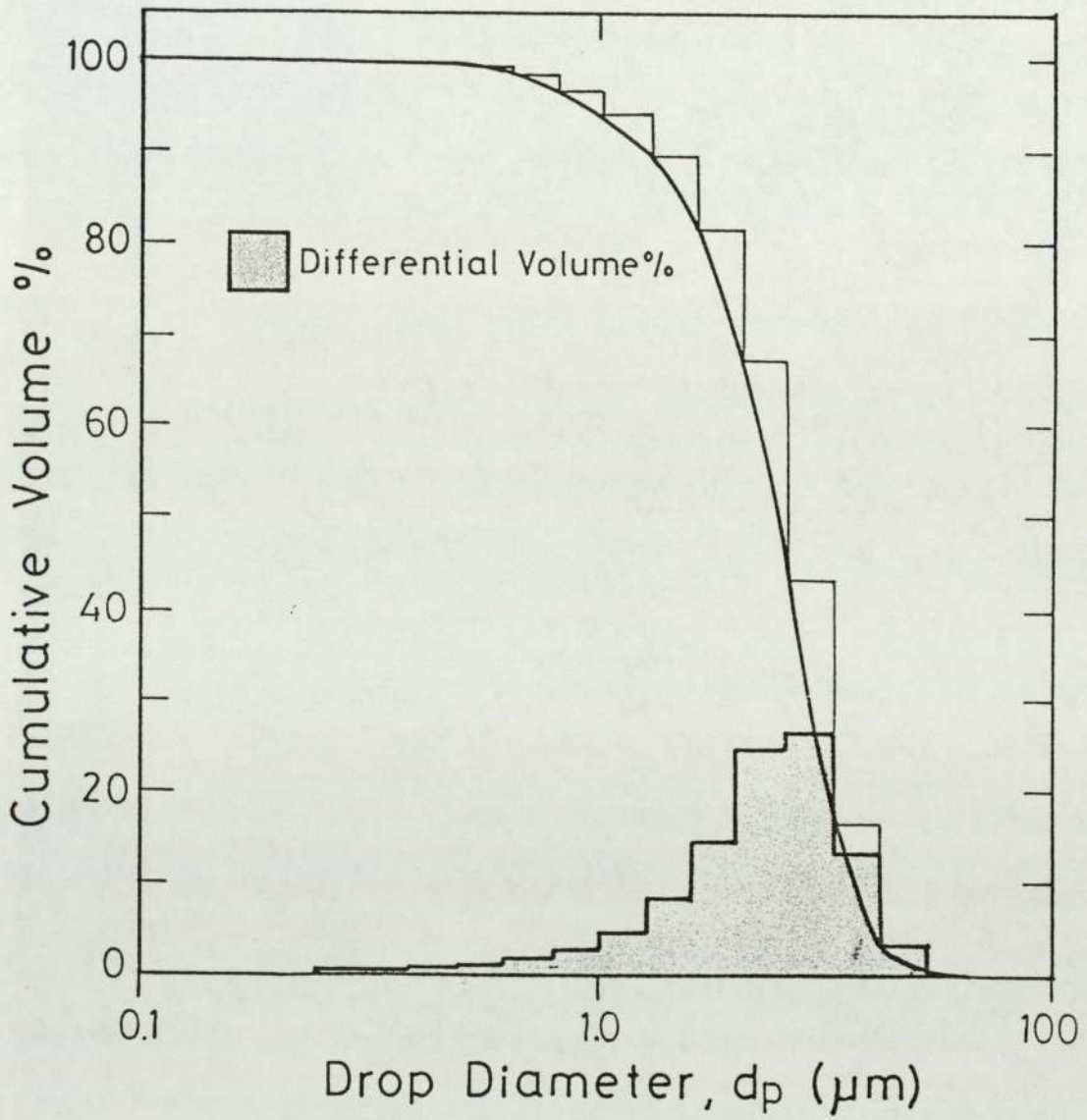
Fig. 6.2(a)   Inlet Drop Size Distribution (Log-Linear)
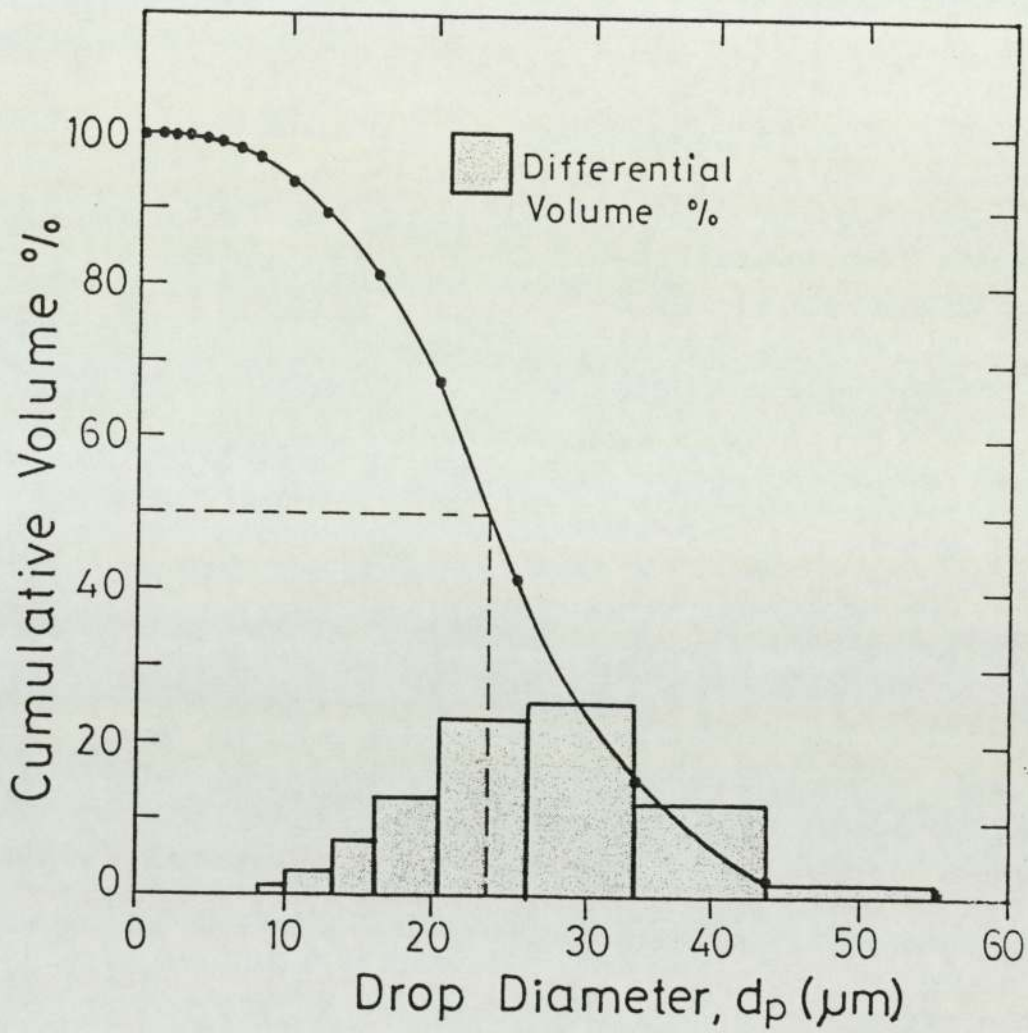
Fig. 6.2(b)   Inlet drop Size Distribution ($d_{50\%} = 23.5\,\mu m$)

(LOG-LINEAR) from the recorder. Apart from this
standard plot of linear percent weight/log diameter
there are other forms which may be useful when
manually plotted. Including:

- Logarithmic probability
- Linear probability
-Rosin-Rammler
- Double linear

The instrument must be calibrated for each orifice
tube and electrolyte combination prior to use.

Calibration is ideally performed using smooth
particles of constant, known density or using 'monosized'
particles supplied by Coulter Electronics Ltd. Most
effective calibration results when the particle size
is between 5 % and 20% of the aperture diameter of the
orifice tube selected.

The size range over which the instrument may
operate is from approximately 2% to 40% of the aperture
diameter, but there is a measurable non-linearity above
20% since the equations that describe the aperture
response do not actually predict a truly linear response
(81). For a 140 μm aperture tube, the working range is
between 2.8 μm and 56 μm.

6.7. LASER TECHNIQUES

This is an alternative method to size secondary dispersions. A laser beam may be used either to produce holograms or directly to measure the drop size through the Malvern particle sizer (14, 15). More details about these techniques can be found in literature (77,78,79,80).

6.7.1 Malvern Particle Sizer

The Malvern Particle Sizer (70) measures particle size distributions in the range of 1 to 100 microns. It uses the principle of 'Fraunhofer Diffraction' from the drops as means of measurement. A low power visible laser transmitter produces a parallel, monochromatic beam of light which is arranged to illuminate the particles by use of an appropriate sample cell. The incident light is diffracted by the droplets illuminated to give a stationary diffraction pattern regardless of droplet mo-vement. As drops enter and leave the illuminated area the diffraction pattern "evolves" always reflecting the instantaneous size distribution in this area. Thus by integration over a suitable period and a continuous flux of droplets through the illuminated area, a repre-sentative bulk sample of the droplets may contribute to the final measured diffraction pattern.

A Fourier transform lens focusses the diffraction
pattern on to a multi-element photo-electric detector
which produces an analogue signal proportional to received
light intensity. This detector is interfaced directly
to a desk top computer allowing it to read the diffraction
pattern and perform the necessary integration digitally.

Having measured a diffraction pattern the computer
uses the method of non-linear least squares analysis
to find the size distribution that gives the closest
fitting diffraction pattern. The size distribution can
be analytically generated by either the well known two
parameter models: Rosen-Rambler, Log normal or Normal.

The result of the analysis, a size distribution of
the sample by weight, may be displayed graphically on
the VDU screen of the computer or printed as a hard copy
result on a line printer.

The experimental procedure used by Poleo (14) and
Al-Meshan (15) involves loading the computer with the
analytical model processing, checking the optical align-
ment of the equipment, and taking a background reading
with the continuous phase in the sample cell. A suitable
background reading should be less than 30. If the level
exceeds 30, realignment should give an improvement.
Sources of high level of background reading are misa-

lignment and dirty or scratched optical components.
The general arrangement is shown in Fig. 6.3. Further
details on the technique and the mode of operation are
to be found in Malvern 2200 particle sizer Handbook (70).

6.8 PHOTOGRAPHY

Photography was used to analyse the effluent
primary dispersion because of its simplicity and relia-
bility. This technique was used successfully by many
workers (1, 14, 15, 16).

Photographs of the dispersion leaving the coalescer
were obtained with a Cannon A2 camera, fitted with a
50 mm micro-lens and using 100 and 400 ASA films. Shutter
speeds of less than 4×10^{-3} S were employed to eliminate
image distortions caused by drop movement. Illumination
of the dispersion from the rear was provided by 250 W
photo-flood bulb through a diffuser.

The circular pipe section, which retained the flowing
dispersion did not cause detectable distortion or magni-
fication of the drops thus eliminating the need for any
special optical arrangement. Enlargements of the
prints to 9x13 cm were found to be satisfactory with
respect to size and contrast for the counting procedure;
typical photographs are reproduced as Figures 7.12 - 14.
A metric scale was placed on the outer tube wall for
calibration purposes.

94
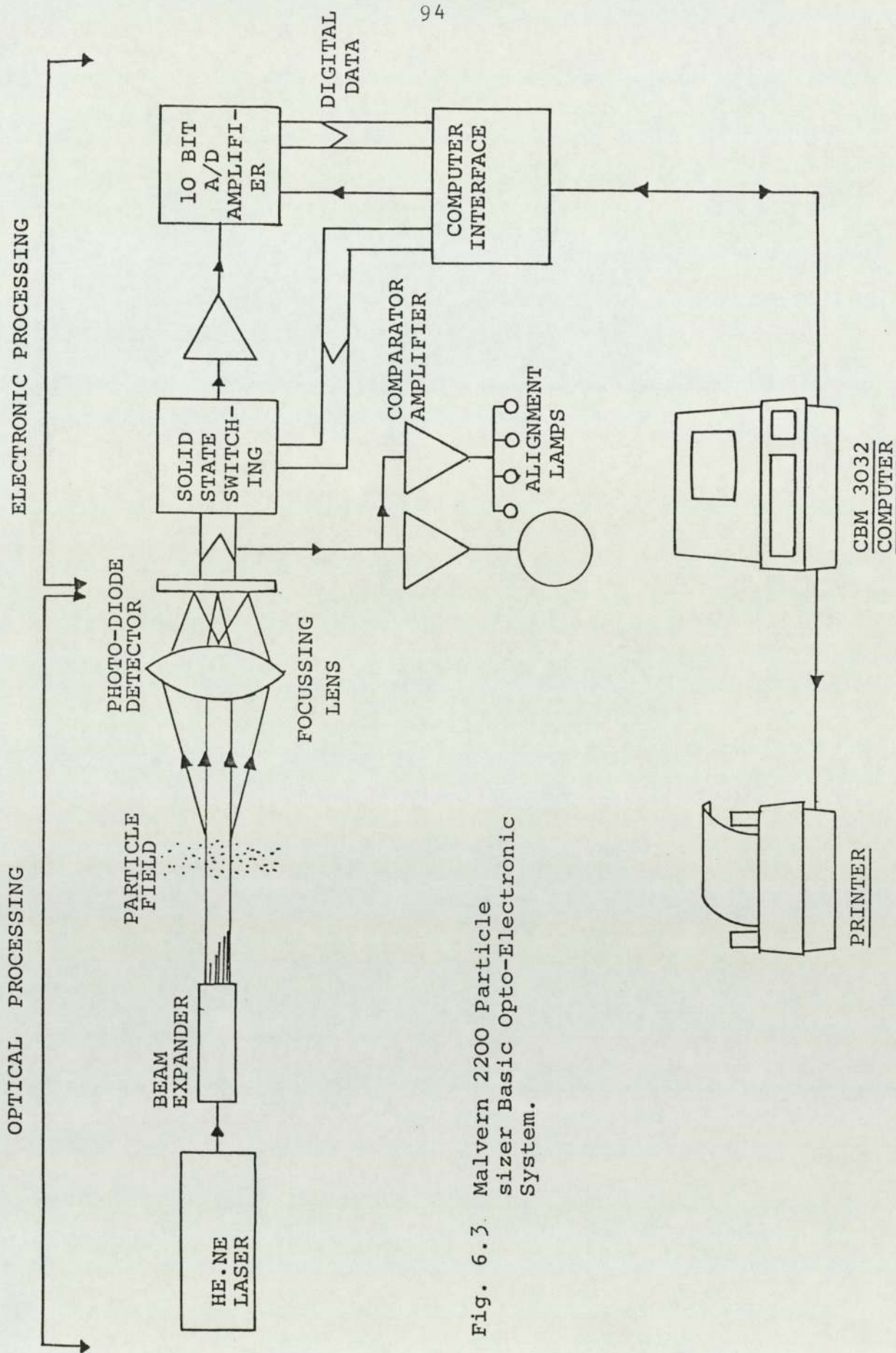
Fig. 6.3. Malvern 2200 Particle sizer Basic Opto-Electronic System.

Manual counting of the drops recorded on the pho-
tographs was accomplished by an OPTON TG-3 Particle
Sizer to identify and record linear drop dimensions,
which are the diameter and the number of drops of that
diameter. A typical size distribution is shown in
Fig. 6.4.
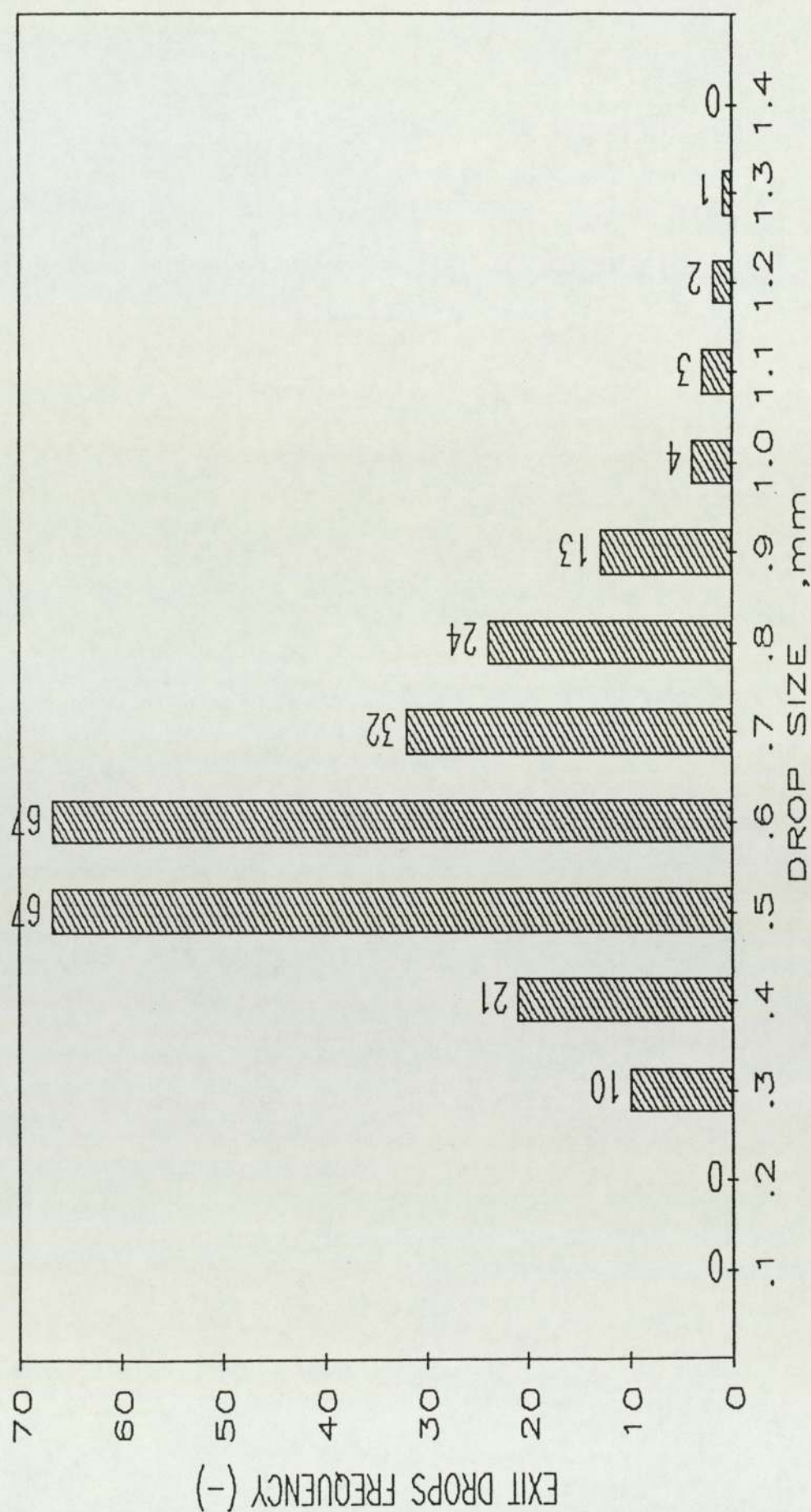
Fig. 6. 4 Exit Drop Size Distribution

CHAPTER   7

EXPERIMENTAL RESULTS

AND DISCUSSION

CHAPTER SEVEN

EXPERIMENTAL RESULTS AND DISCUSSION

7.1. INLET DROP SIZE

Previous workers on coalescence of secondary dispersi-
ons concluded that the mean drop size depends on the centr-
ifugal pump speed (1, 14, 15, 16, 42, 43). The drop break-
up has been found to occur by viscous shear in the vicinity
of the pump impeller (117). In this study the centrifugal
pump, connected to the emulsification loop, was operated
at constant speed. The inlet dispersion was analysed for
each velocity, which when increased the residence time of
the dispersion in the loop decreased. Results of the analy-
sis, presented in Fig. 7.1, indicate that mean drop size
was independent of superficial velocity above 1.5×10^{-2} m/s
but decreased at lower velocities. Fig. 7.2 shows that the
mean drop size increased with increasing phase ratio for
low velocities.

7.2. COALESCED DROP SIZE

The mean size of coalesced drops, determined as the mean
linear diameter from photography, was found to increase
with an increase in superficial velocity up to a certain limit
after which it decreased with increase of velocity. This is
shown in Fig. 7.3. This limit could correspond to a critical
velocity after which the residence time is insufficient for drops to increase
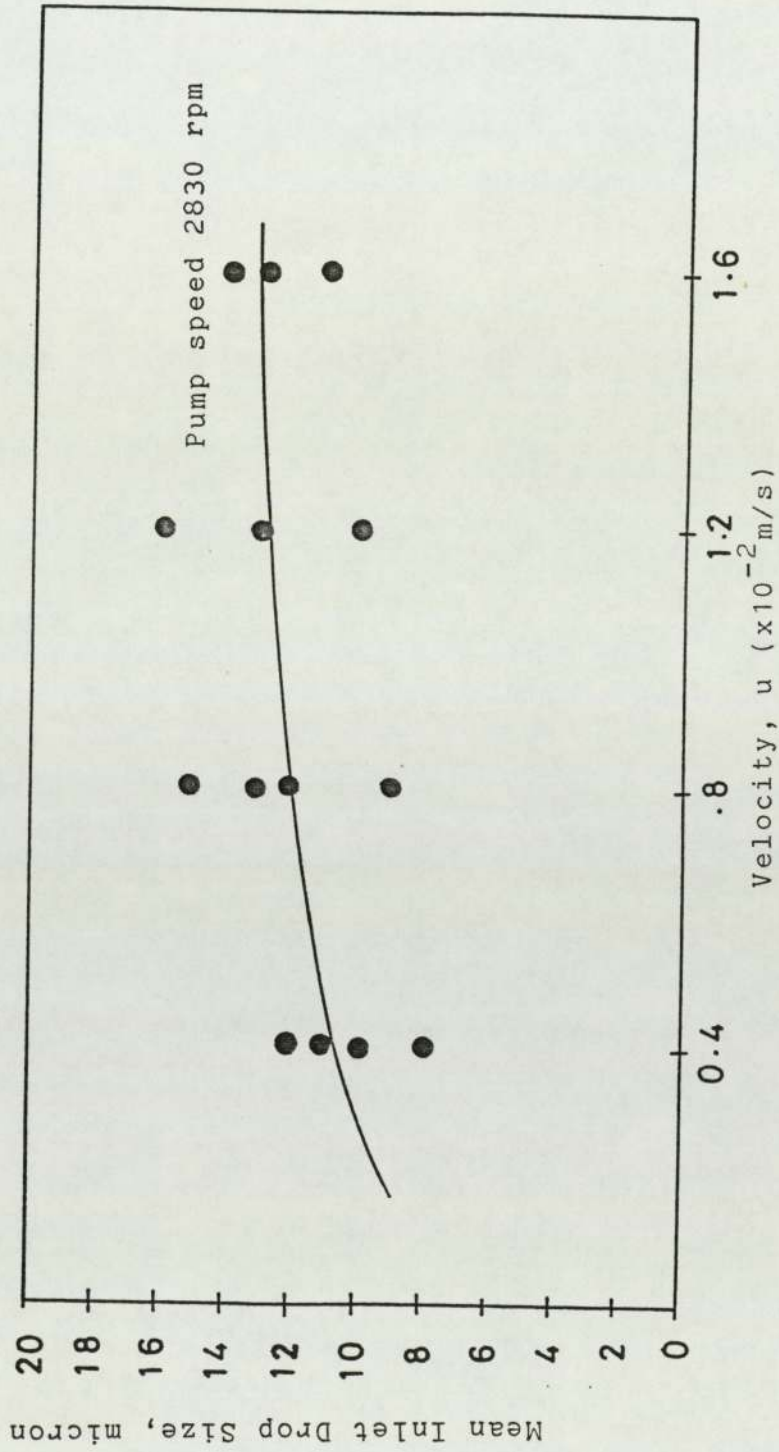
FIG. 7.1 VARIATION OF INLET DROP SIZE WITH VELOCITY FOR TOLUENE-WATER SYSTEM
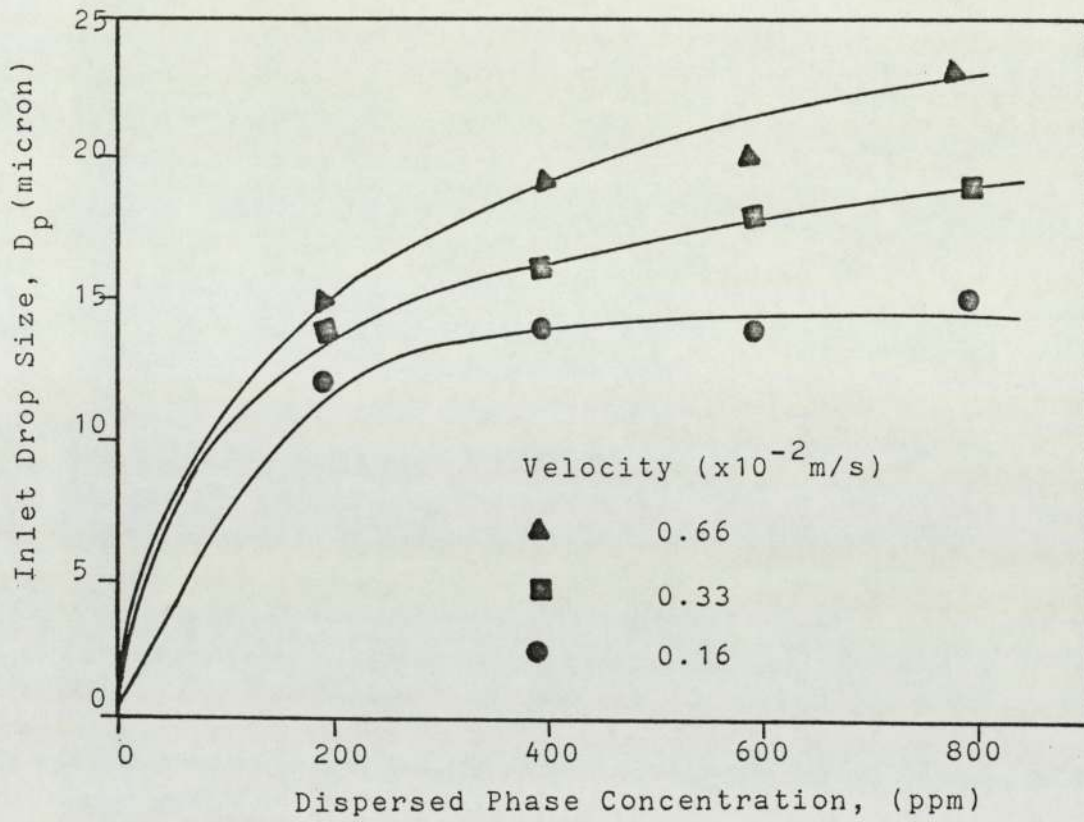
FIG. 7.2 EFFECT OF PHASE RATIO ON INLET DROP SIZE
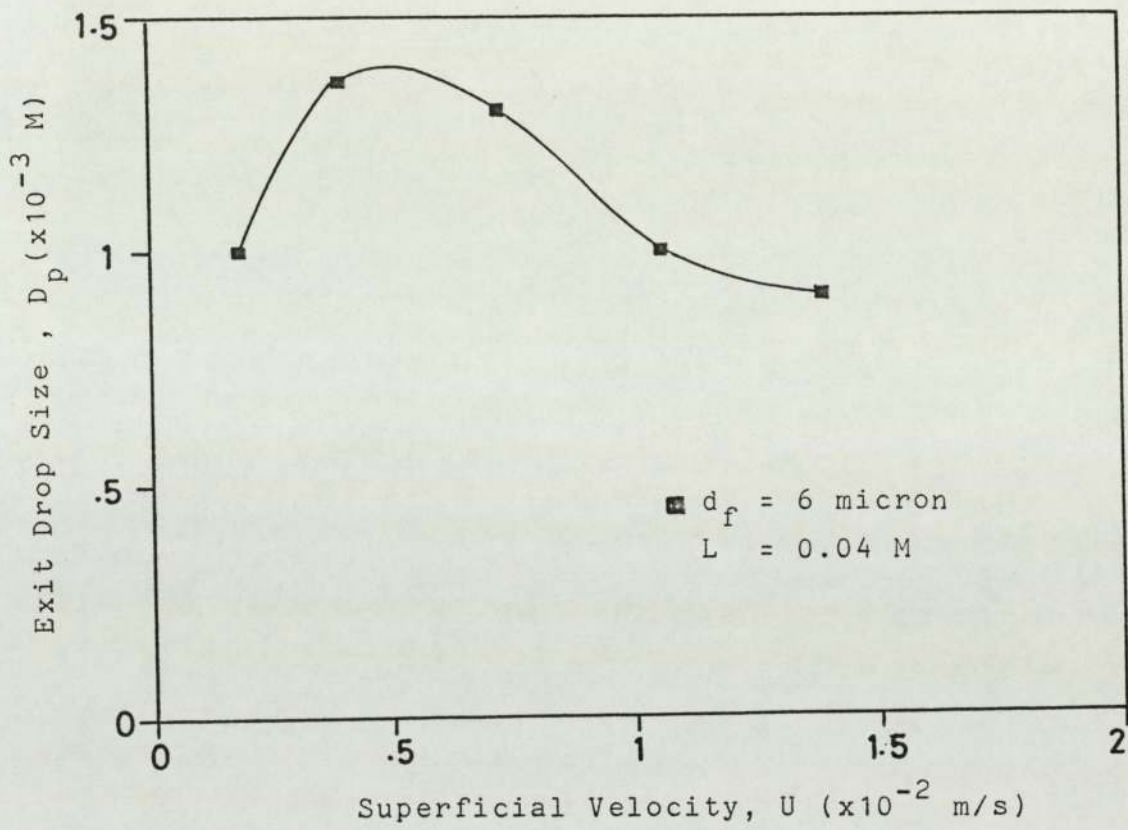
FIG. 7.3 EFFECT OF VELOCITY ON EXIT DROP SIZE

in size by re-coalescence. This velocity was approximately

0.6×10^{-2} m/s. Other workers similarly found the exit

drop size to decrease with increase of velocity (1, 12,

14, 15, 43). Austin (1) suggested that the 'critical

velocity' is associated with break-through of the secondary

haze but this phenomenon did not occur in this study

until the superficial velocity exceeded about 1.5×10^{-2} m/s

compared with 3.5×10^{-2} m/s in Austin's investigation.

7.2.1 Effect of Fibre Diameter on Coalesced Drop Size

Changes in the fibre diameter resulted in a corresp-

onding change in the exit drop size. Increasing the fibre

diameter, for any random packing, leads to an increase in

the mean void diameter which affects the exit drop size, i.e.

exit drop size would be expected to increase with increase

in fibre diameter.

Wilkinson (113) studied the effect of packing size

in the exit layer. He showed that a relationship does

exist between the packing size and exit drop size which

could be altered by simply altering the exit layer of

the packing. This is of importance in the design of

coalescers, since assuming coalescence takes place within

the packing, an increase in exit packing size will

result in an increase in separation efficiency.

This approach was tested by performing an experiment with a fibre diameter of 6 μm and recording the exit drop size. The experiment was repeated with the addition of a layer of 11 μm fibre diameter at the exit face of the coalescer. The exit drop size was found to increase by about 50% . This is shown in Fig. 7.4.

7.2.2 Effect of Phase Ratio on Coalesced Drop Size

Within the range of 200 ppm to 1000 ppm, the exit drop size was found to be independent of phase ratio. Table 7.1 illustrates the values of exit drop size at different velocities and different phase ratios. This is in total agreement with the results obtained in parallel studies (14, 16, 42, 68).

7.2.3 Exit Drop Size Distribution

The histogram representing the exit drop size distribution is given in Fig. 6.4. A computer program, given in Appexdix J (120), was used to calculate the Sauter mean diameter. The results are shown in Table 7.2, and Fig. 7.5.

7.3 SEPARATION EFFICIENCY

The separation efficiency is defined as that fraction of droplets which have coalesced inside the bed to a larger size and can therefore be separated by gravity.
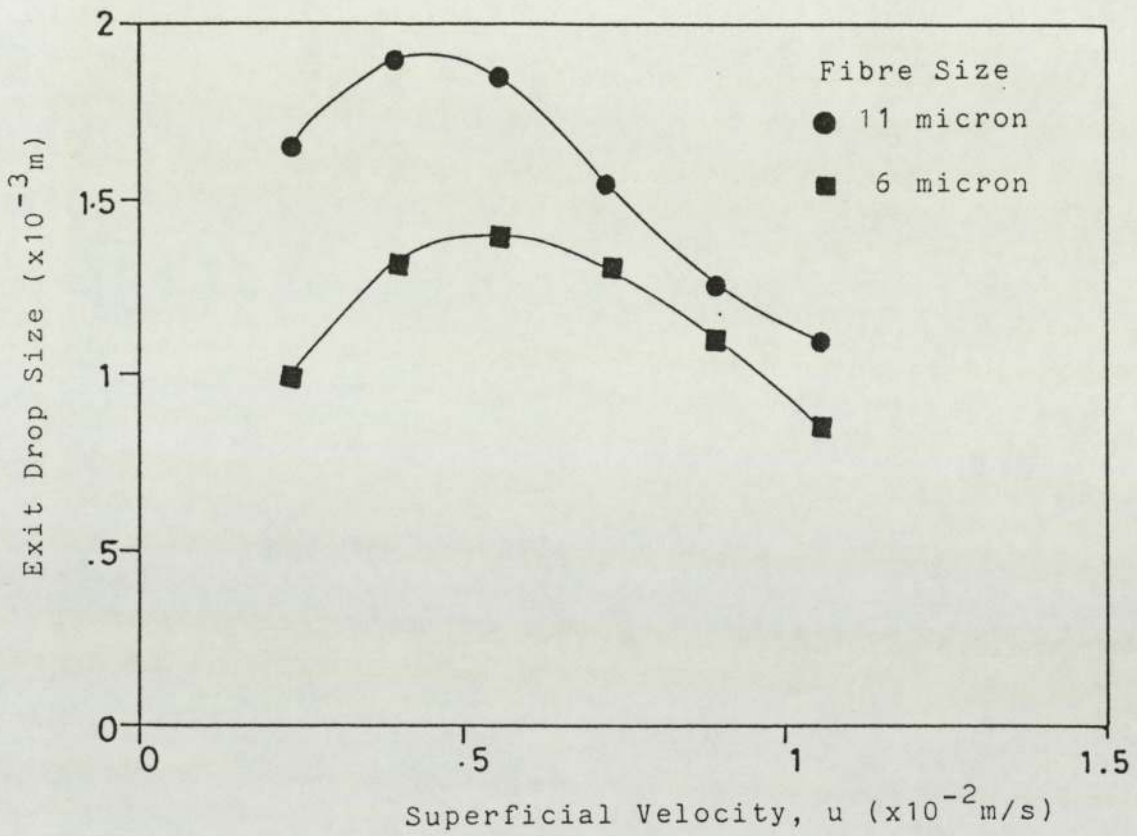
FIG. 7.4 EFFECT OF FIBRE SIZE ON EXIT DROP SIZE

Velocity x 10^{-2} m/s	Phase ratio ppm	Exit drop size x 10^{-3}m
0.166	200	1.18
0.66	200	1.32
0.166	400	0.9
0.66	400	1.14
0.166	600	2.8
0.66	600	1.96
0.166	1000	1.4
0.66	1000	1.54

Table 7.1   Effect of Phase Ratio on Exit
Drop Size for Fibre Diameter 6 μm.

```
    ***  D R O P   S I Z E   D I S T R I B U T I O N  ***


    DM              DA            F            FV              FCV
    ==              ==            =            ==              ===

    .1000           .1000         0            .0000           .0000
    .2000           .2000         0            .0000           .0000
    .3000           .3000        10            .1413           .0381
    .4000           .4000        21            .8447           .1897
    .5000           .5000        67           5.2276          1.1821
    .6000           .6000        67          12.8013          2.0427
    .7000           .7000        32          18.5454          1.5492
    .8000           .8000        24          24.9761          1.7344
    .9000           .9000        13          29.9357          1.3377
   1.0000          1.0000         4          32.0290           .5646
   1.1000          1.1000         3          34.1187           .5636
   1.2000          1.2000         2          35.9274           .4878
   1.3000          1.3000         1          37.0771           .3101
   1.4000          1.4000         0          37.0771           .0000
```

SAUTER MEAN DIAMETER =   .716   mm

Table 7.2   Exit Sauter Mean Diameter
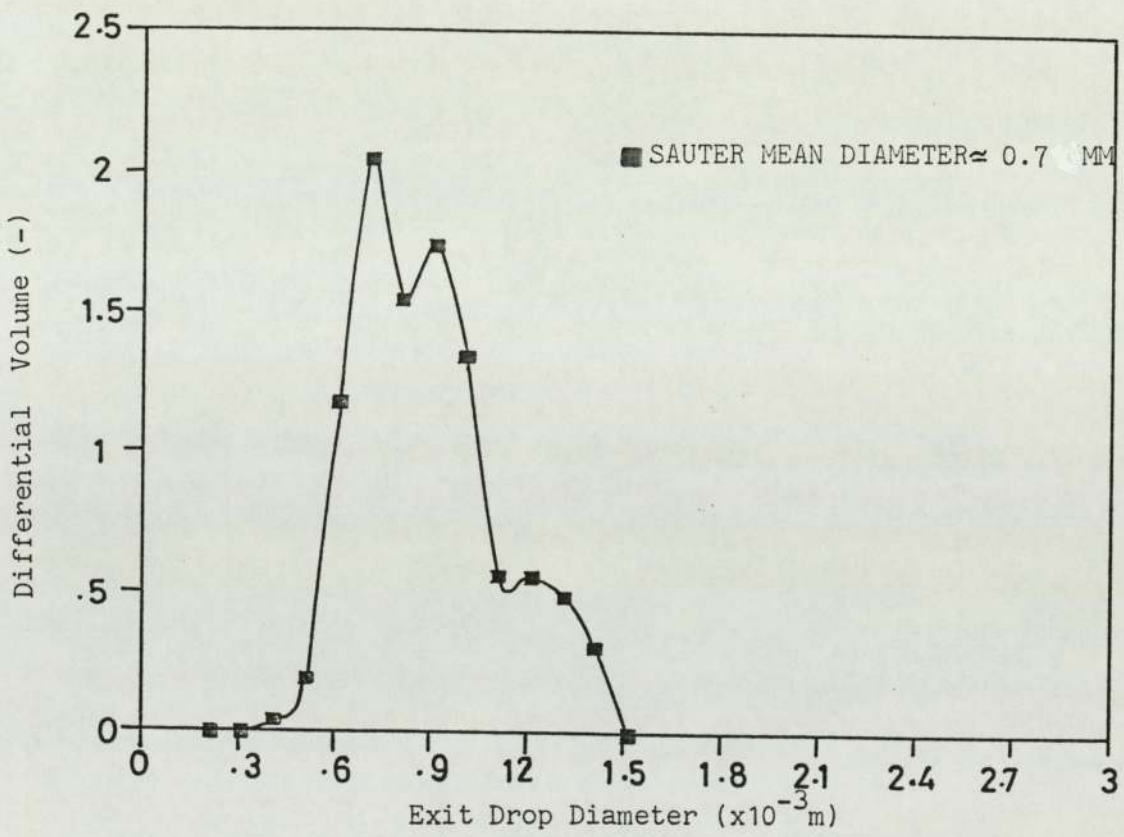
FIG. 7.5 CALCULATION OF SAUTER MEAN DIAMETER

It can be determined from a material balance over the
coalescer. Fig. 7.6 illustrates the effect of superficial
velocity on separation efficiency for different phase
ratios. The separation efficiency was high (close to
unity) at low velocities, and decreased rapidly with
increase in velocity. This is understandable since as
the velocity is increased the drag force detaches some
drops before completion of coalescence and thus reduces
the separation efficiency. As shown in Fig. 7.6, an
increase in the dispersed phase ratio increased the
separation efficiency, and decreased the time required
to achieve steady-state operation. This suggests that
as the number of inlet drops increases they fill the
interstices of the bed faster than at a lower rate
of inlet drops, thus reaching steady state faster. Also
a decrease in fibre diameter should lead to an increase
in the separation efficiency, as shown in Fig. 7.7.

7.4. EFFLUENT PHASE RATIO

It is important to determine the amount of dispersed
phase which leaves the coalescer uncoalesced, termed
entrainment or the effluent concentration. This was done
by analyzing the outlet continuous phase using a HORIBA
Oil Analyzer. The sample was left to settle for 10 minutes
before being analysed. One of the important characteristics
of the coalescer is the ability to handle wastewater
streams (dispersions) with high oil loading (high phase
ratio) without break-through, occurring. The break
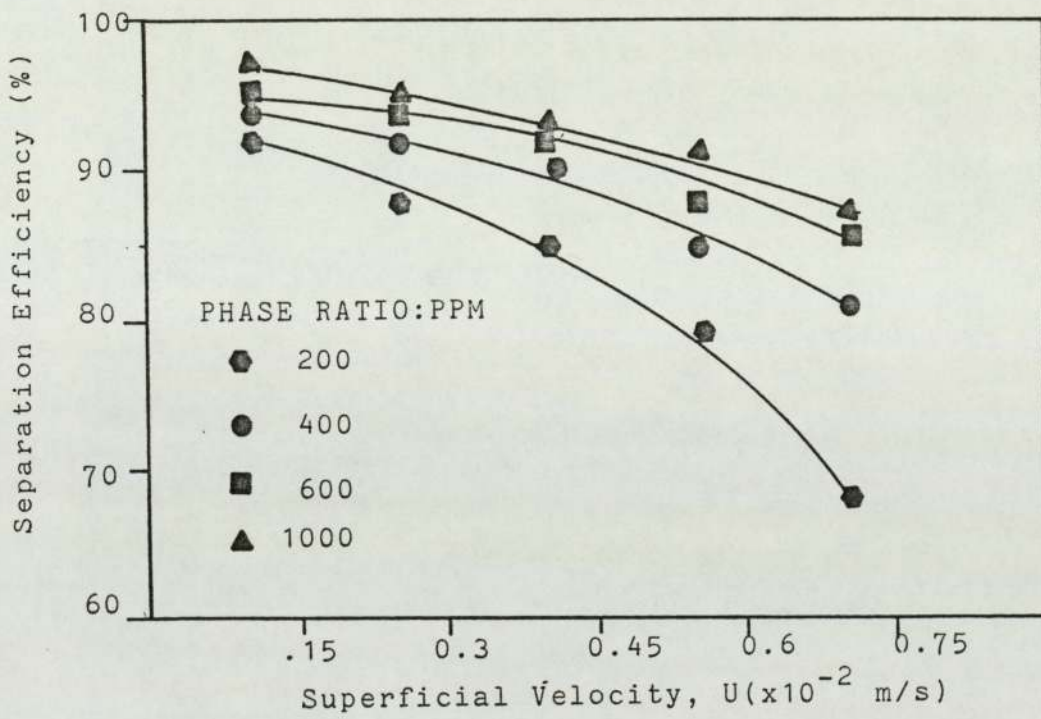
FIG. 7.6 EFFECT OF PHASE RATIO ON SEPARATION EFFICIENCY
$(L = 2.4 \times 10^{-2}$ M)
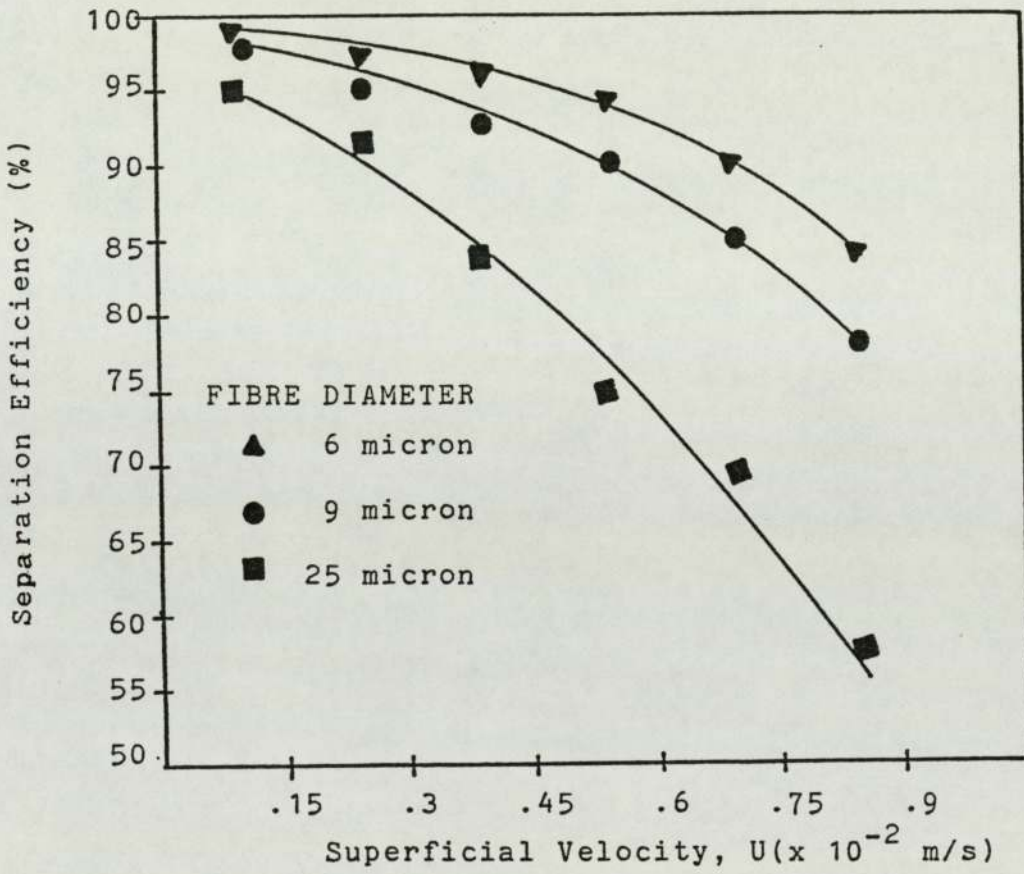
FIG. 7.7 EFFECT OF FIBRE DIAMETER ON SEPARATION EFFICIENCY
(PHASE RATIO 1000 ppm) , (L= .04 M)

through represents the point at which the secondary
haze entrainment in the effluent stream exceeds a certain
limit, generally specified by environmental pollution
control standards.   Examination of entrainment concen-
tration of the effluent stream in Fig. 7.8 reveals
that it may be necessary to operate at lower flow rates
in order to avoid excessive entrainment higher than a
specified limit. Consequently the entrainment graphs form
the basis of selection of operating conditions. Fig. 7.9
illustrates the effect of fibre diameter on effluent
entrainment. It is clear from this graph that the lower
the fibre diameter the lower the effluent entrainment
which leads to a better separation efficiency.

7.5. EFFECT OF BED HEIGHT

With regard to the effect of bed height on the coal-
escence process, increasing the bed height resulted in
an increase in separation efficiency up to a certain
limit, as shown in Fig. 7.10. Above this limit increase
in bed height did not result in a corresponding increase
in the separation efficiency. The effluent entrainment
was also observed to decrease with increase in bed
height, which is reasonable, Fig. 7.11 . However,
the decrease in effluent entrainment was limited to a
certain height above which there was no corresponding
decrease in entrainment with further increase in bed
height; this is illustrated in Fig. 7.11. These results
demonstrate the need to choose an optimum height for
the fibrous bed coalescer and are in agreement with
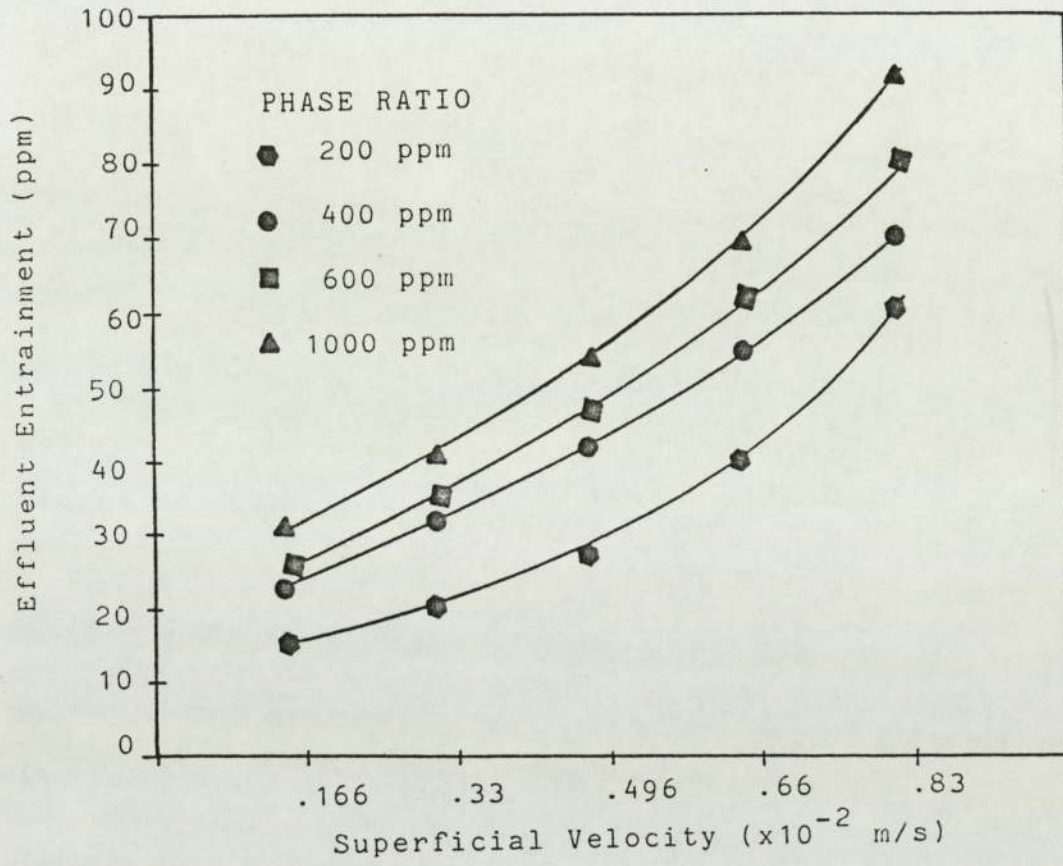
FIG. 7.8 EFFECT OF PHASE RATIO ON EFFLUENT
ENTRAINMENT FOR BED HEIGHT 2.4×10^{-2} M
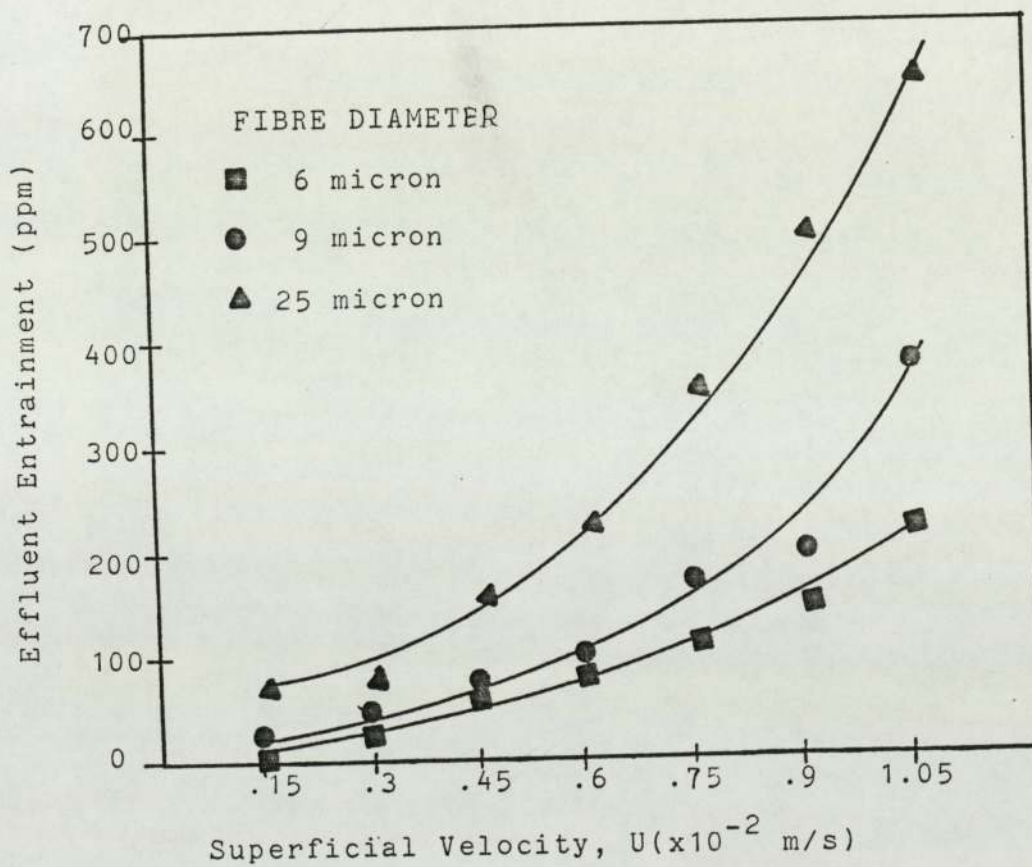
FIG. 7.9 EFFECT OF FIBRE DIAMETER ON EFFLUENT ENTRAINMENT

(PHASE RATIO : 1000PPM) , (L= 4×10^{-2}M)
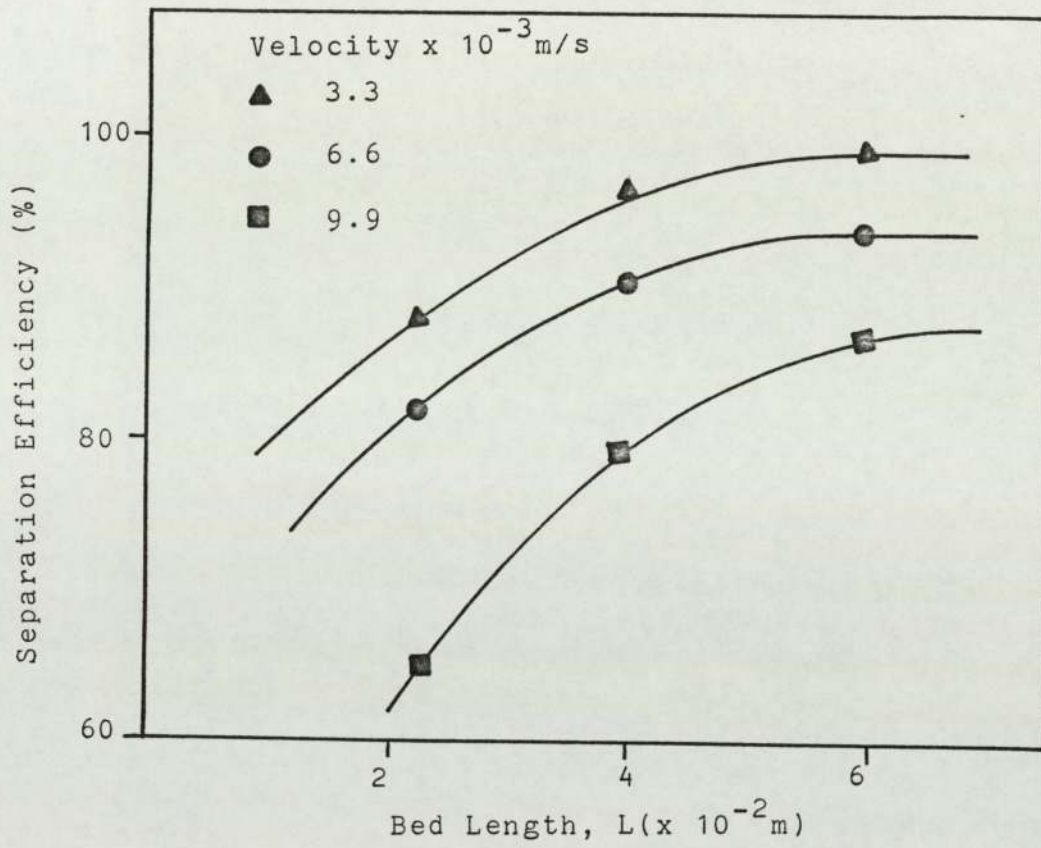
FIG. 7.10 EFFECT OF BED HEIGHT ON SEPARATION EFFICIENCY
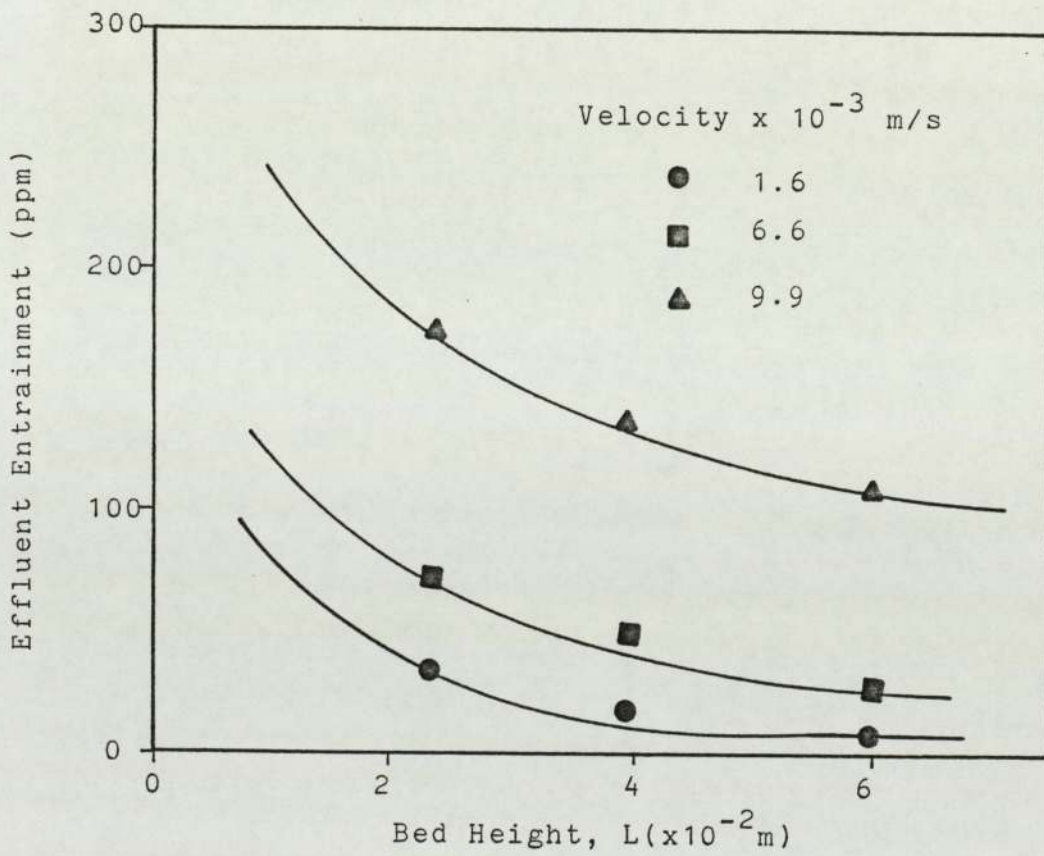
FIG. 7.11 EFFECT OF BED HEIGHT ON EFFLUENT ENTRAINMENT

other workers (1, 14).

7.6. OBSERVATION OF DROP RELEASE SITES

Observations were made of the coalesced drops to determine the release mechanisms. Numerous microphotographs were taken of conditions at the exit face of the bed. The predominant mechanism of drop formation was by drip-point, by which many drops of consistent size brokeout from fixed points. This observation tends to support the assumption of the existence of a dispersed phase continuum . Similar observations were reported by Austin (1). Drops were formed initially, from a large number of sites on the exit face of the bed, but as steady state conditions were approached, the dispersed phase flowed in relatively fewer channels. In some runs there were 10 active channels as shown in Fig. 7.12, with the exit drops from a certain channel leaving in a queue of consistent drop size and with an almost consistent drop-drop separation distance of about 1.5 mm. This supports the suggestion of Austin (1) regarding a queueing drop model. The exit drops, forming a queue, moved upward following a straight flow pattern near the exit face of the bed, then due to fluctuation of continuous phase they moved slowly in a zig-zag pattern, Fig. 7.13. This phenomenon was also observed from the glass ballotini beds used by Poleo (14). This phenomenon was observed at low velocities, <

DRIP-POINT MECHANISM FOR COALESCED DROPS
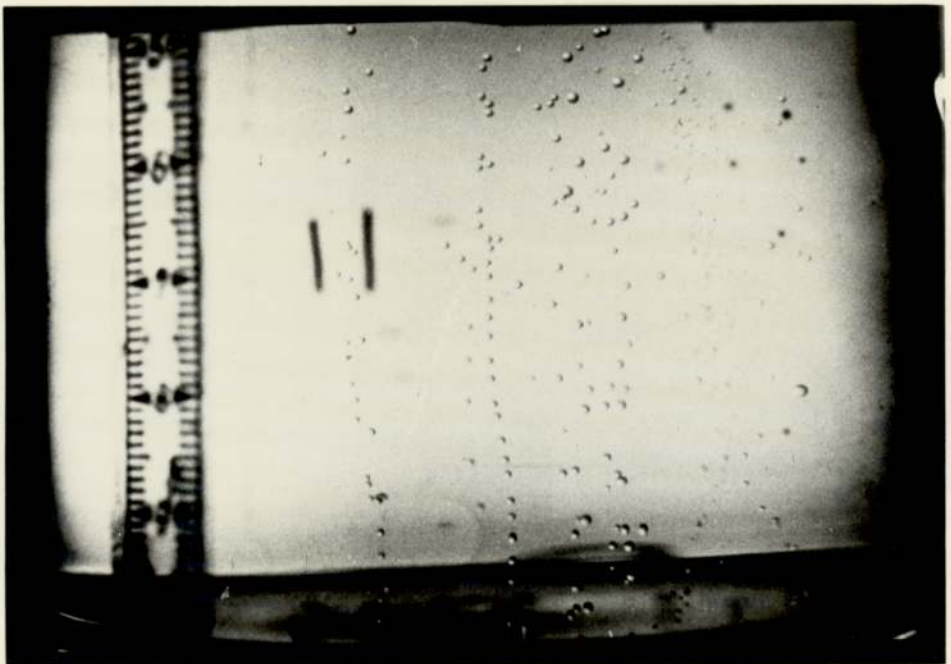
FIGURE 7.12   EXIT DROPS RELEASING FROM DIFFERENT
CHANNELS IN THE EXIT FACE OF THE BED.
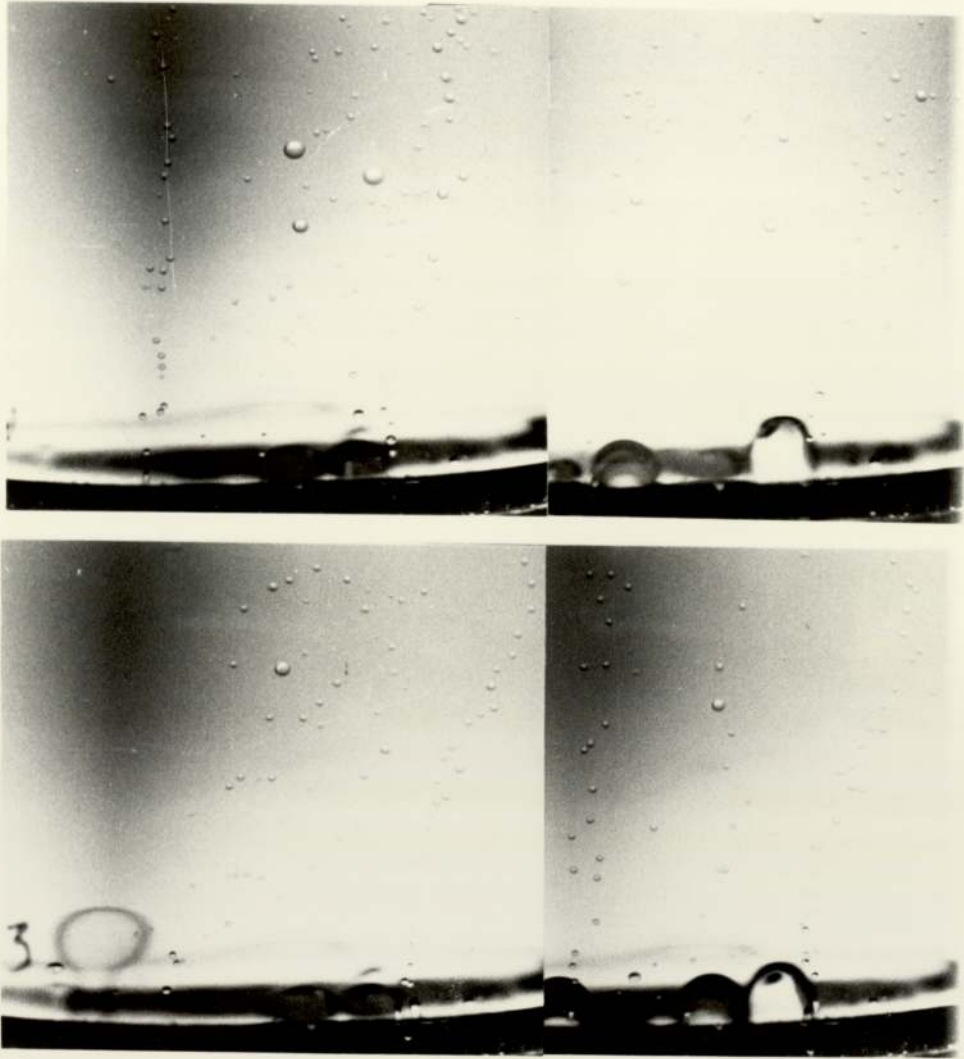
FIGURE 7.13   ZIG-ZAG FLOW PATTERN OF RELEASED DROPS

0.5×10^{-2} m/s, but at high velocities the drops were formed at apparently random positions on the exit face, Fig. 7.14. At high velocities 'jetting', when drops of small size broke out rapidly, was observed.

Froth-type drop formation was also recorded. In this the continuous phase is trapped within a film of the dispersed phase; the drop formed becomes bigger and bigger until it bursts out. This mechanism is shown in Fig. 7.15. The ballooning mechanism was observed at different velocities and produced an average drop size of approximately 5 mm. The steps of drop growth, neck formation and release are illustrated in Fig. 7.16. These different observed mechanisms are shown in Fig. 7.17.

The mechanisms, observed in this study, were also reported, by Attarzadeh (68) for fibrous beds, and by Poleo (14) and Al-Meshan (15) for glass ballotini.

FIGURE 7.14   EFFECT OF VELOCITY ON NUMBER OF ACTIVE
CHANNELS AND DROP SIZE.
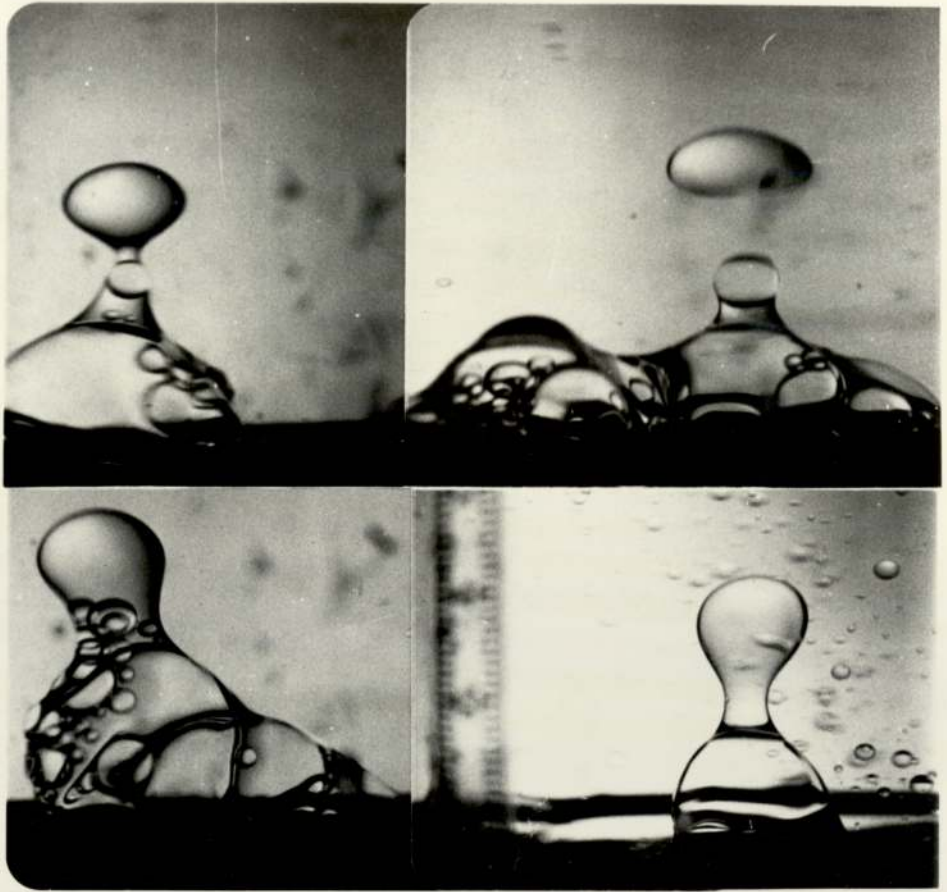
FIGURE 7.15 FROTH-TYPE DROP FORMATION (graping)
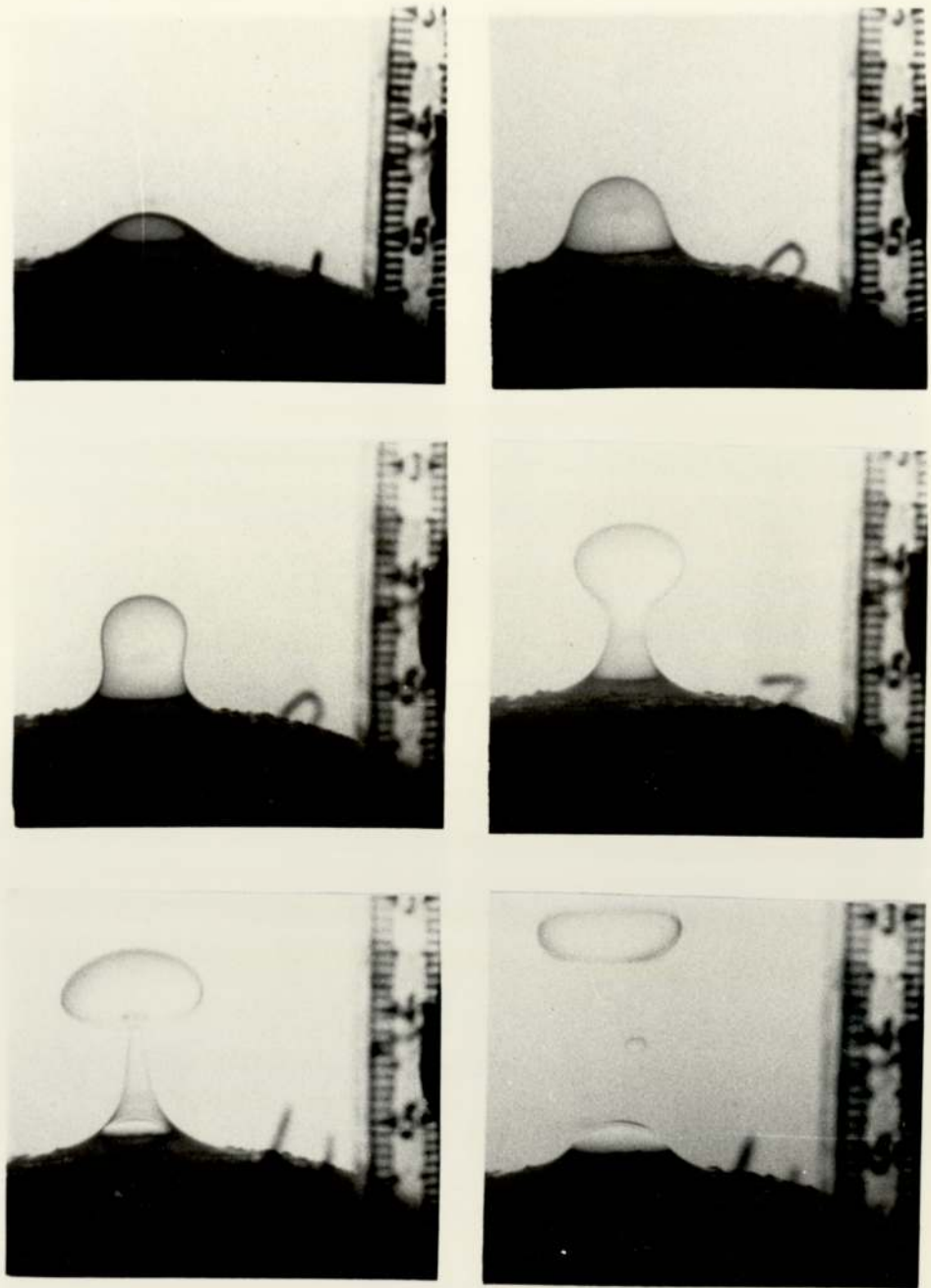
FIGURE 7.16   STEPS OF BALLONING MECHANISM
L = 0.04 M, PHASE RATIO = 1000 PPM
d_f = 25 μM,   VELOCITY = 0.33×10^{-2} M/S
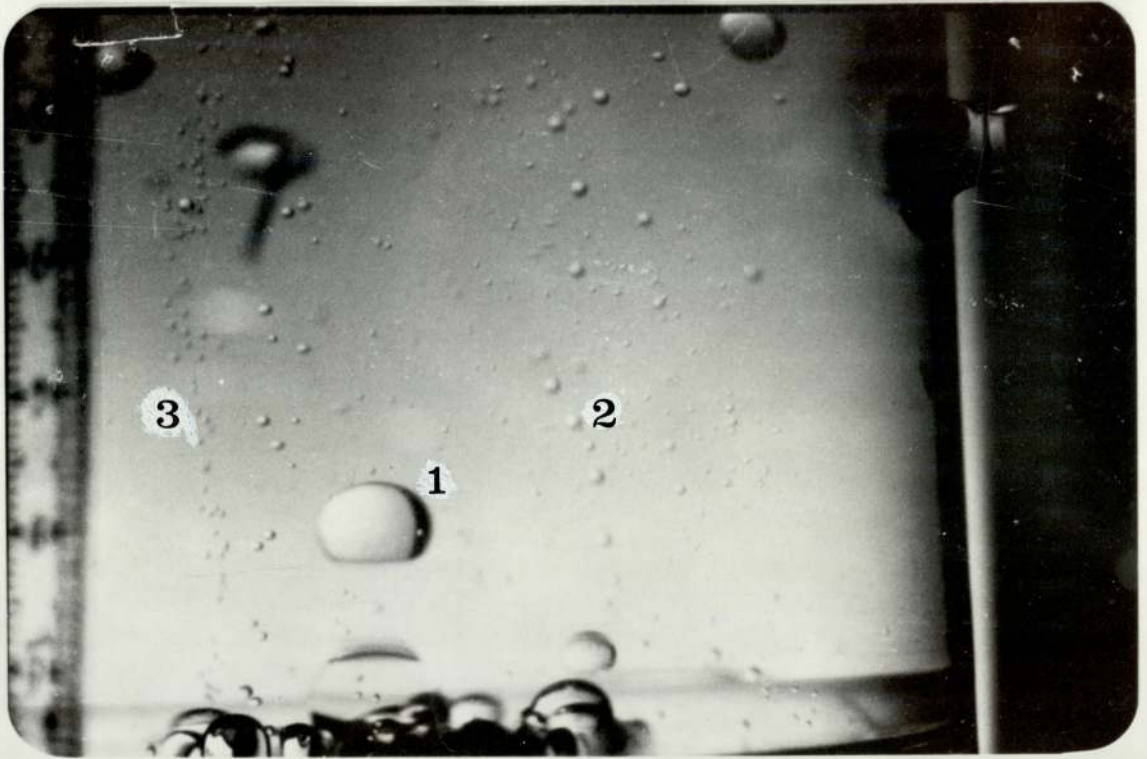
FIG. 7.17 DIFFERENT OBSERVED DROP RELEASE MECHANISMS

1. BALLOONING
2. DRIP-POINT
3. JETTING

CHAPTER 8

ANALYSIS OF PRESSURE DROP DATA

CHAPTER EIGHT

ANALYSIS OF PRESSURE DROP DATA

8.1 FLUID FLOW EQUATIONS

Fluids flowing through a bed of particles, such as
sand or ballotini glass beads, or other porous medium,
such as fibres, distinct from a conduit, flow through
passages between the particles of the bed. Actually
there are two different model approaches to analyse the
single phase flow. Either the flow is analysed inside
conduits or the flow is considered around solid objects
immersed in the fluid. The conduit flow approach is
generally used for low and intermediate, in the range
50 - 90%, void fractions, while the second approach is
used for very high ,greater than 90%, void fractions (14).

Within the conduit flow approach, there is a disti-
nction between the "geometrical" and "statistical" models.
The simplest kind of geometrical model consists of a bun-
dle of straight cylindrical capillaries of uniform cross
section. In the statistical models the random nature
of the interconnections and/or orientation has been
emphasized.

Channel flows have been treated by an approximation
which neglects all but one velocity component, resulting
in Hagen-Poiseuille type-flow equations. Recently, the

complete Navier-Stokes equation has been solved for special channel geometries (124).

The continuum approach to modelling porous media does not distinguish between conduit flow or flow around submerged objects. This is essentially a deterministic approach because certain basic physical laws (the continuity equation for mass and the momentum equation) are assumed and these equations are averaged over the volume under consideration.

The approaches considering flow around solid objects, sometimes termed "drag theories", are variants, extensions, or generalizations of Stoke's Law.

The first relation to express the flow by the specific permeability (k) of the medium was proposed by Darcy (85).

$$u = \frac{k}{\mu_c} \cdot \frac{\Delta p}{L} \qquad (8.1)$$

This relation, termed as Darcy's Law, has subsequently been confirmed by many workers.

The resistance of the porous medium can be expressed in terms of friction factor f_p; defined by the equation.

$$f_p = \frac{d_c}{\mu_c u^2} \cdot \frac{\Delta p}{L} \qquad (8.2)$$

as a function of the superficial or particle Reynolds
number, N_{Re}

$$N_{Re} = \frac{d_c \, u \, \rho_c}{\mu_c} \qquad (8.3)$$

A review of these models is given in the dissertation
of Poleo (14).

8.2. SINGLE PHASE FLOW PRESSURE DROP

Analysis of the single phase pressure drop helps
in determination of the flow characteristics of the
fibres used for coalescence. It also serves to check
the reproducibility of the packing technique and to
detect ingress of air or particulate matter into the bed.

The Ergun equation (86) is used to describe single
phase flow in packed beds.

$$f_p \, (e_1^3 / \, (1-e_1)) = (150/N_{Re}) \, (1-e_1) + 1.75 \qquad (8.4)$$

Substituting for f_p and N_{Re} and rearranging,

$$\frac{\Delta p_1}{L} = \frac{150 \, \mu_c \, u \, (1-e_1)^2}{d_c^2 \, e_1^3} + \frac{1.75 \, \rho_c \, u^2 (1-e_1)}{d_c \, e_1^3} \qquad (8.5)$$

For low values of Reynolds number, $N_{Re} < 1$, the second
term on the right hand side is negligible and equation
(8.5) reduces to the Blake-Kozeny equation.

Macdonald et.al (87) suggested a modified Ergun equation,:

$$\frac{\Delta P_1}{L} = \frac{180 \; \mu_c \; u \; (1-e_1)^2}{d_c^2 \; e_1^3} + \frac{1.8 \; \rho_c \; u^2 \; (1-e_1)}{d_c \; e_1^3} \quad (8.6)$$

which reduces to the Carman-Kozeny equation for low Reynolds number.

An analysis of variance, by Austin (1), for quadratic regression on pressure drop data showed that the lack of fit and random errors were more significant than the second order term. This evidence, together with the high correlation coefficients obtained for linear regression analysis on the data, further justify sole consideration of a first order dependence on velocity.

In equation (8.6) the constant 180 is equal to the product of the Kozeny constant, k and another constant relating the characteristic fibre diameter to the specific surface. The commonly accepted value for the Kozeny constant is 5. However, k is dependent on the structure of the bed, voidage fraction and particle shape among other factors. Poleo (14) reviewed the effect of the following factors on the value of the Kozeny constant:

1. Shape factor and tortuosity

2. Wall effect

2. Voidage

4. Sphericity of the particles

5. Surface roughness of the particles

6. Orientation of the particles

7. The average diameter value used

   when working with mixed particles.

It was concluded from the literature (88, 89, 90, 91, 92, 93) that,

a) Widely different values may be obtained
   for the tortuosity, T, some of which
   lack any physical meaning, when using
   different models of pore structure.

b) If the model incorporates the most important
   features of the pore structure, the value
   of tortuosity factor should normally
   lie in the range $1 < T < 3$.

Regarding the wall effect, no correlation is necessary since e_1 represents the average voidage of the whole bed including the region at the wall, but it might be necessary to include a correlation for the friction of the walls of the container. Coulson (94) determined

experimentally the correlation factor f_w for this effect as

$$f_w = (1 + \tfrac{1}{2} \ \frac{A_c}{a}) \tag{8.7}$$

where A_c is the surface area of the container per unit
volume of bed. Carman (88) concluded that the wall
effect is negligible if $D/d_c > 10$, where D is the diameter
of the container and d_c the particle diameter. No corre-
ction is made in this study for the wall effect since
the ratio of D/d_c for the largest size fibre used is
over 2000.

Spheres and particles which are approximately isometric
do not pack to give beds with voidages in excess of about
0.6. Different arrangements of spheres and their voidages
are given in Fig. 8.1 (95). With fibres and some ring
packings, however, values of e_1 near unity can be obtained
and rapidly increasing values of k are required to obtain
agreement with experiments.

Sphericity of the particle, indicated by Ψ , is
defined as the area of the sphere having the same volume
as the particle divided by the area of the particle.
The voidage is closely related to the sphericity. The
sphericity could be used as the sole determining factor
of porosity if particles of a single size were always
oriented in the same spatial arrangement.

Top View

Front View

5 Tetragonal Sphenoidal (clear passage) Porosity 0.3019

Top View

Front View

10 Rhombohedral (blocked passage) Porosity 0.2595

Top View

Front View

4. Orthorhombic Porosity 0.3954

Top View

Front View

9 Rhombohedral (clear passage) Porosity 0.2595

Top View

Front View

3 Orthorhombic (blocked passage) Porosity 0.3954

Top View

Front View

8 Rhombohedral Porosity 0.2595

Top View

Front View
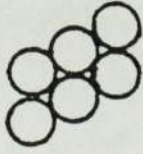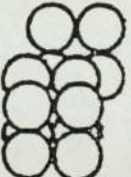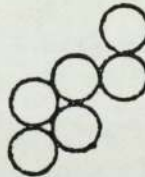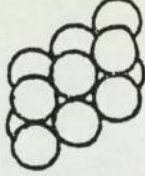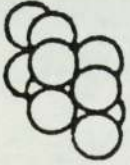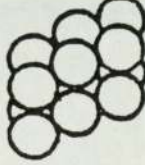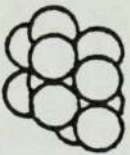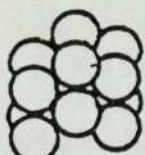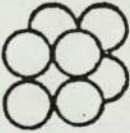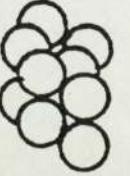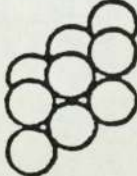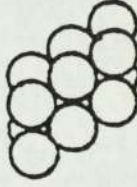
2 Orthorhombic (clear passage) Porosity 0.3954

Top View

Front View

7 Tetragonal Sphenoidal (blocked passage 2) Porosity 0.3019

Top View

Front View

1 Cubic Porosity 0.476

Top View

Front View

6 Tetragonal Sphenoidal (blocked passage 1) Porosity 0.3019

Figure 8.1   Systematic arrangement of spheres and their porosities.

Roughness of the particle is of less significance than the other variables but may become important in the highly turbulent region. Experimental data in the laminar and early turbulent region indicate that roughness has little effect on pressure drop and should not be included in fluid flow correlations for porous media in this flow range.

Orientation is an important variable in special cases. In some experiments pressure drops were determined for different arrangements of stacked spheres, as in Fig. 8.1. These different packing arrangements are special cases and serve to indicate the maximum effect of orientation. Such variations in orientation do not occur with random packing as encountered with ordinary industrial packings.

Diameter of the particle, d_p, could be determined from permeability measurements by the use of Darcy's equation.

8.3. ANALYSIS OF SINGLE PHASE PRESSURE DROP DATA

Applying the modified Ergun equation suggested by Macdonald (87) and neglecting the second order dependence on velocity, since the maximum value of the Reynolds number N_{Re} was always < 1 for the range of variables investigated, yields

$$\frac{\Delta P_1}{L} = \frac{36 \; k \; \mu_c \; u \; (1-e_1)^2}{d_f^2 \; e_1^3} \qquad (8.8)$$

'which is the Carman-Kozeny equation. Rearrangement
of equation 8.8 gives,

$$\frac{\Delta P_1}{\mu_c} \left[\frac{e_1^3 \; d_f^2}{(1-e_1)^2 \; 36 \; L} \right] = k \; u \qquad (8.9)$$

The first term, $\dfrac{\Delta P_1}{\mu_c}$ describing the pressure drop, con-
tains the only property pertaining to the continuous
phase, and therefore is independent of temperature
fluctuations. Properties of the packing, which were
evaluated experimentally are included in the second term.

The single phase pressure drop data were correlated
against superficial velocity by linear regression
analysis using equation (8.9). The correlations obtained
for different fibre sizes are illustrated in Fig. 8.2,
where the slope of the best fit line is equal to the
Kozeny constant. The results are shown in Table 8.1
Clearly the values of the Kozeny constant exhibit vari-
ation from 1.43 to 4.1 with the increase corresponding
to an increase of fibre diameter. This variation in
Kozeny constant can be justified by considering the change
in bed voidage at higher velocities, where the bed is
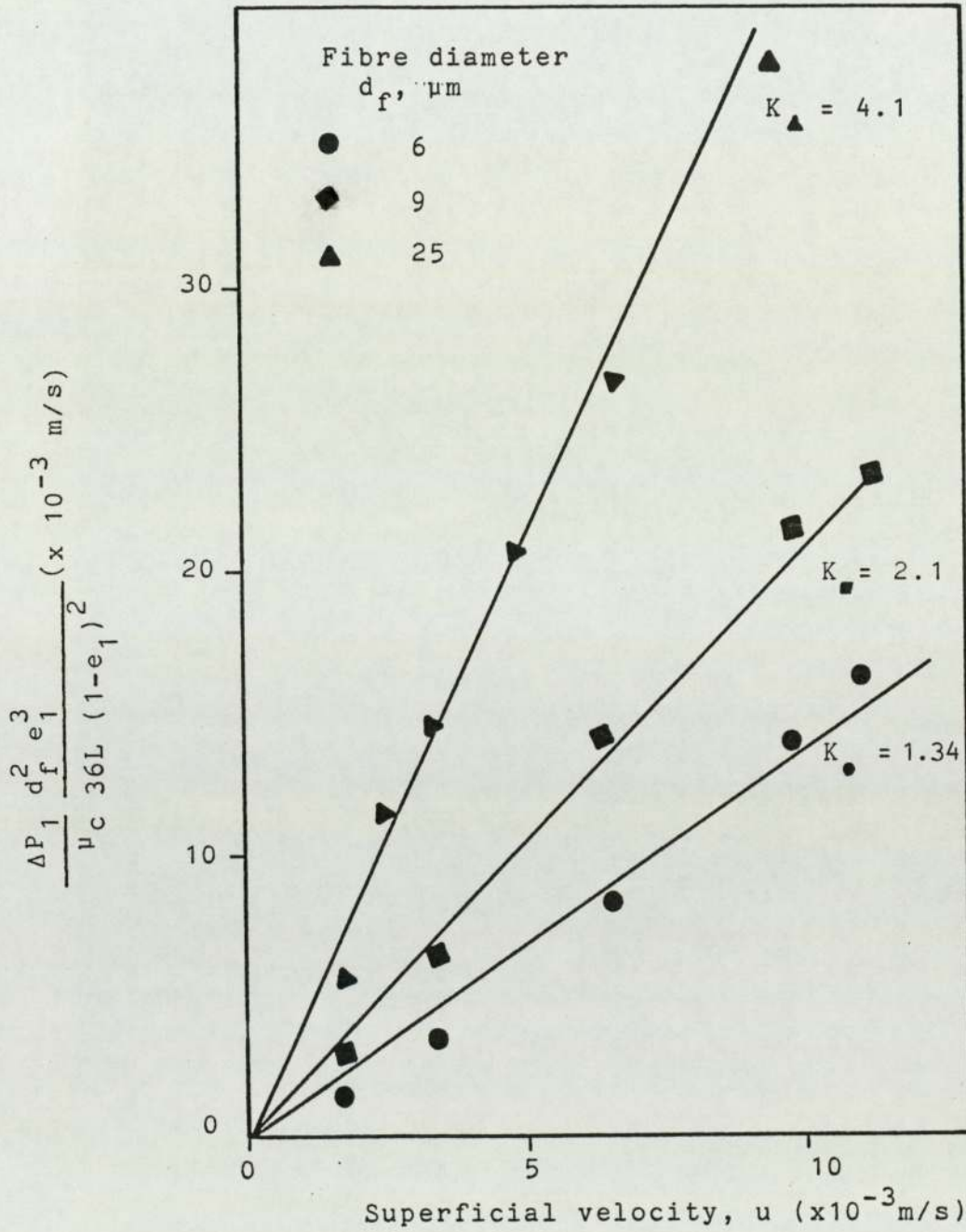
FIG. 8.2 CORRELATION OF SINGLE PHASE PRESSURE DROP FOR
DIFFERENT FIBRE DIAMETERS

Fibre Diameter d_f(m)	Voidage e_1	Kozeny Constant K
6×10^{-6}	0.86	1.34
9×10^{-6}	0.91	2.1
25×10^{-6}	0.88	4.1

Table 8.1   Single Phase Pressure Drop

Correlation

compressed under the effect of pressure and the voidage of
the bed is reduced. A lower voidage will produce a
lower Kozeny constant. To minimize the effect of this
variation it is suggested that two phase pressure drops
be expressed as the ratio $\dfrac{\Delta P_2}{\Delta P_1}$.

8.4 TRANSIENT PRESSURE DROP DATA

The overall pressure drop across the coalescer was
recorded at regular intervals after the dispersion was
introduced to the inlet face. A typical example of the
transient behaviour observed prior to attainment of steady
state conditions is shown in Fig. 8.3. If the dispersed
phase in the system exists as discrete drops, not forming
a continuum within the packed bed, most of the hydrodynamic
forces contributing to the pressure drop should come from
the continuous phase. Also, if the single pressure drop
is presented as $\dfrac{\Delta P_1}{\mu_c}$, the two phase pressure drop data
should be handled in the same way in order to calculate
the contribution of the dispersed phase present within
the packing. Since the dispersed phase viscosity is
lower than the continuous phase viscosity the effect of
the dispersed phase can be easily over-estimated. Thus
as discussed in Section 8.6, when calculating the dispersed
phase saturation from relative permeability calculations,
the difference between the saturation values obtained
by using the dispersed phase viscosity instead of the
continuous phase can be in excess of 10% in some cases.
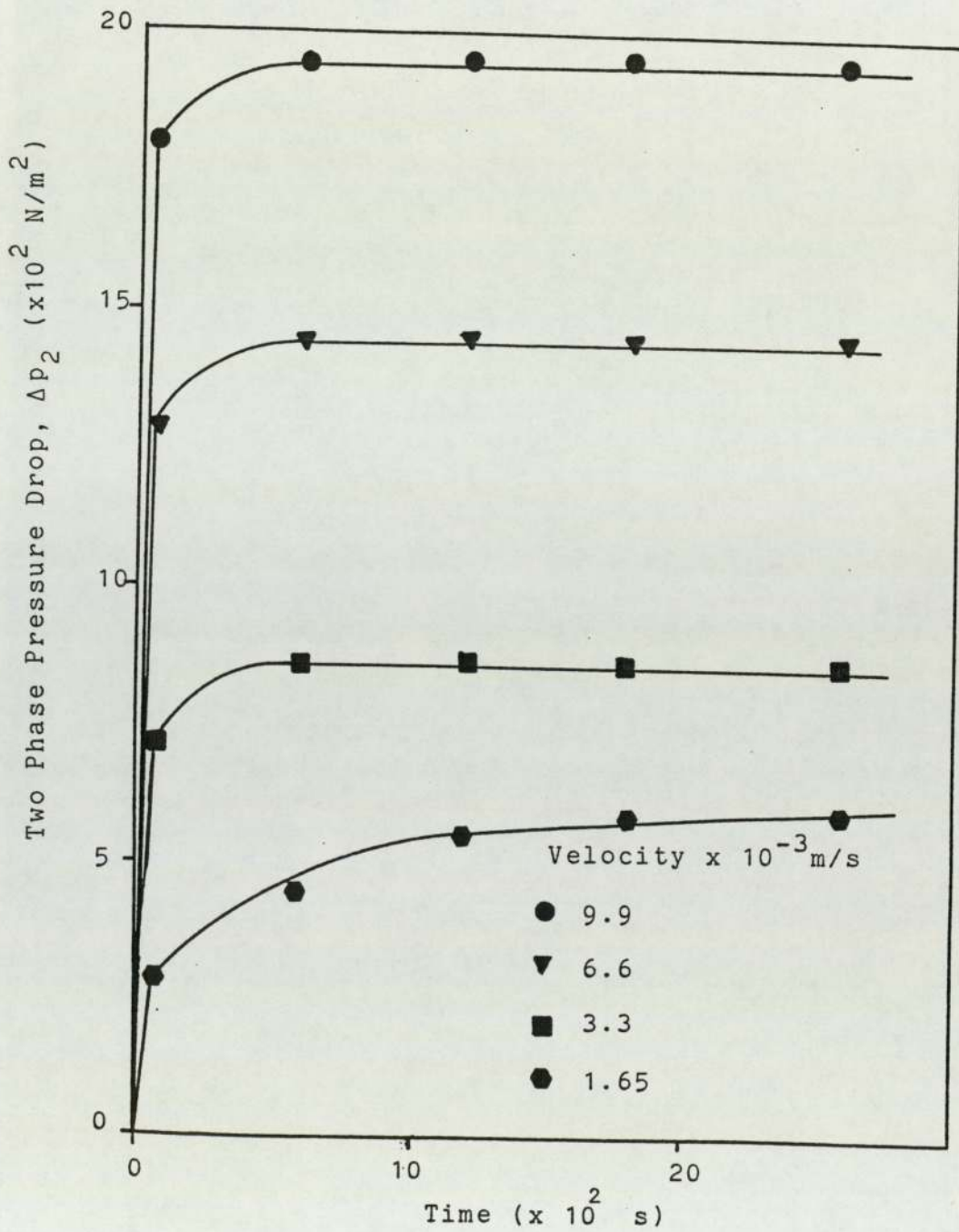
FIG. 8.3 TYPICAL TRANSIENT BEHAVIOUR OF TWO PHASE PRESSURE

DROP (d_f = 25 µm, L = 4×10^{-2} m)

Therefore both the single phase and two phase pressure

drop will be presented as $\dfrac{\Delta p}{\mu_c}$.

Fig. 8.3 shows the effect of superficial velocity
on pressure drop. As expected, pressure drop increased
with increasing superficial velocity. It increased rapidly
at first after start-up in any experiment but then
remained almost constant throughout the experiment.

8.5 TWO PHASE PRESSURE DROP

Pressure drop during two phase flow is known to
increase as the dispersed phase accumulates in the bed.
The plot of two phase pressure drop against superficial
velocity, illustrates non-linear relationships and the
shapes of the curves are dependent on the bed height,
fibre diameter and inlet drop size. Fig. 8.4 shows the
effect of phase ratio on two phase pressure drop, while
Fig. 8.5 shows the same data plotted on a log-log scale
to show the linearity of pressure drop data in this case.
Fig. 8.6 illustrates the relation between the ratio
$(\dfrac{\Delta p_2}{\Delta p_1} \dfrac{\mu c_1}{\mu c_2})$ and superficial velocity for different phase
ratios. This ratio, $(\dfrac{\Delta p_2}{\Delta p_1} \dfrac{\mu c_1}{\mu c_2})$ is used to account for
the variations in packing technique and operating temperature.
The ratio was found to decrease as either velocity or
bed depth were increased. It also increased rapidly
with increasing phase ratio or dispersed phase concen-
tration for the same operating time.
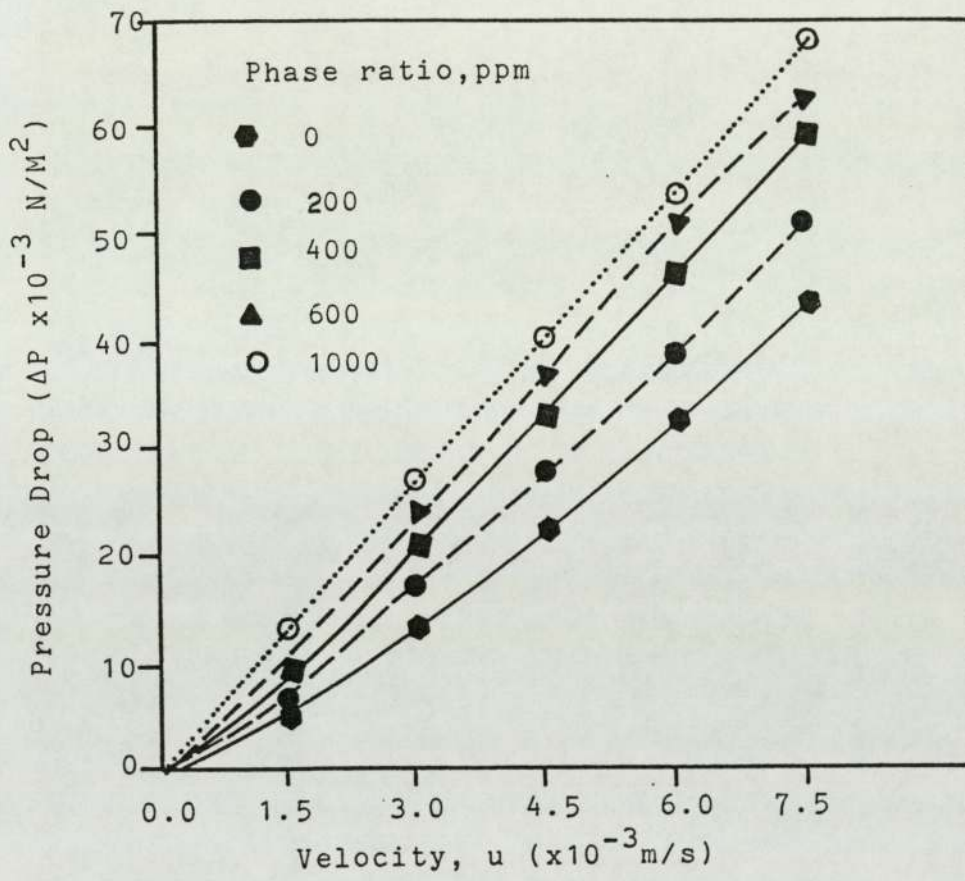
FIG. 8.4 EFFECT OF PHASE RATIO ON TWO PHASE PRESSURE DROP (ΔP_2)
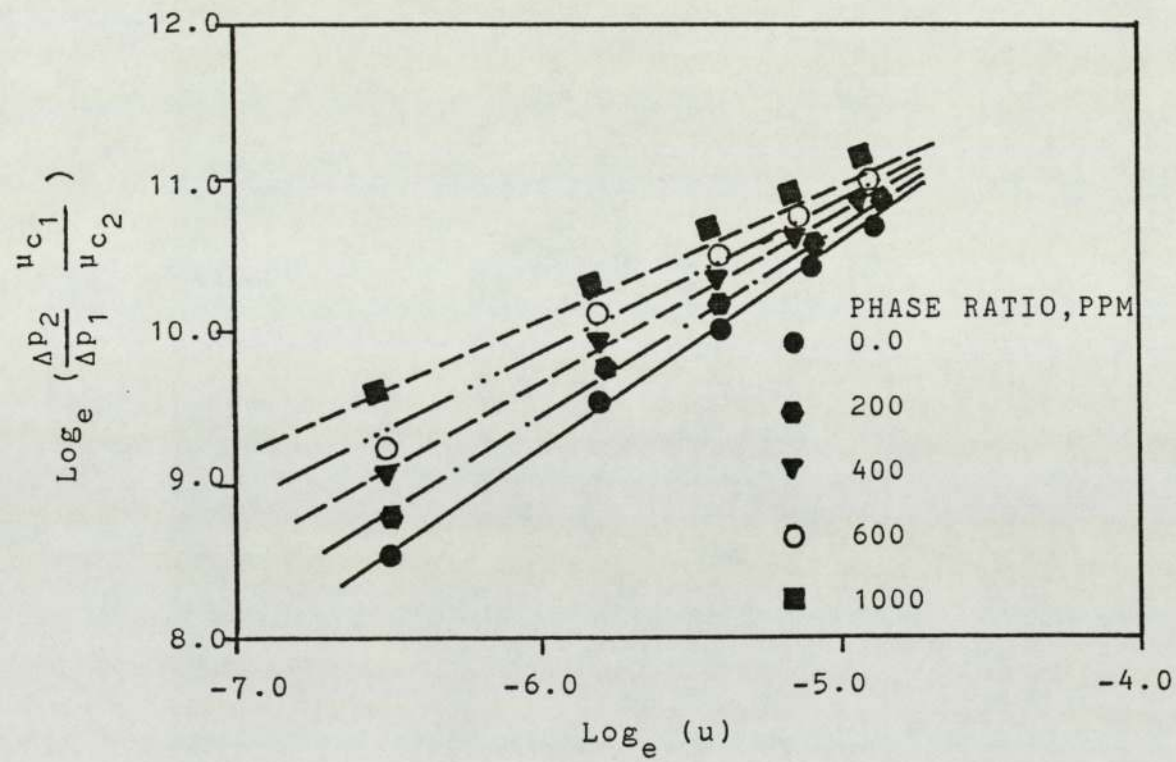
FIG. 8.5 EFFECT OF PHASE RATIO ON PRESSURE DROP $(\frac{\Delta P_2}{\Delta P_1} \frac{\mu c_1}{\mu c_2})$
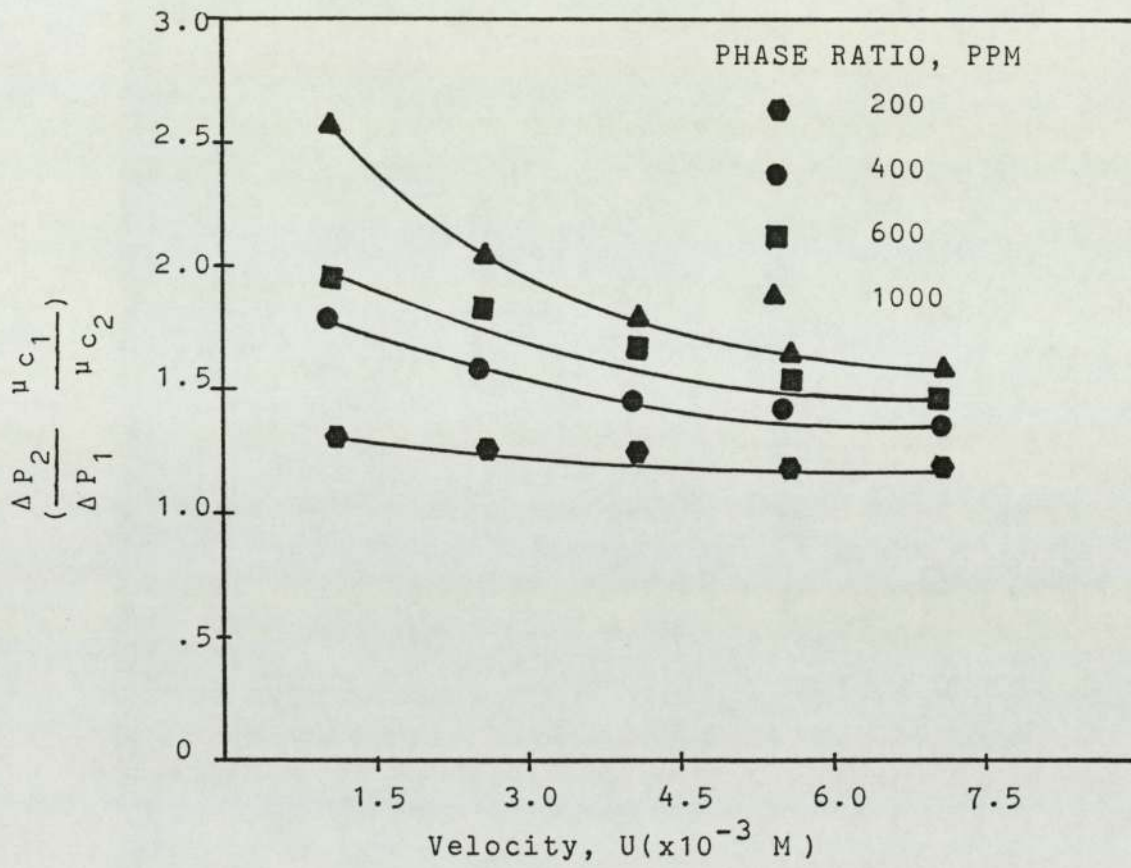
FIG. 8.6 EFFECT OF PHASE RATIO ON TWO PHASE PRESSURE DROP

For different fibre sizes, the individual pressure drops increased with decreasing fibre size, as shown in Fig. 8.7.

8.6 RELATIVE PERMEABILITY METHOD OF SATURATION PROFILES

The measurement of relative permeability consists, essentially, of the determination of two flow rates under a given pressure drop and the determination of saturation. Many relative permeability curves have been published for oil-water, air-water and oil-air-water systems(62, 63, 64).

Leverett (62) investigated the relative permeabilities of unconsolidated sands to different pairs of oil-water mixtures. The oils used were hydrocarbon products including a close-cut hexane fraction, kerosene and a commercial lubricating oil, with viscosities ranging from 76.5×10^{-3} Ns/m^2 to 0.31×10^{-3} Ns/m^2. The relative permeabilities were found to be substantially independent of the viscosity of either phase. Relatively small variations in interfacial tension, porosity, permeability and liquid density differences were found to have an insignificant influence on the relative permeability at a particular value of oil saturation.

Jones (63) correlated relative permeability data with the continuous or dispersed phase saturation using the expressions
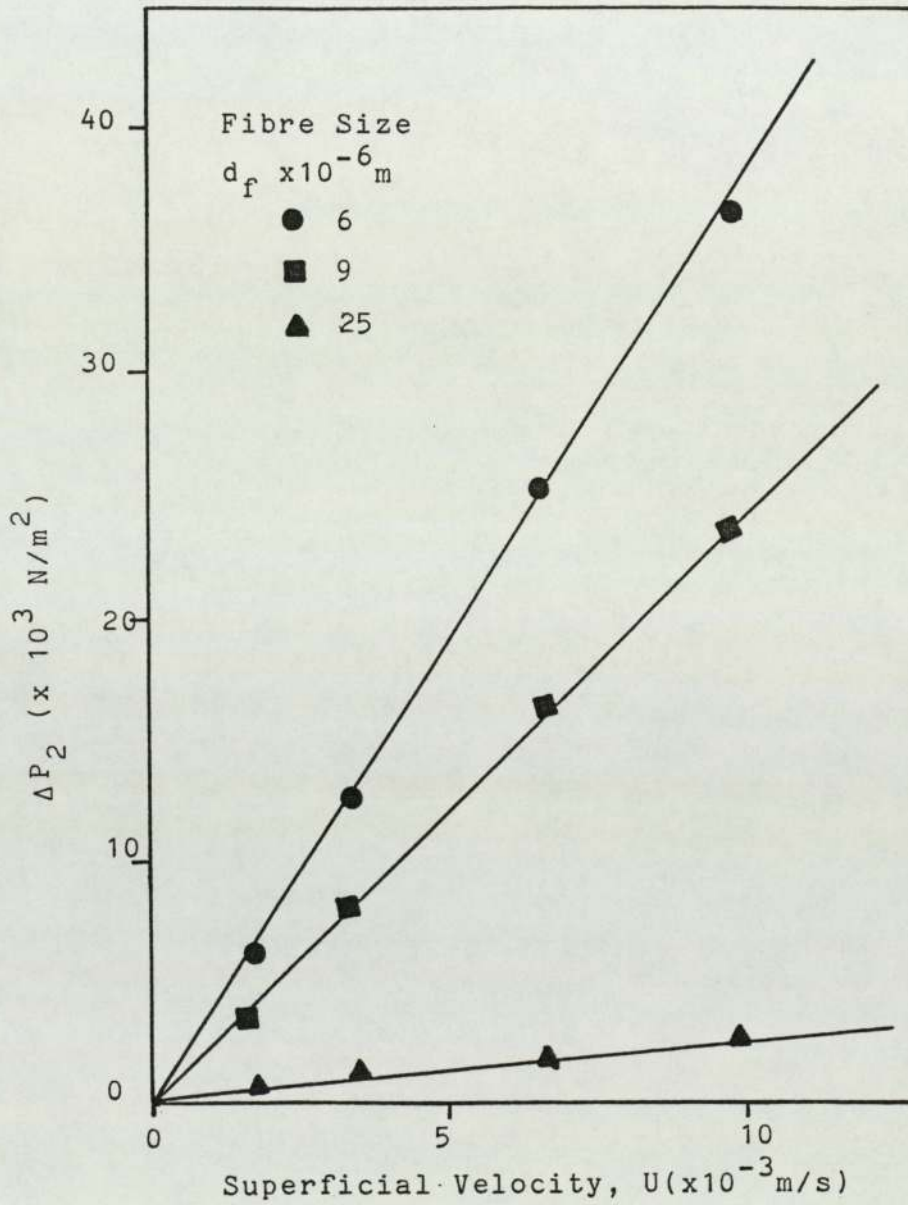
FIG. 8.7 EFFECT OF FIBRE SIZE ON INDIVIDUAL TWO
PHASE PRESSURE DROP (L = 4 x 10^{-2}m)

$$\frac{kd}{ko} = (1 - 1.11\ S_c)^2 = (1.11\ s_d - 0.11)^2 \qquad (8.10)$$

$$\frac{kc}{ko} = (1 - s_d)^3 = s_c^3 \qquad (8.11)$$

from experiments using oil as the non wetting phase, and water as the wetting phase flowing through granular media.

Carpenter et.al (64) published relative permeability data for glass beads using hydrocarbon oils or refined white oils and an aqueous phase consisting of various mixtures of water, lithium bromide and alcohol. The results of Leverett, Jones and Carpenter, showing typical relative permeability curves are plotted in Fig. 8.8 for comparison (62, 63, 64).

All the data show that relative permeability to the wetting aqueous phase is reproducible under different experimental conditions. This water relative permeability curve could therefore be used as a calibration curve to obtain the oil saturation from the measured relative permeability to the water phase during a coalescence experiment. The discrepancy between Jone's data and Carpenter's data in predicting the oil saturation is less than 15% for any predicted value.

For two phases flowing through a short column of porous medium with uniform cross section, the effective permeability to the water phase may be defined as

$$k_c = \frac{u_2 \; \mu_c \; \Delta L}{\Delta P_2} \qquad (8.12)$$

where ΔL is the depth of the porous medium, ΔP_2 is the total pressure drop within the water phase and u_2 is the superficial velocity of the water phase. The permeability of the medium to a single (water) phase is defined by Darcy's law as

$$k_o = \frac{u_1 \; \mu_c \; \Delta L}{\Delta P_1} \qquad (8.13)$$

where ΔP_1 is the total pressure drop. If the superficial velocity $\ddot{u}_1$ for one phase flow is adjusted to equal the value u_2, the superficial velocity of the water phase in two-phase flow at the same temperature conditions, the ratio $\frac{\Delta P_1}{\Delta P_2}$ is equal to $\frac{k_c}{k_o}$ the relative permeability to water phase.

Therefore, the relative permeability can be calculated from the ratio of $\frac{\Delta P_1}{\Delta P_2}$ for each pressure drop, to find the oil saturation from Fig. 8.8 (or equations 8.10 and 8.11) so that
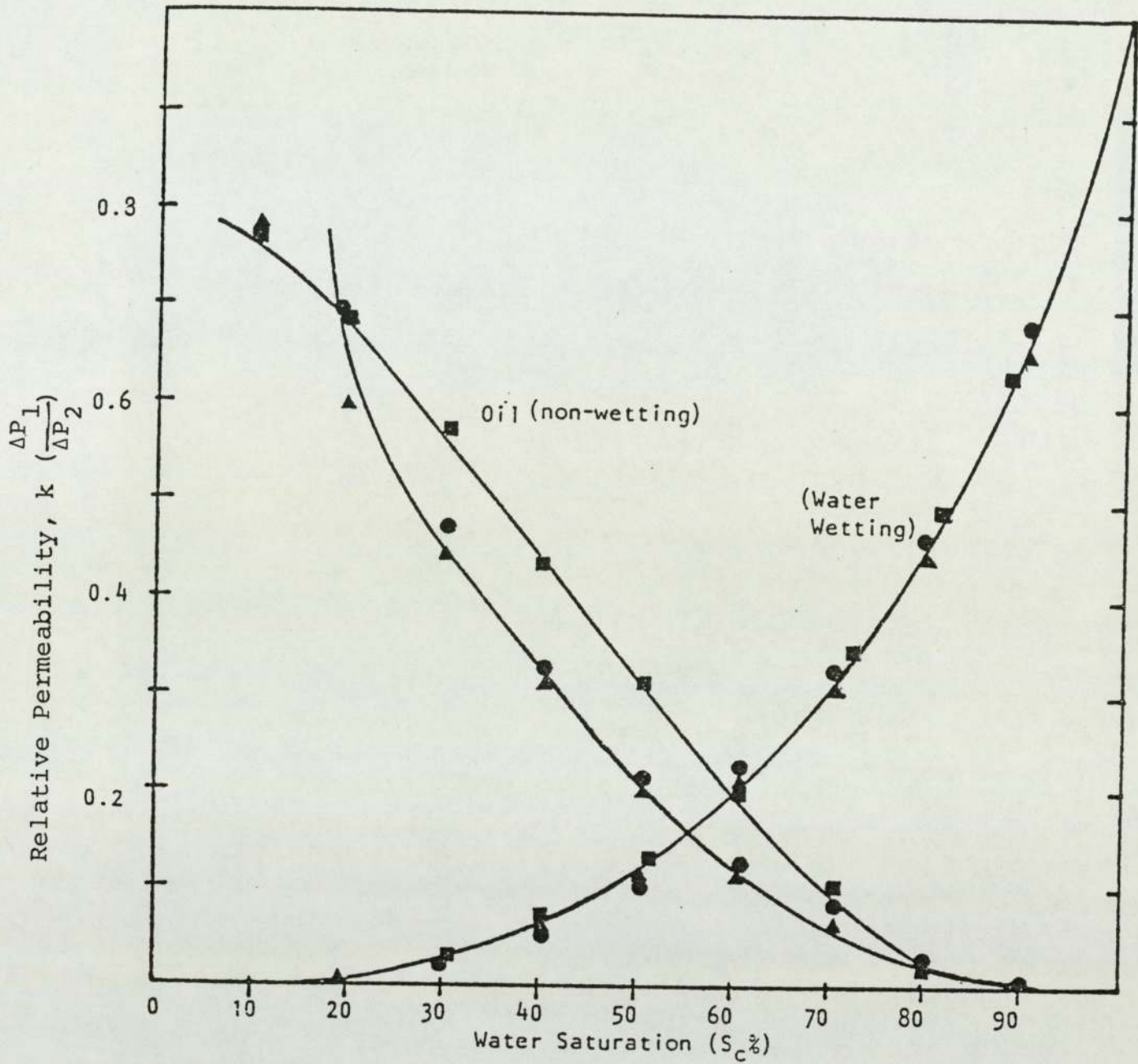
- Leverett $3.1 - 6.7 \times 10^{-2} m^2$ sand with 41% porosity
  $\gamma_{12} = 24-34 \times 10^{-3}$ N/m

- Carpenter $10.4 \times 10^{-2} m^2$ glass bead with 38% porosity
  $\gamma_{12} = 53 \times 10^{-3}$ N/m

- Correlation curve by Jones

Figure 8.8 Relative Permeabilities Vs Saturation
Curves.

$$\frac{\Delta P_1}{\Delta P_2} = \frac{k_c}{k_o} \qquad (8.14)$$

The Carman-Kozeny equation gives

$$k_o = \frac{d_c^2 \, e_1^3}{180(1-e_1)^2} \qquad (8.15)$$

from which a theoretical value for the permeability of
the medium to water can be calculated, and compared with
the experimental value obtained by using equation (8.13).
These values are shown in Table 8.2 for different fibre
sizes. Both values are very close which supports the
assumption that the Carman-Kozeny equation can be used
to predict the single phase flow of the system.

Fig. 8.9 shows the variation of average saturation
with velocity, while Fig. 8.10 shows the effect of fibre
size on saturation profiles. It is clear that the inlet
oil saturation is higher for the lowest superficial
velocity, which suggests a higher contribution of sedimenta-
tion to the drop capture efficiency with lower superfi-
cial velocity. Concerning the effect of fibre diameter,
the inlet saturation is higher for the small fibre size,
suggesting that drop capture by interception is aided
as the size of the interstice is decreased.
Fig. 8.11 shows that the saturation increases slightly
with increase of dispersed phase ratio, which is in
agreement with the increase of separation efficiency

Permeability	Fibre Size ($\times 10^{-6}$ m)		
	6	9	25
Measured $K_0 = \dfrac{\mu_c \, \dot{u} \, L}{\Delta P_1}$	7.65×10^{-12}	4.4×10^{-11}	1.6×10^{-10}
Theoretical $K_0 = \dfrac{e_1^3 \, d_f^2}{180(1-e_1)^2}$	6.49×10^{-12}	4.18×10^{-11}	1.64×10^{-10}
$\dfrac{\text{Measured}}{\text{Theoretical}}$	1.17	1.05	0.975

Table 8.2 Comparison of Theoretical vs.

Experimental Permeability.
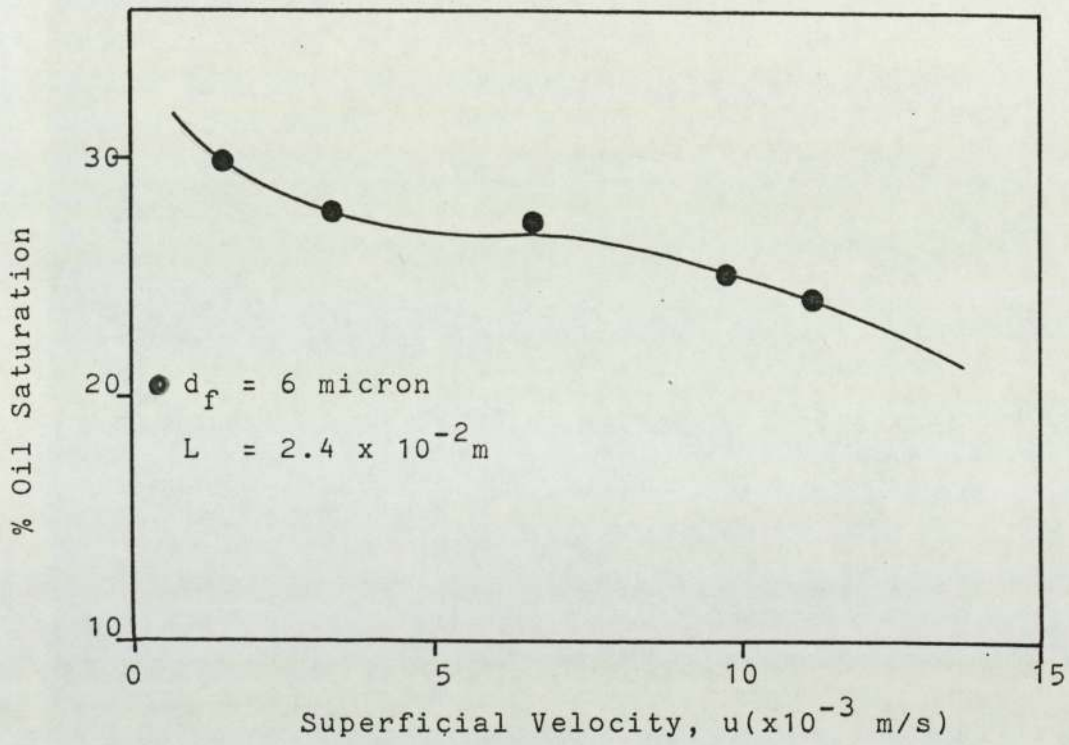
FIG. 8.9 VARIATION OF AVERAGE SATURATION WITH VELOCITY
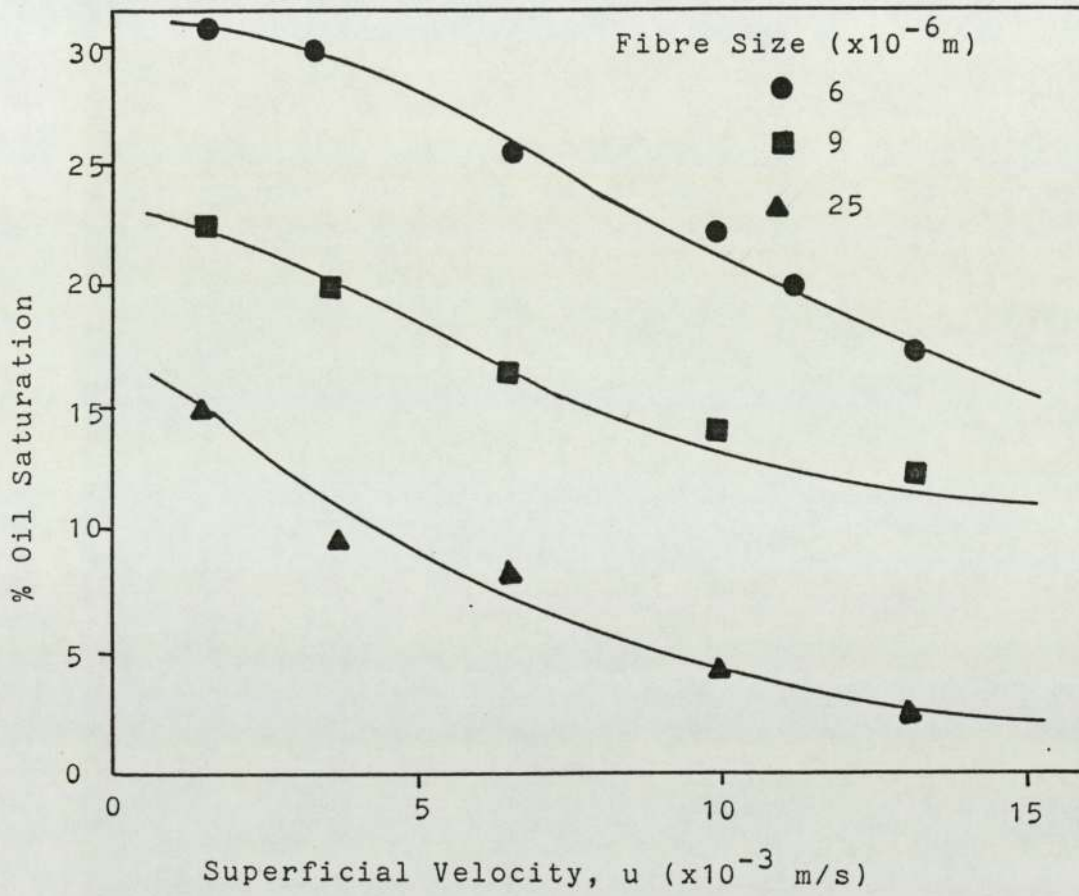
FIG. 8.10 EFFECT OF FIBRE SIZE ON SATURATION PROFILE

(PHASE RATIO: 1000 PPM)
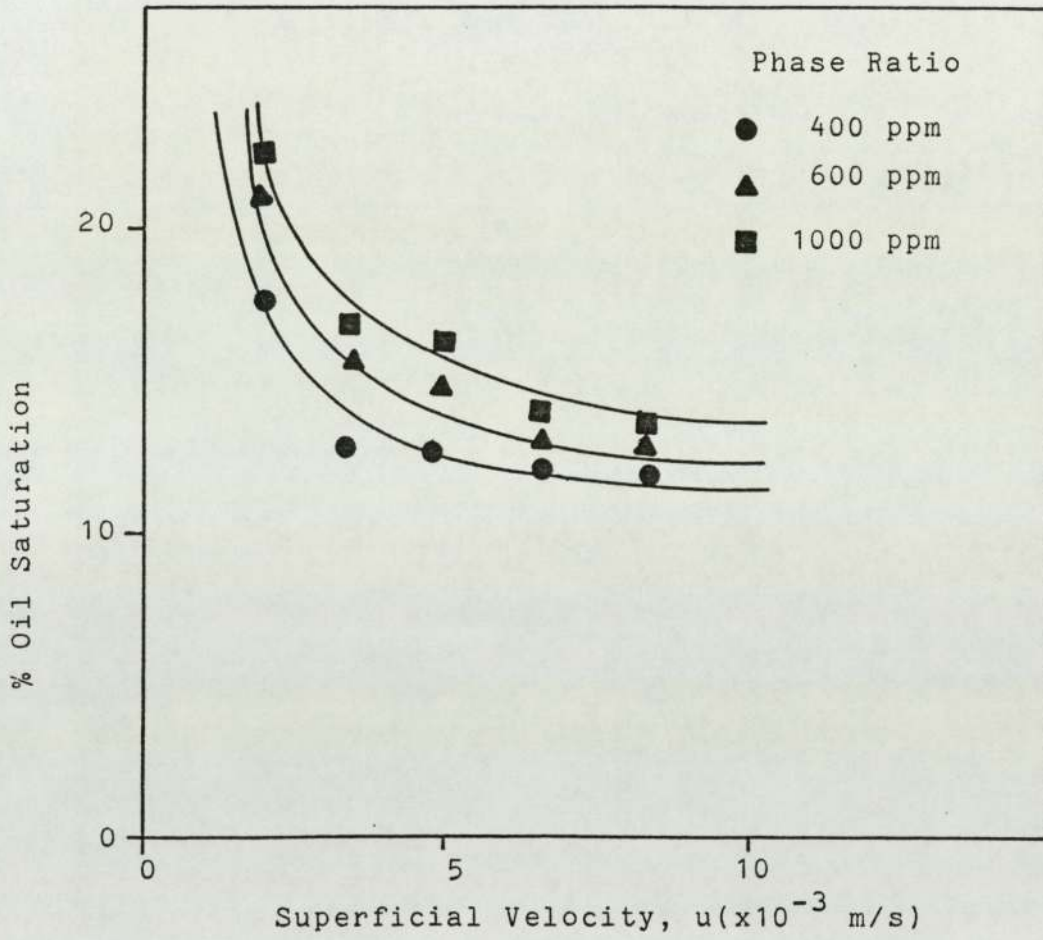
FIG. 8.11 EFFECT OF PHASE RATIO ON SATURATION PROFILES

with phase ratio.

The saturation profile starts at a high value at the inlet face of the bed, then decreases with increase of bed height, but only up to a certain limit above which no further significant decrease occurs, as shown in Fig. 8.12. This indicates the optimum height of bed.
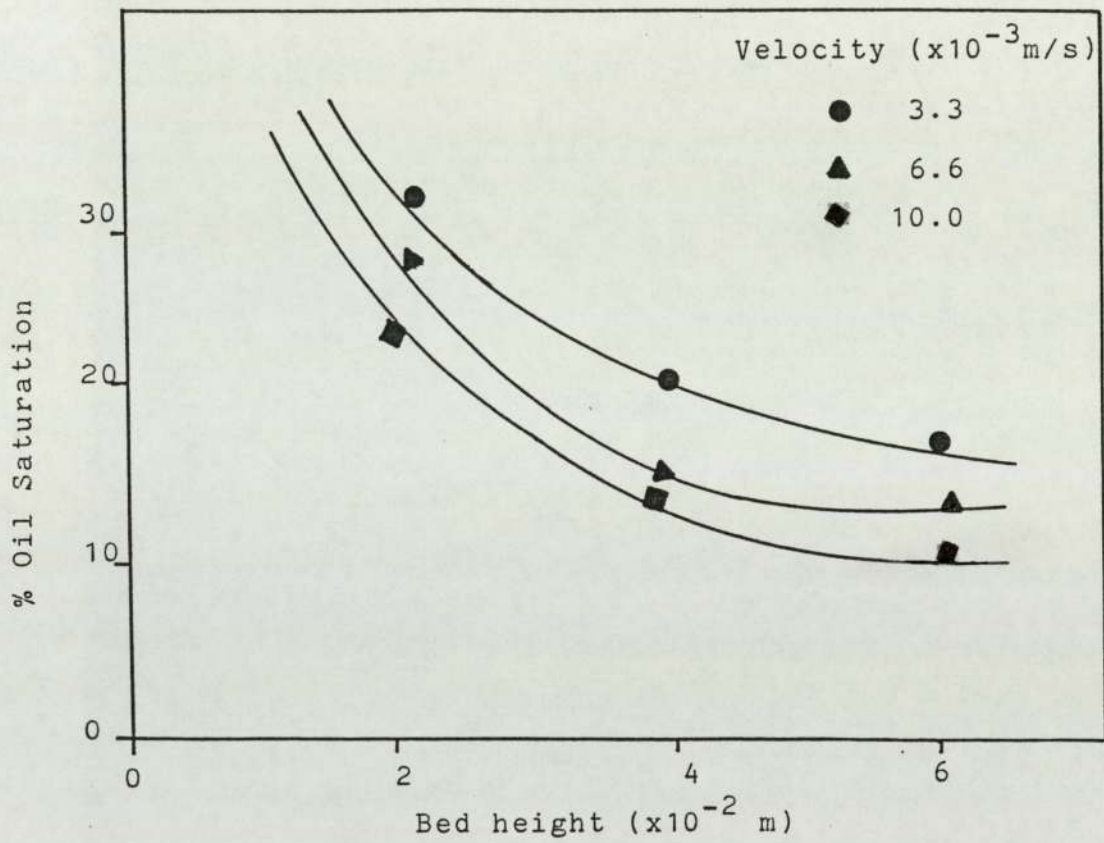
FIG. 8.12 EFFECT OF BED HEIGHT ON SATURATION PROFILES

CHAPTER 9

MODELS FOR THE SEPARATION OF DISPERSIONS

IN FIBROUS BED COALESCERS

CHAPTER NINE

MODELS FOR THE SEPARATION OF DISPERSIONS IN FIBROUS
BED COALESCERS

9.1 MODELS OF PREDICTION OF FILTER COEFFICIENT

The filter coefficient provides a measure of the
overall drop coalescence efficiency of a bed. It is
defined as

$$\lambda = \frac{-\log_e(\frac{\text{Outlet drop number density}}{\text{inlet drop number density}})}{L} \quad (9.1)$$

Mathematical models which have been derived to
assist in the design of fibrous bed coalescers attempted
to predict the filter coefficient. A review and a
comparison of these models is given below.

9.1.1 Vinson and Churchill's Model

This model considers the probability of retaining
a drop when it collides with a fibre. This drop then
moves along the fibre onto other fibres and coalesces
with other retained drops. The mechanism of coalescence
is interception. The size of a drop at detachment
depends upon the thickness of the threads attenuated
by fluid forces.

Their equation represents the best fit of the data
taken for a system were photoetched screens were used
to simulate a fibrous bed (55).

The filter coefficient is presented by:

$$\lambda = \frac{- \log_e (0.128(u \, d_f \, \mu_c)^{-0.4} - 0.089)}{L} \qquad (9.2)$$

where the units of the independent variable are (gm)
(micron)/s^2.

9.1.2 Rosenfeld and Wasan's Model

Rosenfeld and Wasan assumed that drops flow along
the streamlines of the fluid and if they come close to
a held drop or fibre, they will strike it. An effective
fibre diameter, d_{fe} was introduced to account for held
drops and a factor, β was used to relate the collision
frequency to coalescence efficiency (28):

$$\lambda = \frac{8 \, \beta \, (1-e_1) \, d_f}{\pi^2 \, d_f^2 \, e_1(1-s_d)} \quad \frac{2d_{fe} + d_p}{d_{fe} + d_p} \qquad (9.3)$$

where

$$d_{fe} = d_f(\frac{1-e_1(1-s_d)}{1-e_1})$$

This equation (9.3) is valid at low velocities.
At higher velocities an adjustable parameter, referred
to as the critical velocity, must be evaluated experiment-
ally. The value of β was determined by Sherony (31) to
be 0.41.

9.1.3 Sherony and Kintner's Model

The model by Sherony and Kintner (31) was the first
one developed for fibrous bed coalescers. It uses the
'travelling drop' hypothesis in which drop capture is
assumed to occur by interception and inertial impaction.
An equation was presented in terms of an overall coalescence
efficiency, η_c and the average saturation:

$$\lambda = \frac{0.75}{d_f} \left(\frac{s_d}{1-s_d}\right) \quad (1-e_1) \quad \left(1 + \frac{d_p}{d_f}\right) \eta_c \qquad (9.4)$$

The major shortcoming in this model is that it predicts
an increase in separation efficiency with higher velocity.
This is in contradiction to the results of all other workers
(1, 14, 22, 27, 43, 55).

9.1.4 Spielman and Goren's Model

Spielman and Goren assumed that coalesced liquid,
attached to fibres, drains through the bed and leaves it
at the same rate as suspended drops are coalesced within
the bed. Each immiscible fluid is considered to flow within
a fixed channel, with the non-wetting fluid flowing on the
inside. Each channel is described by Darcy's Law. It
was suggested that London-Van der Waals' forces should
be included in the evaluation of capture efficiency.
The equation proposed for continuous phase wetted beds,
was obtained by correlation of experimental data with
a modified adhesion number (32, 51):

$$\lambda = 0.29 \frac{d_p^2}{d_f^3} \left(\frac{Q \; d_f^2}{\mu_c \; u \; d_p^4}\right)^{0.25} \tag{9.5}$$

This model is not general and needs a considerable amount of data to determine the constant and exponent.

9.1.5 Austin's Queue Model

Austin's model is based on the hypothesis that drops are captured in the forepart of the bed where they accumulate and coalesce (1). They are then conveyed in channels to the release sites located on the exit face of the coalescer. The model recognises an analogy between drops waiting to coalesce and 'customers' queueing at a service facility. Thus the fraction of 'customers' which join the queue when there are n units in the system is given by,

$$f_n = e^{\frac{-\alpha n}{\mu}} \tag{9.6A}$$

$$f_n = \gamma^{2n} \tag{9.6B}$$

The filter coefficient is related to the fraction of customers, f_n which undergo 'balking'. Applying equation (9.6B) for steady state conditions when $n = L_q$,

$$f_{L_q} = \gamma^{2L_q} \tag{9.7}$$

Then from equation (9.1), the filter coefficient, λ_c is given by,

$$\lambda_c = \frac{-\log_e (1 - f_{L_q})}{L} \tag{9.8A}$$

Substituting for f_{L_q},

$$\lambda_c = \frac{-\log_e (1 - \gamma^{2L_q})}{L} \tag{9.8B}$$

The length of the 'queue' ,L_q, may be estimated from
experimental data, if the quantity of dispersed
phase held in the packing interstices is transformed
into a number of drops of characterisation diameter d_p,
which may be taken as the mean linear diameter of the
inlet dispersion.

The derivation of such 'length' is as follows:

$$\text{Saturation} = \frac{\text{volume of dispersed phase}}{\text{volume of pores}}$$

$$S = \frac{V_d}{V_{pores}}$$

$$V \text{ pores} = e_1 \cdot V_{packing}$$

$$\therefore \quad V_d = S \; e_1 \; V_{packing}$$

$$V_{packing} = \frac{\pi \; D^2 L}{4}$$

$$\therefore \quad V_d = \frac{1}{4}\pi S \; e_1 \; D^2 L \qquad (9.9)$$

assuming L_q: No. of drops, each of diameter d_p

$$V_d = \frac{1}{6}\pi d_p^3 \; L_q \qquad (9.10)$$

then

$$\frac{1}{6} \pi \; d_p^3 \; L_q = \frac{1}{4} \pi \; S \; e_1 \; D^2 L$$

$$\therefore \quad L_q = \frac{3}{2} \; S \; e_1 \; \frac{D^2}{d_p^3} \; L \qquad (9.11)$$

Calculating values of L_q, corresponding values
of γ could be predicted from a correlation relating
the variation of steady state queue length with
degree of balking.

A computer program with a subroutine to predict
γ was used to calculate L_q and λ_c and compare them
with λ_{exp} and is given in Appendix K.

Experimental values of filter coefficient λ_{exp} were
determined using the equation

$$\lambda_{exp} = \frac{-\text{Loge} \left[(1-\eta) \ (\frac{d_i}{d_o})^3 \right]}{L} \tag{9.12}$$

9.1.6 Comparison between the models

A comparison between the different models was
attempted based upon the set of data presented in Table
9.1 and the results are illustrated in Table 9.2. These
results show that the filter coefficient varies over
a magnitude of 800 for the different models. This is not
surprising in view of possible interactions between
operating parameters in the extremely complex coalescence
process. This variation leads to the necessity of
formulating a better expression for the filter coefficient
which takes into consideration all the parameters
affecting the coalescence process.

Parameter	Symbol	Value
Fibre Diameter	d_f	6, 9,25,50 100 μm
Superficial velocity	u	0.5×10^{-2} m/s
Dispersed phase density	ρ_d	867 kg/m^3
Continuous phase density	ρ_c	1000 kg/m^3
Dispersed phase viscosity	μ_d	0.58×10^{-3} Ns/m^2
Continuous phase viscosity	μ_c	1.0×10^{-3} Ns/m^2
Boltzman's constant	k'	1.38048×10^{-23} J/K
Absolute temperature	T	293 K
Hamaker constant	Q	0.401×10^{-20} J
Hydrodynamic function	A	$2 - \log_e N_{Re}$
Bed height	L	0.04 m
Single phase voidage	e_1	0.86

Table 9.1 Basic set of parameters used in

comparision of capture mechanisms

and filter coefficients

Model	Fibre Size, d_f (μm)			
	6	9	25	50
Vinson (55)	21	26	40	50
Rosenfeld (28)	17470	12480	5200	2770
Sherony (31)	2040	292	190	71
Spielman (32)	13840	5020	390	70
Austin (1)	145	220	240	660
Experimental	381	339	277	-

Table 9.2 Comparison of filter coefficients

predicted by different models

9.2 <u>THEORETICAL COMPARISON OF CAPTURE MECHANISMS</u>

As discussed in chapter 4, many mechanisms have
been proposed for drop capture within the coalescer.
The object now is to determine the relative contribution
of each of these mechanisms to the overall capture
efficiency under practical operating conditions. This
comparison will help to produce an equation for prediction
of the rate of drop capture in a coalescer.

Comparison was achieved by taking into consideration
the superficial velocity, fibre size and drop diameter.
The drop diameter was used as a variable since the
inlet dispersion was polydisperse, with drop sizes
ranging from 0.1 to 50 microns.

The basic set of data presented in Table 9.1
was used to determine the drop capture efficiencies
due to interception, London-Van der Waal's forces,
diffusion and sedimentation. Direct interception
mechanism was not included in the analysis since the
efficiencies cannot be compared directly. Inertial
impaction was also excluded since the density of the
drop phase was less than that of the continuous phase
density. The equations for estimation of the individual
mechanisms are summarised in Table 9.3. The calculations
were performed for a range of values of drop diameter
and superficial velocity within the experimental values.

Mechanisms	Characteristic Dimensionless Group	Equation for Capture Efficiency
Interception	Interception number, N_R	$\eta_I = \dfrac{1}{2A}\left[2(1+N_R)\log_e(1+N_R) + \dfrac{1}{(1+N_R)} - (1+N_R)\right]$
Direct Interception	Direct Interception number, N_{RD}	$\eta_{DI} = 1 : (N_{RD} > 1); \quad \eta_{DI} = 0 : (N_{RD} < 1)$
Inertial Impaction	Stokes' number, N_{Stk}	$\eta_{II} = \dfrac{N_{Stk}^3}{N_{Stk}^3 + 0.77\, N_{Stk}^2 + 0.22}$
Sedimentation	Gravity number, N_G	$\eta_G = -N_G$
London Forces	Adhesion number, N_{Ad}	$\eta_L = \dfrac{N_R^2}{A}\left[\dfrac{3\pi A}{2} N_{Ad}\right]^{1/3}$
Diffusion	Peclet number, N_{Pe}	$\eta_D = 2.17\,(2A)^{-1/3}\,(N_{Pe})^{-2/3}$

Table 9.3 Dimensionless Groups and Equations used in Capture Mechanism Evaluation

A computer program, listed with the output in Appendix D, was used to facilitate the calculations.

The overall efficiency is given as:

$$\eta_T = \eta_I + \eta_D + \eta_G + \eta_L \qquad (9.13)$$

Table 9.4 shows the significance of the different mechanisms when the individual contribution is greater than an arbitary 4% of the total efficiency. These values were calculated for fibre diameters of 6, 9, 25, 50, and 100 μm. The results show that all the four mechanisms investigated were relevant to the coalescence of secondary dispersions at the range of velocities used in this study.

Fig. 9.1 shows the variation of total capture efficiency with velocity for different drop sizes at a fibre size of 25 μm. Increasing the velocity is predicted to decrease the total capture efficiency gradually to an almost constant value, except for 0.1 μm drops; in which only diffusion and London-Van der Waal's forces predominate. Going a step further and examining the variation of capture efficiency with velocity at a specific drop diameter indicates that at high velocities, interception is predominant and almost constant, whilst at low velocities, diffusion, London forces and interception predominate and decrease with increase of velocity. This is shown in Fig. 9.2. A plot of the variation of

Drop Diameter d_p (μm)	Superficial velocity, u ($\times 10^{-2}$ m/s)					
	0.1	0.33	0.66	0.99	1.3	1.66
0.1	DL	DL	DL	DL	DL	DL
1	IDL	IDL	IDL	IL	IL	IL
5	IL	IL	IL	IL	I	I
10	IL	I	I	I	I	I
20	IS	I	I	I	I	I
30	IS	I	I	I	I	I
50	IS	I	I	I	I	I

Table 9.4 (a) Significance of different drop capture mechanisms at 4% contri-
bution level for the range of velocities and drop diameters
encountered in this study (d_f = 6 μm)

Key: I : interception,   S : Sedimentation

        D : Diffusion   L : London-Van der Waal's

Drop Diameter d_p (µm)	Superficial velocity, u($\times 10^{-2}$ m/s)					
	0.1	0.33	0.66	0.99	1.3	1.66
0.1	DL	DL	DL	DL	DL	DL
1	IDL	IDL	IDL	IDL	IDL	IDL
5	ILS	IL	IL	IL	IL	IL
10	ILS	IL	IL	IL	I	I
20	ILS	I	I	I	I	I
30	IS	I	I	I	I	I
50	IS	I	I	I	I	I

Table 9.4(b) Significance of different drop capture mechanisms for $d_f = 9$ µm

Drop Diameter d_p (μm)	Superficial Velocity, $u(\times 10^{-2}$ m/s)					
	0.1	0.33	0.66	0.99	1.3	1.66
0.1	D	DL	DL	DL	IDL	DL
1	IDSL	IDL	IDL	IDL	IDL	IDL
5	ISL	ISL	IL	IL	IL	IL
10	ISL	ISL	IL	IL	I	I
20	IS	IS	IS	I	I	I
30	IS	IS	IS	I	I	I
50	IS	IS	IS	I	I	I

Table 9.4.(c) Significance of different drop capture mechanism for d_f = 25 μm

Drop Diameter d_p (µm)	Superficial Velocity, $u(\times 10^{-2}$ m/s)					
	0.1	0.33	0.66	0.99	1.3	1.66
0.1	D	DL	DL	DL	DL	DL
1	IDSL	IDSL	IDL	IDL	IDL	IDL
5	ISL	ISL	ISL	ISL	IL	IL
10	ISL	ISL	ISL	ISL	ISL	IL
20	IS	ISL	IS	IS	IS	I
30	IS	IS	IS	IS	IS	I
50	IS	IS	IS	IS	IS	I

Table 9.4(d) Significance of different drop capture mechanisms for d_f = 50 µm

Drop Diameter d_p (μm)	Superficial Velocity, $u(\times 10^{-2}$ m/s)					
	0.1	0.33	0.66	0.99	1.3	1.66
0.1	D	DL	DL	DL	DL	DL
1	IDLS	IDLS	IDLS	IDL	IDL	IDL
5	IDLS	IDLS	ILS	ILS	ILS	ILS
10	ILS	ILS	ILS	ILS	ILS	ILS
20	IS	ILS	IS	IS	IS	IS
30	IS	IS	IS	IS	IS	IS
50	IS	IS	IS	IS	IS	IS

Table 9.4(e) Significance of different drop capture mechanisms for d_f = 100 μm
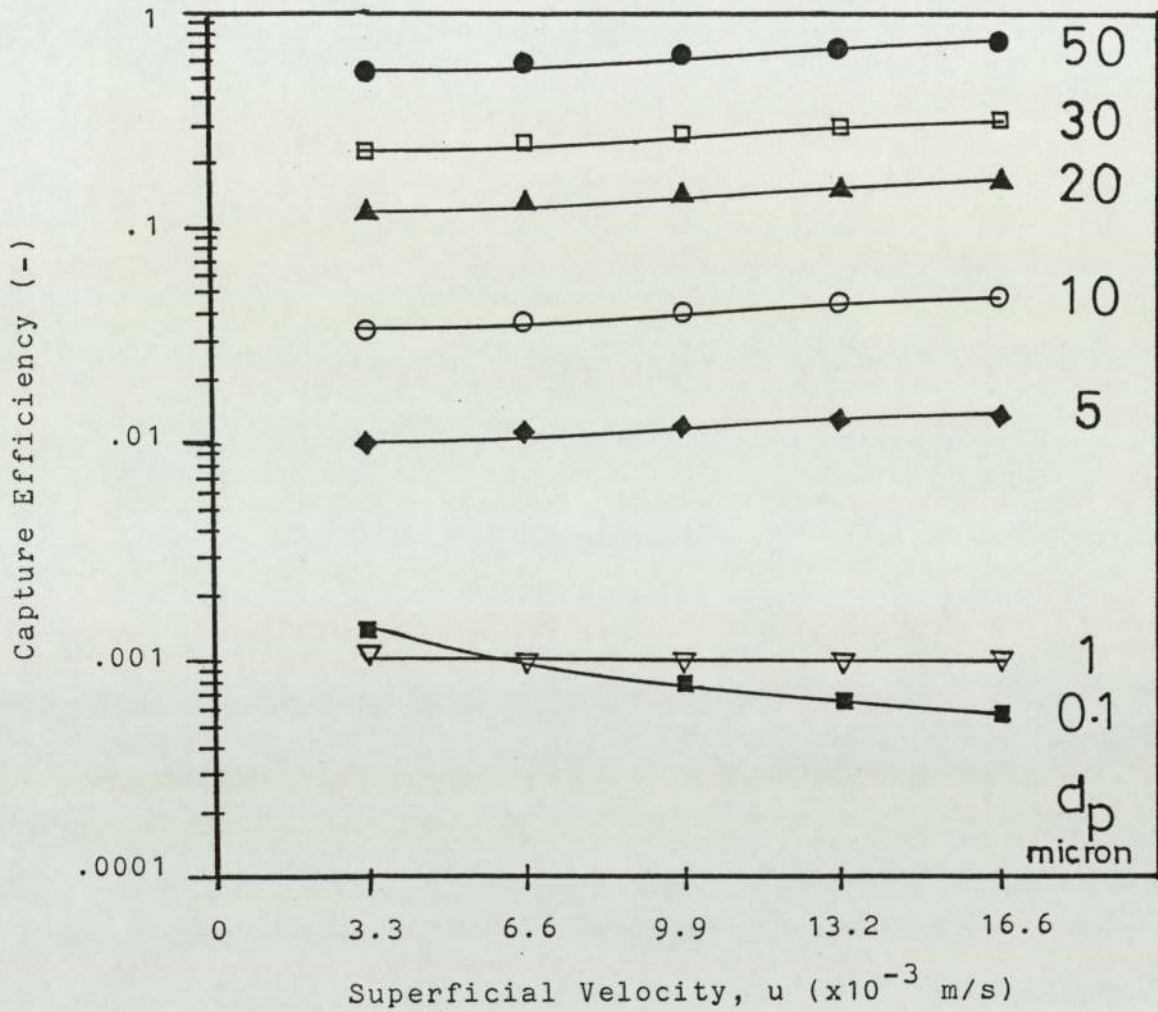
FIG. 9.1 VARIATION OF TOTAL CAPTURE EFFICIENCY WITH
VELOCITY FOR DIFFERENT DROP SIZES AT 25 μm FIBRE SIZE
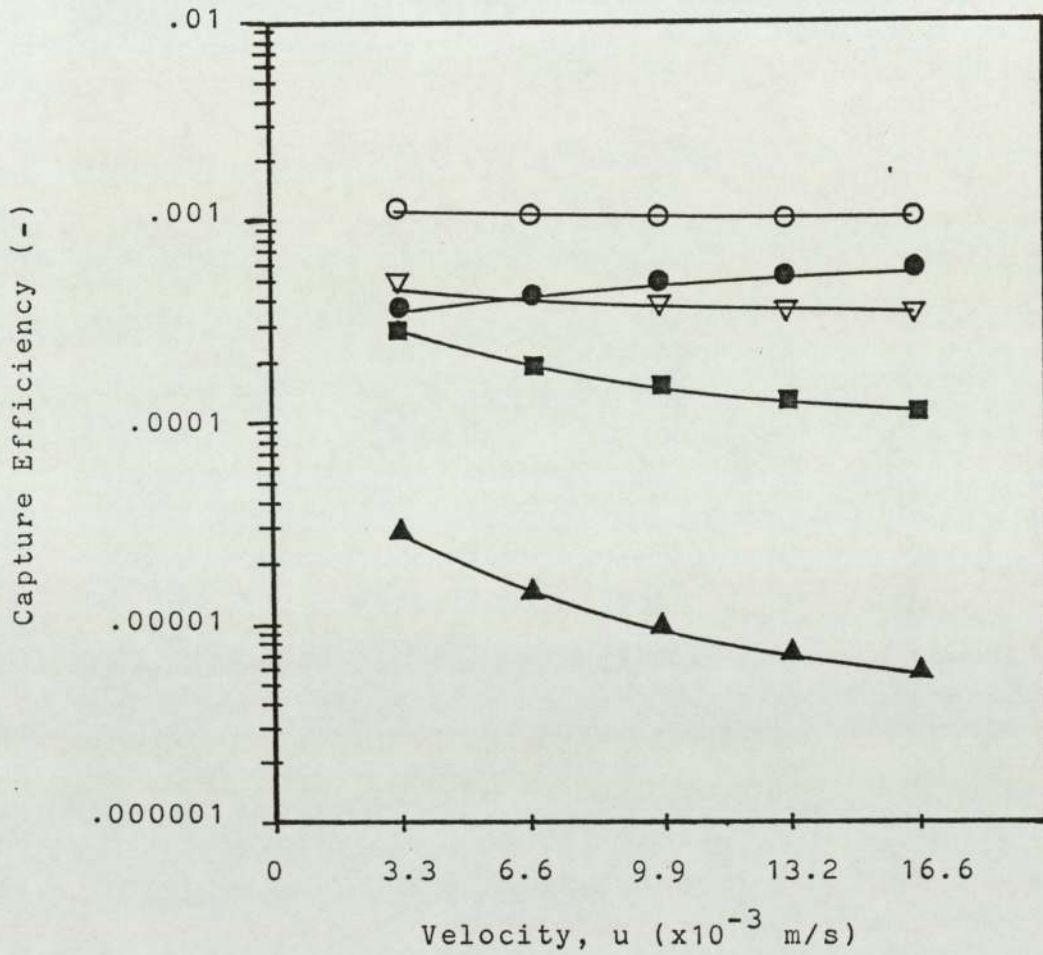
FIG. 9.2 VARIATION OF CAPTURE EFFICIENCY
WITH VELOCITY AT 1 μm DROP SIZE

MECHANISM

● INTERCEPTION   ■ DIFFUSION

▲ SEDIMENTATION   ▽ LONDON FORCES

○ TOTAL EFFICIENCY
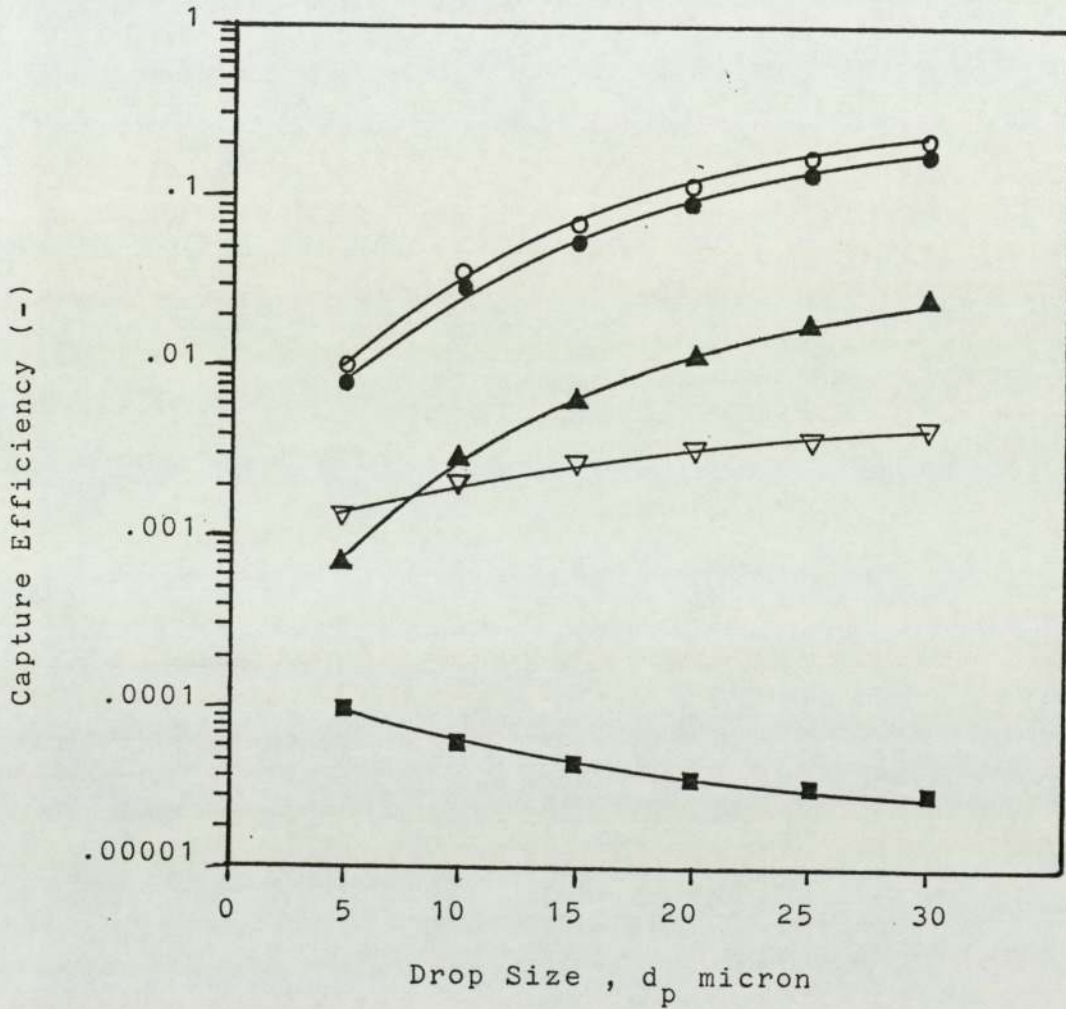
FIG. 9.3 VARIATION OF CAPTURE EFFICIENCY WITH DROP SIZE AT 3.3×10^{-3} M/S VELOCITY

MECHANISM

- INTERCEPTION
- SEDIMENTATION
- O TOTAL EFFICIENCY

- DIFFUSION
- ▽ LONDON FORCES

capture efficiency with drop size at 0.0033 m/s,
Fig. 9.3 exhibits a minimum efficiency since diffusion
is significant for small drops but interception and
sedimentation are responsible for increased high
capture efficiency as the drop size increases.

9.2.1 Screening of Mechanisms

The theoretical results were examined further
in order to formulate an expression representing the
capture efficiency, for the range of variables
investigated in this study.

Table 9.4 indicates that diffusion mechanism is
predominant only for drops smaller than 1 µm; thus
this mechanism need not be considered further.

At high velocities, e.g 0.01 m/s, the contri-
bution of interception mechanism is always higher than
90% of the overall contribution, whilst that of
sedimentation is almost zero, as shown in Fig. 9.4.
But at lower velocities ، Fig 9.5 ، the contribution
of sedimentation increases to about 30% and that of
interception decreases to 70% . This suggests that
sedimentation make a significant contribution for fibre
sizes greater than 50 µm at all drop sizes in the
range 1 to 50 µm, Fig. 9.6. This is also true for
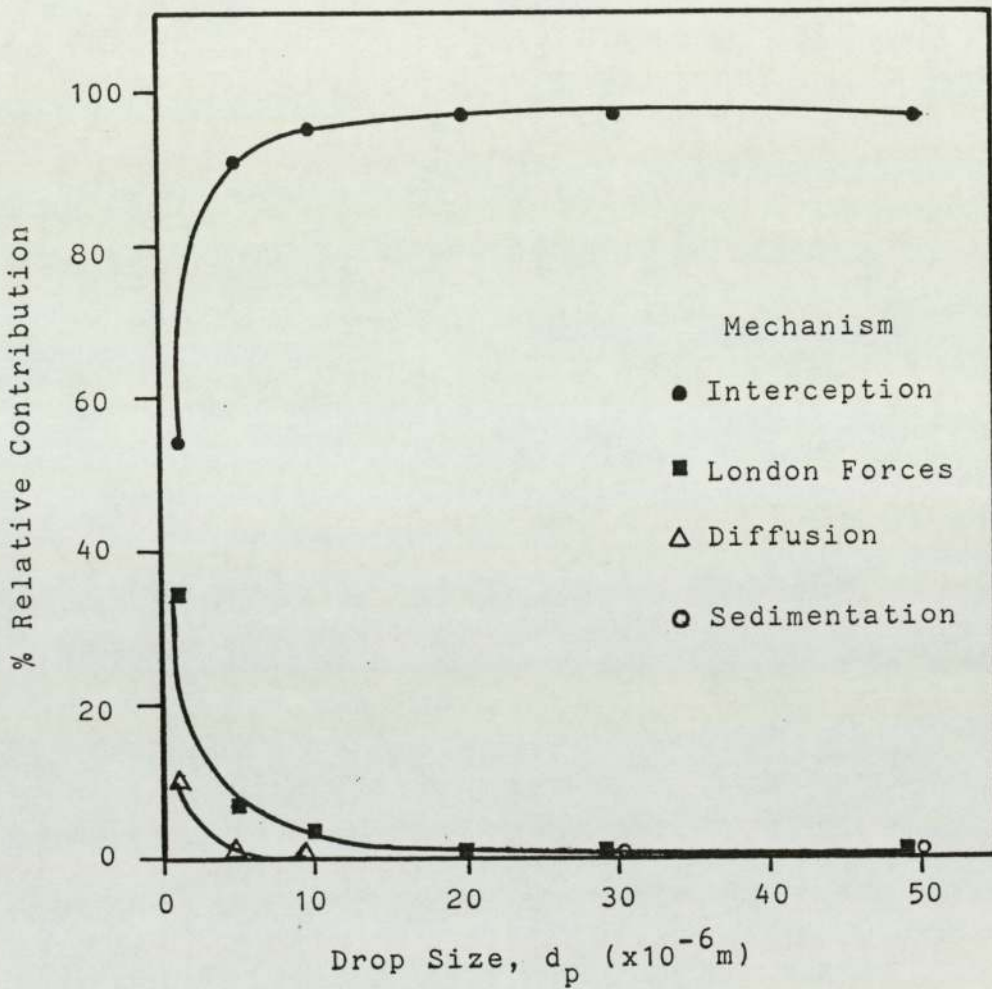
FIG. 9.4 EFFECT OF DROP SIZE ON % RELATIVE
CONTRIBUTION OF CAPTURE EFFICIENCY FOR
d_f = 25 μm AT HIGH VELOCITY (U = 16.6x10^{-3}M/S)
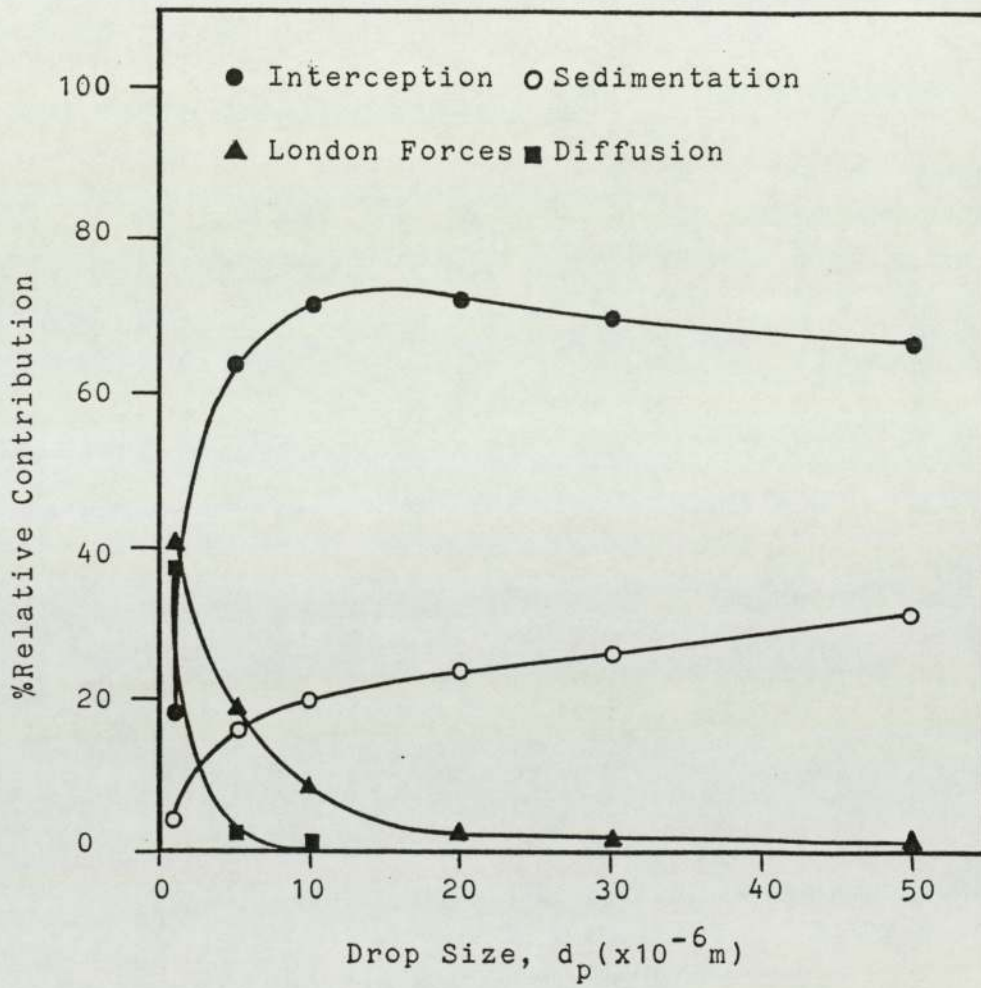
FIG. 9.5 EFFECT OF DROP SIZE ON % RELATIVE CONTRIBUTION
OF CAPTURE EFFICIENCY FOR d_f = 25 μm AT LOW VELOCITY
(U = 10^{-3} M/S)
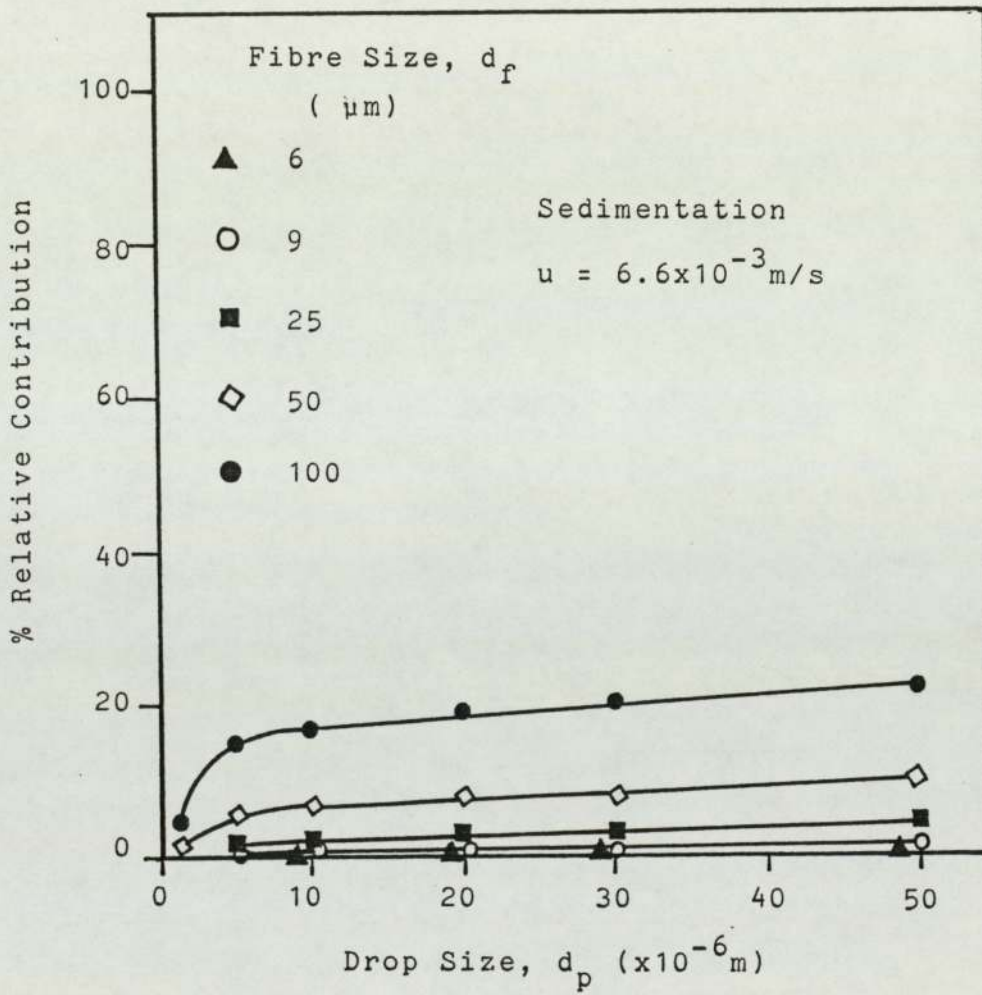
FIG. 9.6 EFFECT OF FIBRE SIZE ON CAPTURE EFFICIENCY BY
SEDIMENTATION MECHANISM AT DIFFERENT DROP SIZES.

velocities lower than 0.01 m/s with the same range of fibre
size, Fig. 9.7. Since the coalescence process produces
larger drops, the effect of this mechanism should not be
neglected.

The contribution of interception mechanism increases with
the decrease of fibre size at a certain drop size, Fig. 9.8,
and at a certain velocity, Fig. 9.9.

London-Van der Waal's forces are only significant when
the overall efficiency is less than 0.001, Fig. 9.2, and at
drop size less than 5 μm, Fig. 9.4.

In conclusion the interception and sedimentation mechani-
sms are the two to be considered within the range of velocities,
drop sizes and fibre sizes used in this study.

In order to account for the combined effect of these
two mechanisms Prieve and Ruckenstein (102) showed that
it may be represented by:

$$n_{GI} = n_G + n_I \tag{9.14}$$

Emi (103) proposed the following equation:

$$n_{GI} = \frac{1+N_R}{1+N_G} \left[\frac{1}{2A} \left(\frac{1}{(1+N_R)^2} - 1 + \log_e (1+N_R)^2 \right) + N_G \right] \tag{9.15}$$
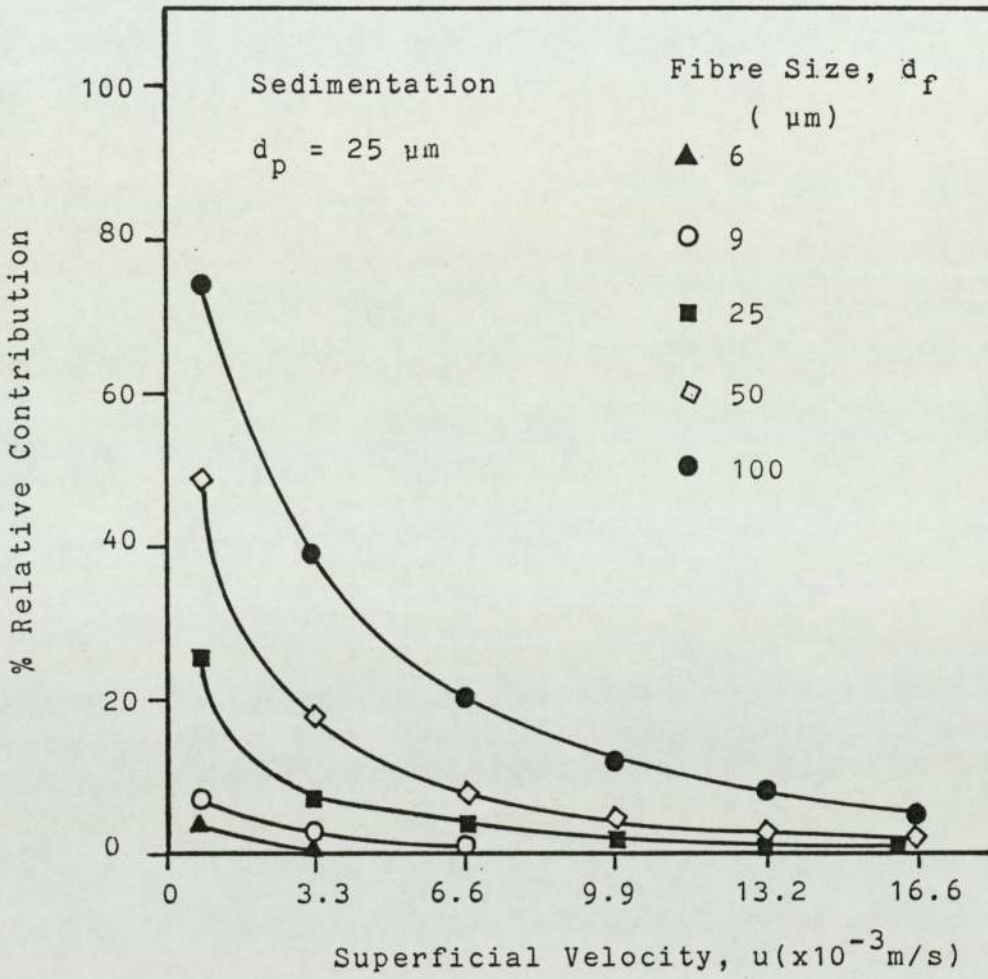
FIG. 9.7 EFFECT OF FIBRE SIZE ON CAPTURE EFFICIENCY
BY SEDIMENTATION MECHANISM AT DIFFERENT VELOCITIES.
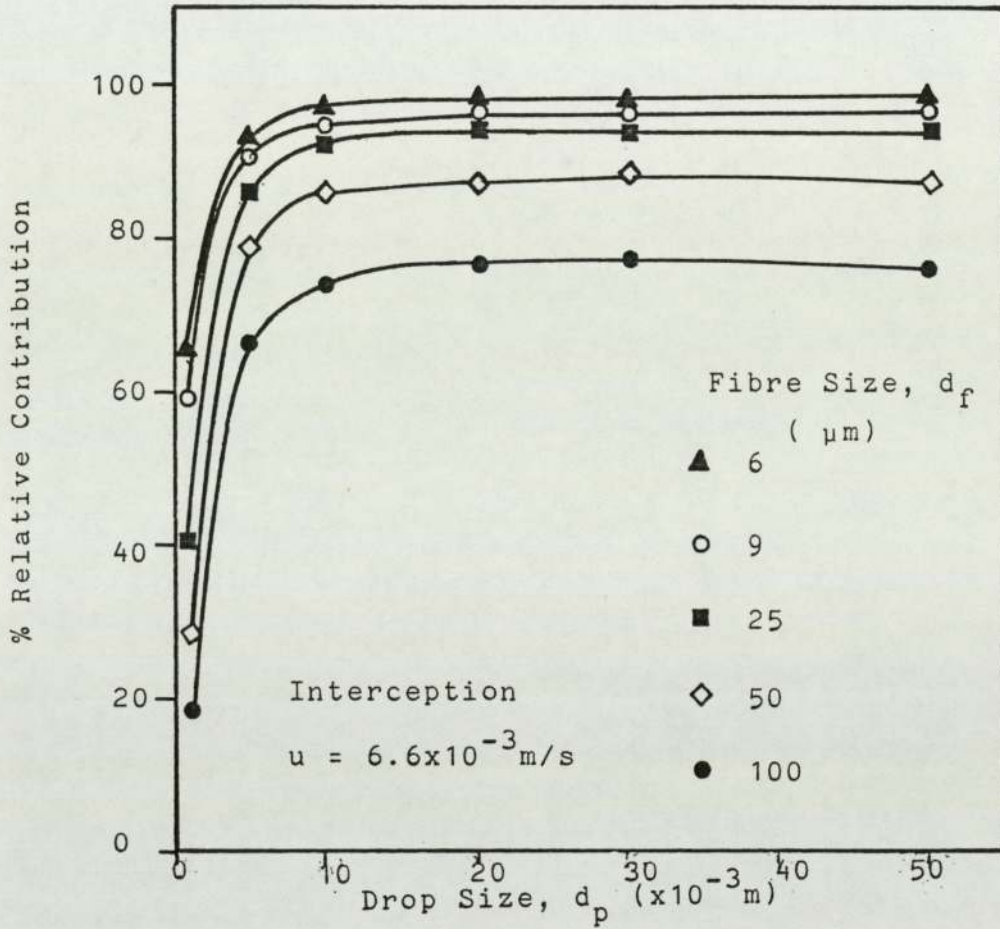
FIG. 9.8 EFFECT OF FIBRE SIZE ON CAPTURE EFFICIENCY BY
INTERCEPTION MECHANISM AT DIFFERENT DROP SIZES.
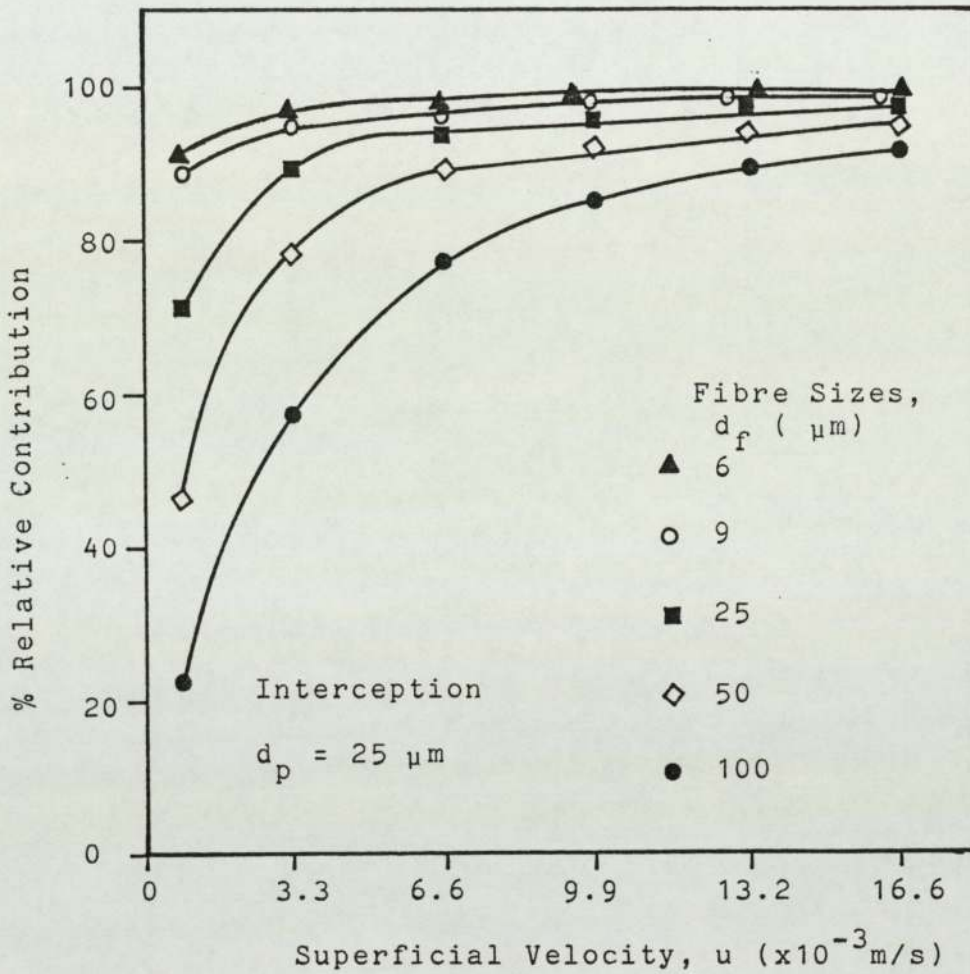
FIG. 9.9 EFFECT OF FIBRE SIZE ON CAPTURE EFFICIENCY BY
INTERCEPTION MECHANISM AT DIFFERENT VELOCITIES.

Pich (104) investigated the variation of capture by gravity forces with the angular position of a particle relative to a collector, and suggested an alternative form:

$$\eta_{GI} = \eta_I + \eta_G + N_R \, N_G \qquad (9.16)$$

According to the results of this study, sedimentation was most significant when the velocity was 0.66×10^{-2} m/s, the drop diameter 30 μm and fibre diameter 25 μm.

Then from table 9.3 N_R = 1.2

$$N_{Re} = 0.165$$

$$N_G = -0.015$$

$$\eta_I = 0.2268$$

$$\eta_G = 0.015$$

For the combined effects of interception and sedimentation,

From equation (9.14) η_{GI} = 0.24

From equation (9.15) η_{GI} = 0.197

From equation (9.16) η_{GI} = 0.224

From these results, the expression proposed by Emi yields a negative effect by combining the mechanisms, which cannot be valid. Pich's equation gives an efficiency which differs by only 6% from the efficiency obtained using the additivity rule. Therefore, Pitch's equation (9.16) was selected

as the equation for calculation of the drop capture
efficiency.

9.3 RATE OF DROP CAPTURE

It is important to formulate an expression
representing the rate of drop capture within the fibrous
bed coalescer. A material balance of droplets over a
bed consisting of uniform cylindrical fibres, of height
dl and a change dn in dispersed drop number concentration
would give

$$- u \frac{dn}{dl} = j \left(\frac{\alpha}{\frac{\pi}{4} d_f^2 \cdot L_f} \right) \qquad (9.17)$$

where α is the volume fraction of solids and j is the
average rate of drop capture by cylindrical fibres.
The filter coefficient λ is defined by:

$$- \frac{dn}{dl} = \lambda n \qquad (9.18)$$

and the dimensionless fibre collection efficiency as:

$$\eta = \frac{j}{\frac{\pi}{4} d_f^2 u n} \qquad (9.19)$$

Then $\qquad j = \frac{\pi}{4} d_f^2 \eta u n \qquad (9.20)$

Substitution for λ and j in equation (9.17) gives

$$\lambda = \frac{\eta \alpha}{L_f} \qquad (9.21)$$

Integration of equation (9.18) over a depth
of bed $0 \rightarrow L$ gives

$$\lambda = \frac{-\log_e(\frac{n_1}{n_o})}{L} \qquad (9.21)$$

where n_o and n_1 are the inlet and outlet drop density
numbers entering and leaving a depth of bed L.
Substituting and rearranging for n_1 in equation (9.21)

$$n_1 = n_o e^{-(\frac{\alpha \eta L}{L_f})} \qquad (9.22)$$

Whilst the fibre diameter is not included in
equation (9.22), it is included in the calculation
of capture efficiency η .

The capture efficiencies discussed in section
9.2 were based upon the projected area of the fibres
and therefore the efficiency of a single layer η_i is
related to the fractional open area of fibres,

$$\eta_i = \eta \left(1 - (\frac{d_a}{d_a + d_f})^2\right) \qquad (9.23)$$

In order to analyze the rate of drop capture within
the coalescer with respect to the height, the inlet
drop size distribution curve, Fig. 6.2 was fitted
to a distribution function by polynomial regression

and the resulting expression was employed to calculate
the number of drops in each drop diameter interval
(2 μm). The total capture rate for a fibre layer of
height 1 was calculated by application of equations
(9.13) and (9.23). The number of drops, n_1, leaving
the bed interval was then obtained using equation
(9.22). Assuming no drop redispersion, n_1 was used
as the input of suspended drops to the next interval
of bed depth and a new value of n_1 was obtained. This
set of calculations was repeated, using a computer
program, for a bed of 20×10^{-2} m bed height. The listing
of the program and a specimen set of results are presented
in Appendix E. Fig. 9.10, plotted from the program
output, shows the removal rate of suspended drops as
a function of bed depth. Increasing the value of velocity
decreases the rate of drop capture to a minimum after
which, any further increase in velocity does not cause
a further decrease in drop capture. As discussed in
section 9.2, at high velocities, interception is the
predominant capture mechanism and this is independent
of velocity. Hence there is a minimum capture efficiency
and thus a minimum rate of drop removal, supporting
the predictions in Figure 9.10.

9.4 TWO PHASE PRESSURE DROP PREDICTION

Many workers have attempted to predict two phase
pressure drop in packed beds. Their trials were
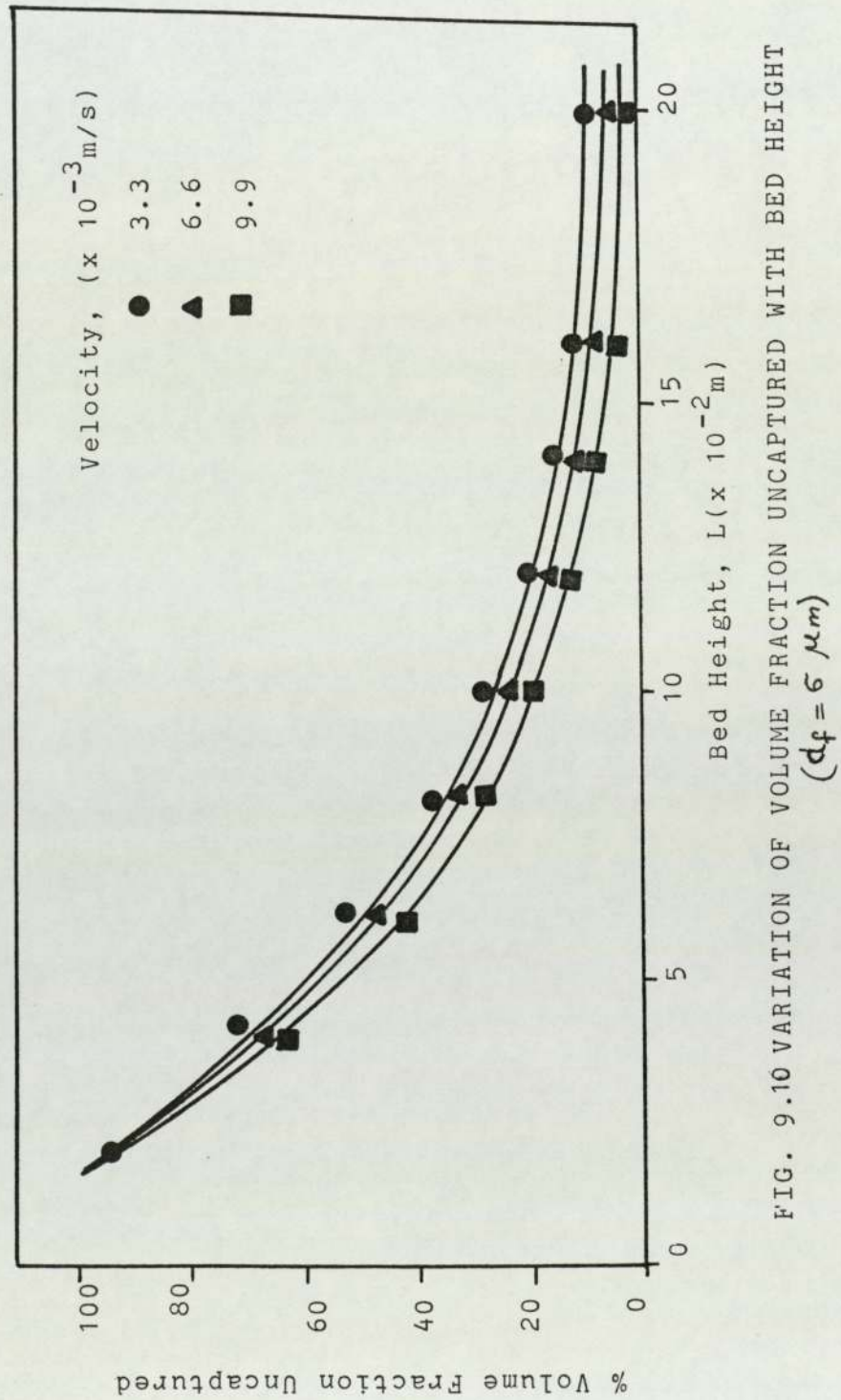
FIG. 9.10 VARIATION OF VOLUME FRACTION UNCAPTURED WITH BED HEIGHT
$(d_f = 6 \mu m)$

restricted to the assumption of constant saturation
throughout the length of the bed. Sherony (31)
proposed an equation based on the Blake-Kozeny equation,

$$\frac{\Delta P_2}{\Delta P_1} = \frac{(1 - e_1 (1-\bar{S}))^2}{(1-e_1)^2 (1-\bar{S})^3} \qquad (9.24)$$

Rosenfeld and Wasan (28) suggested a more simplified
equation

$$\frac{\Delta P_2}{\Delta P_1} = (1 + \frac{e_1 \bar{S}}{1-e_1})^{2/3} \qquad (9.25)$$

where $\bar{S}$ is correlated with superficial velocity using,

$$\bar{S} = \frac{C(1-e_1)u^n}{e_1} \qquad (9.26)$$

C and n have been determined to be 0.8 and 0.2
respectively when u is measured in ft/min. However,
contrary to the experimental results these models
predict that the pressure drop ratio is independent
of bed depth.

9.4.1 Derivation of Proposed Equation

Based on the Blake-Kozeny equation, an expression
can be formulated to predict the two phase pressure
drop. In this study, during two phase flow, the fibrous
bed consists of a mixture of 'cylinders' and 'spheres'
which possess different values of specific area, a.

Derivation of this specific area is given in Appendix F.

For single phase flow through an element of
bed depth δl, the Blake-Kozeny equation can be written as:

$$\frac{\delta P_1}{\delta l} = \frac{k\ \mu_c u(1-e_1)^2 a_1^2}{e_1^3} \tag{9.27}$$

Where a_1 = specific surface of the bed consisting of
a mixture of 'cylinders' and 'spheres'.

Rewriting equation (9.27) by analogy for two
phase flow:

$$\frac{\delta P_2}{\delta l} = \frac{k\ \mu_c u(1-e_2)^2 a_2^2}{e_2^3} \tag{9.28}$$

where $e_2 = e_1 (1 - s)$

and $\qquad a_2 = \dfrac{\left[\dfrac{6e_1 S}{d_p} + \dfrac{4(1-e_1(1-S))}{d_f}\right]}{1-e_1(1-S)}$

Substituting for e_2 and a_2 into (9.28) and taking
the limit as $\delta l \to o$

$$dp_2 = \frac{k\ \mu_c u}{e_1^3} \cdot \frac{\left[\dfrac{6\ e_1 S}{d_p} + \dfrac{4}{d_f}(1-e_1(1-S))\right]^2}{(1-S)^3}\ dl \tag{9.29}$$

The total two phase pressure drop may hence be
determined by integration of equation (9.29) between
the limits of 0 and L.

$$\Delta P_2 = \frac{k \; \mu_c u}{e_1^3} \int_0^L \frac{\left[\frac{6e_1 S}{d_p} + \frac{4}{d_f}(1-e_1(1-S)) \right]^2}{(1-S)^3} \; dl \qquad (9.30)$$

Similarly from equation (9.27)

$$\Delta P_1 = \frac{16 \; k\mu_c u(1-e_1)^2 L}{d_f^2 \; e_1^3}$$

then $\dfrac{\Delta P_2}{\Delta P_1} = \dfrac{d_f^2}{16(1-e_1)^2 L} \displaystyle\int_0^L f(S) \; dl \qquad (9.31)$

where $f(s) = \dfrac{\left[\dfrac{6 \; e_1 S}{d_p} + \dfrac{4}{d_f} (1 - e_1(1-S)) \right]^2}{(1 - S)^3} \qquad (9.32)$

by letting $a' = \dfrac{6}{d_p}$, $b' = \dfrac{4}{d_f}$

then the numerator of the right-hand side of equation
(9.32) becomes $(a'e_1 S + b'(1-e_1 + e_1 S))^2$ and after
rearrangement, $(e_1(b'+a')S + b'(1-e_1))^2$

Let

$$d' = e_1(b' + a') \; , \quad e' = b'(1-e_1)$$

$\therefore \quad f(S) = \dfrac{(d'S + e')^2}{(1-S)^3}$

$$f(s) = \frac{d'^2 S^2 + 2 \; d'e'S + e'^2}{(1 - S)^3}$$

Let $a = d'^2$, $b = 2d'e'$, $C = e'^2$

Due to discontinuity in mathematical description
of the saturation profiles the integration cannot
be performed in one stage.

when $\qquad 0 < 1 < L_I$, $\quad S = S_I$

$$\therefore \quad \int_0^{L_I} F(s)\, dl = \left[\frac{a\, S_I^2 + b\, S_I + C}{(1 - S_I)^3} \right] L_I \qquad (9.33)$$

but when $L_I \leq 1 \leq L$, $\quad S = (S_I - S_E) e^{-k(1-L_I)} + S_E$

let $\qquad g = (S_I - S_E), \quad h = S_E$

and substituting $\quad V = g\, e^{-k(1-L_I)} + h$

$$\frac{dV}{dl} = -k\, g\, e^{-k(1-L_I)}$$

$$dl = -\frac{d\, V}{k(v-h)}$$

when $1 = L_I$, $\quad V = g + h$

$\qquad 1 = L$, $\quad V = g\, e^{-k(L-L_I)} + h$

$$\therefore \quad \int_{L_I}^{L} f(s)\, dl = \int_{g+h}^{g\, e^{-k(L-L_I)} + h} f(V)\, \frac{-dV}{k(V-h)}$$

$$= \frac{1}{k} \int_{g\, e^{-k(L-L_I)} + h}^{g+h} \frac{aV^2 + bV + C}{(v-h)(1-v)^3} \cdot dv \qquad (9.34)$$

Evaluation of the integral given by equation
9.34 has been completed in Appendix G.

The final result of the integration is lengthy, but is quite feasible since this is an analytical solution. The total pressure drop ratio across the bed will be predicted using,

$$\frac{\Delta P_2}{\Delta P_1} = \frac{d_f^2}{16(1-e_1)L} \int_0^{L_I} F(s)dl + \int_{L_I}^{L} f(s) \, dl \qquad (9.35)$$

where $\int_0^{L_I} F(s) \, dl$ is determined using equation (9.33)

and $\int_{L_I}^{L} f(s) \, dl$ is determined using equation G.7

9.5 PREDICTION OF SATURATION PROFILES

From a study of the coalescence of oil-in-water suspensions by flow through porous media, Spielman and Su (19), suggested that the total saturation at any point in a coalescing bed is equal to the sum of three distinct regimes; initially captured drops s''', an intermediate phase of coalescing drops, s'', and a continuum of the dispersed phase flowing in capillaries to the exit face, s'

$$\text{i.e.} \qquad S = s''' + s'' + s' \qquad (9.36)$$

A qualitative representation of these regimes is illustrated in Fig. 9.11.

.
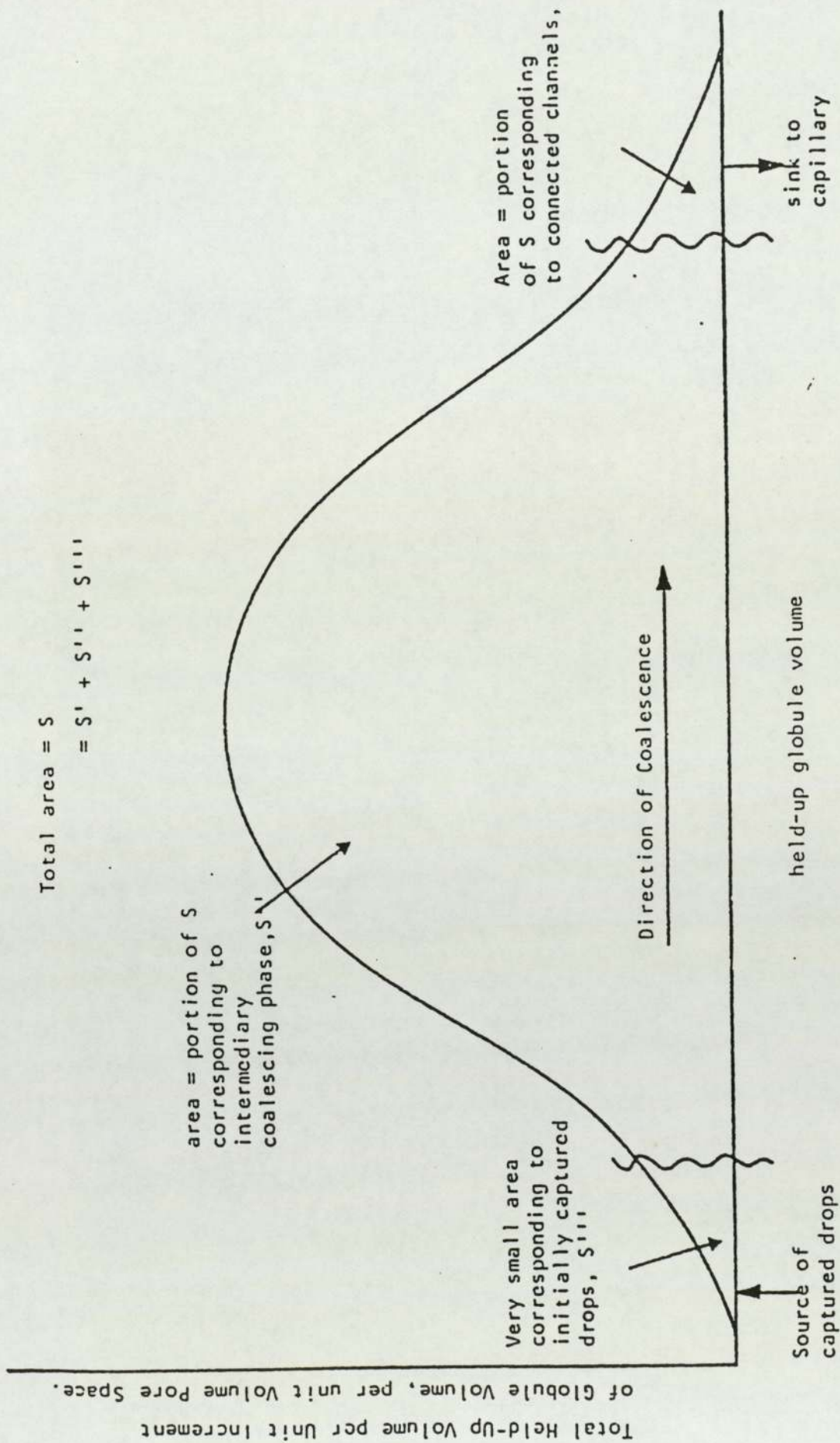
Figure 9.11 Qualitative distribution of the total volume of held-up oil over individual held-up globule volumes. Drops are captured at the left hand of the spectrum. Dispersed phase is transferred to successively larger drops by coalescence eventually leaving capillary conduction at the right.

Based on general trends shown by experimental data, Austin (1) proposed an idealised saturation profile, illustrated in Fig. 9.12. A small length, L_I where the saturation has a constant value, S_I was proposed. This constant saturation is assumed to be independent of velocity. Subsequently the saturation profile decays exponentially at a rate characterised by the value of the decay factor, k, which is a function of velocity. The decrease continues until a final value of saturation, S_E is reached which is dependent on velocity.

$$\text{i.e.} \qquad S = S_I \qquad 0 < 1 \leq L_I$$

$$S = (S_I - S_E)\ e^{-k(1-L_I)} + S_E \qquad L_I \leq 1 \leq L \qquad (9.37)$$

The average saturation at steady state, $\bar{S}$, was determined by the integration of the profile between 0 and the total height of the bed, L. The integration ,shown in Appendix H , is given as

$$\bar{S} = S_E + (S_I - S_E)\ \frac{L_I}{L} + \frac{(S_I - S_E)}{kL}(1 - e^{-k(L-L_I)})\qquad (9.38)$$

In order to evaluate the parameters S_E and k, it is necessary to estimate the values of the inlet saturation, S_I and the height L_I.

$$S = (S_I - S_{E1})e^{-k_1(I-L_I)} + S_{E1}$$

$$S = (S_I - S_{E2})e^{-k(I-L)} + S_{E2}$$

$$S = (S_I - S_{E3})e^{-k_3(I-L_I)} + S_{E3}$$

Increasing velocity, u

Bed depth

S

S_I

S_{E1}

S_{E2}

S_{E3}

L_I

0
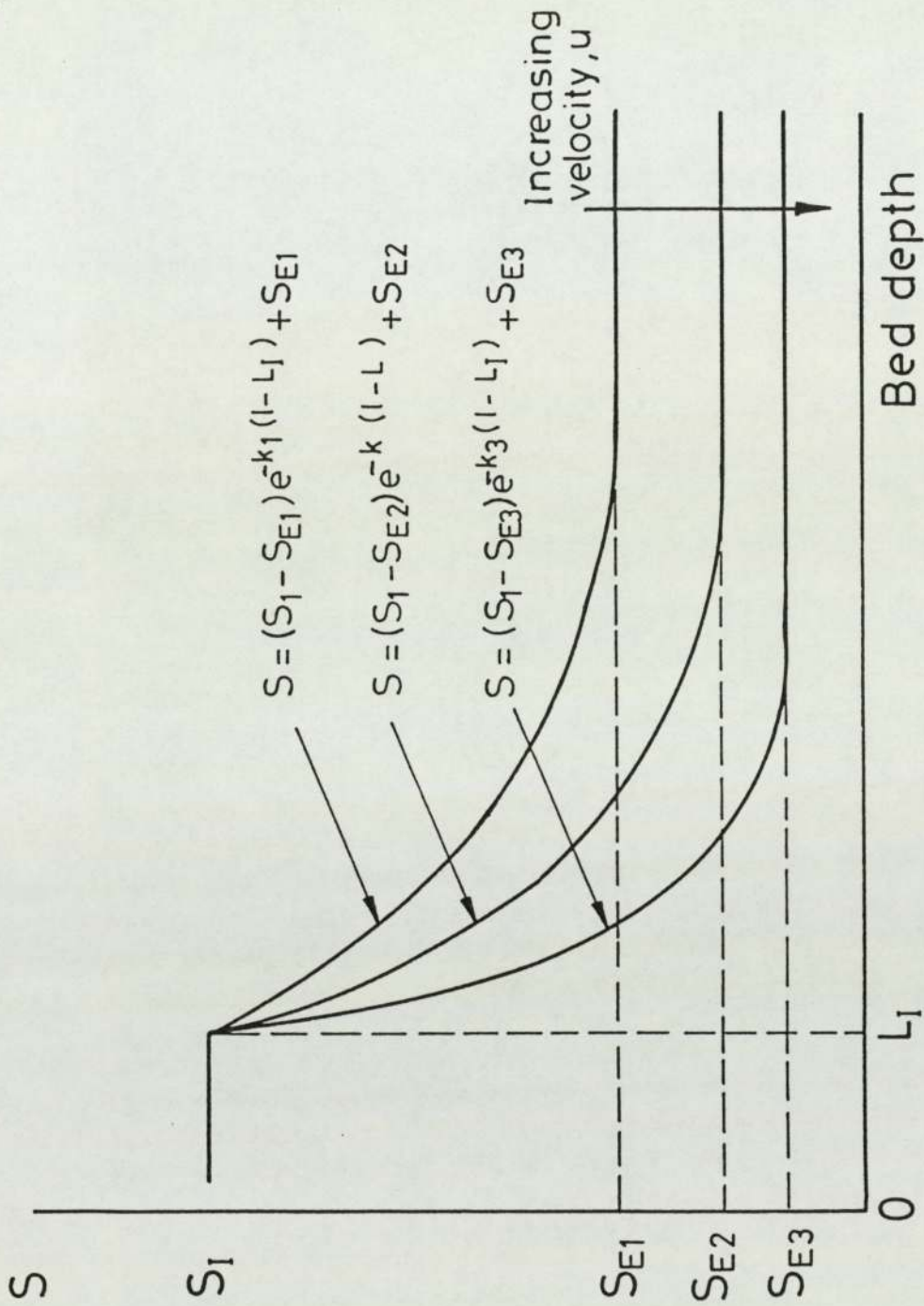
Figure 9.12 Idealised saturation profiles

Referring to equation (9.35), the pressure drop data could be used to find the values of parameters S_E and k. To do this the value of L_I was assumed to be equal to twice the fibre diameter, i.e. the fibre bed was assumed to have the thickness of two fibres. Brown (95) gives a correlation between void fraction and the diameter ratio, $\frac{d_p}{d_a}$, Fig. 9.13. For an average drop size of 25 μm and aperture diameter of 50 μm, $\frac{d_p}{d_a}$ = 0.5 which gives, for smooth cylinders as in the present case, e_p = 0.56 corresponding to a saturation of 0.44. This value is in close agreement with the data of Poleo (14) and will be used as an initial estimate of S_I.

Inspection of equation (9.38) shows that if the parameter, k is large, then the decay will approximate to a step change in saturation at L_I from S_I to S_E and equation (9.38) becomes

$$\bar{S} \simeq S_E + (S_I - S_E) \frac{L_I}{L} \quad \text{for large k} \qquad (9.39)$$

A computer program was used to determine S_E and k and then the saturation profile. The program listing and sample results are given in Appendix I. The saturation profile is shown in Fig. 9.14 for different velocities. S_E and k were both found to decrease as velocity increased.
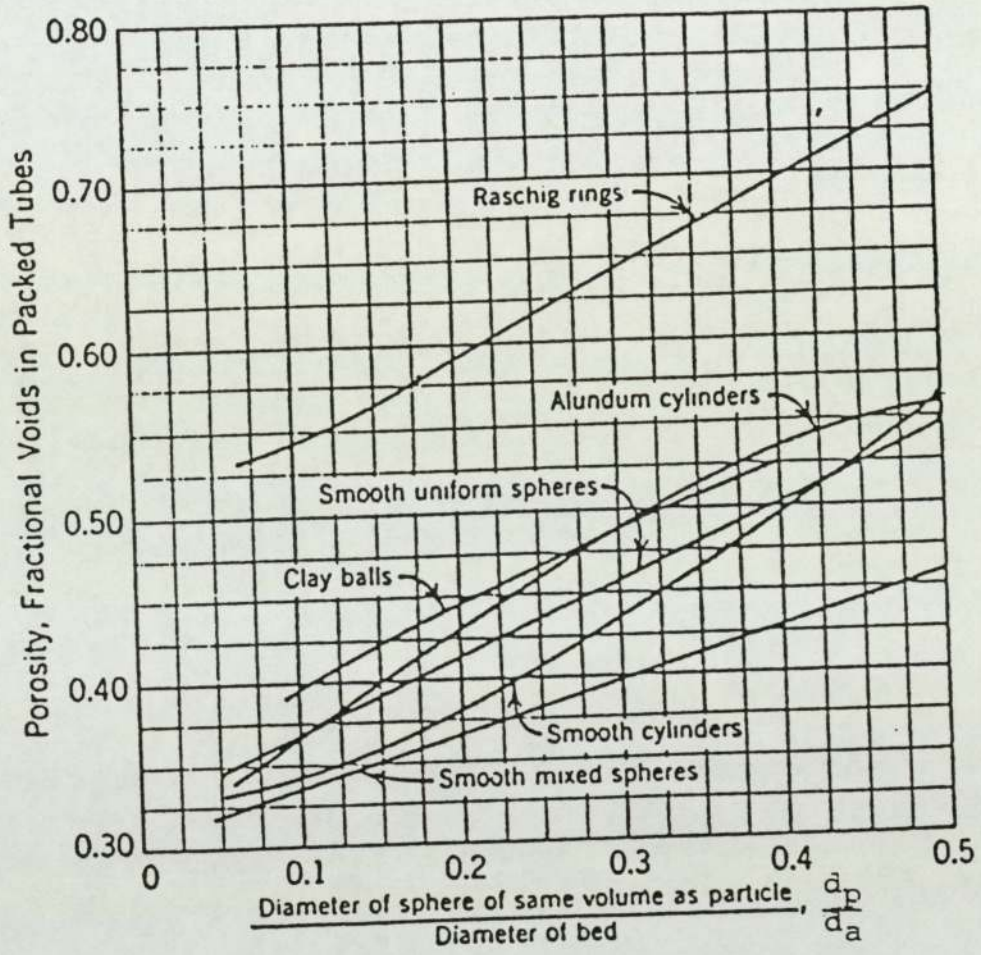
Fig. 9.13   Porosity as a function of the ratio of diameters
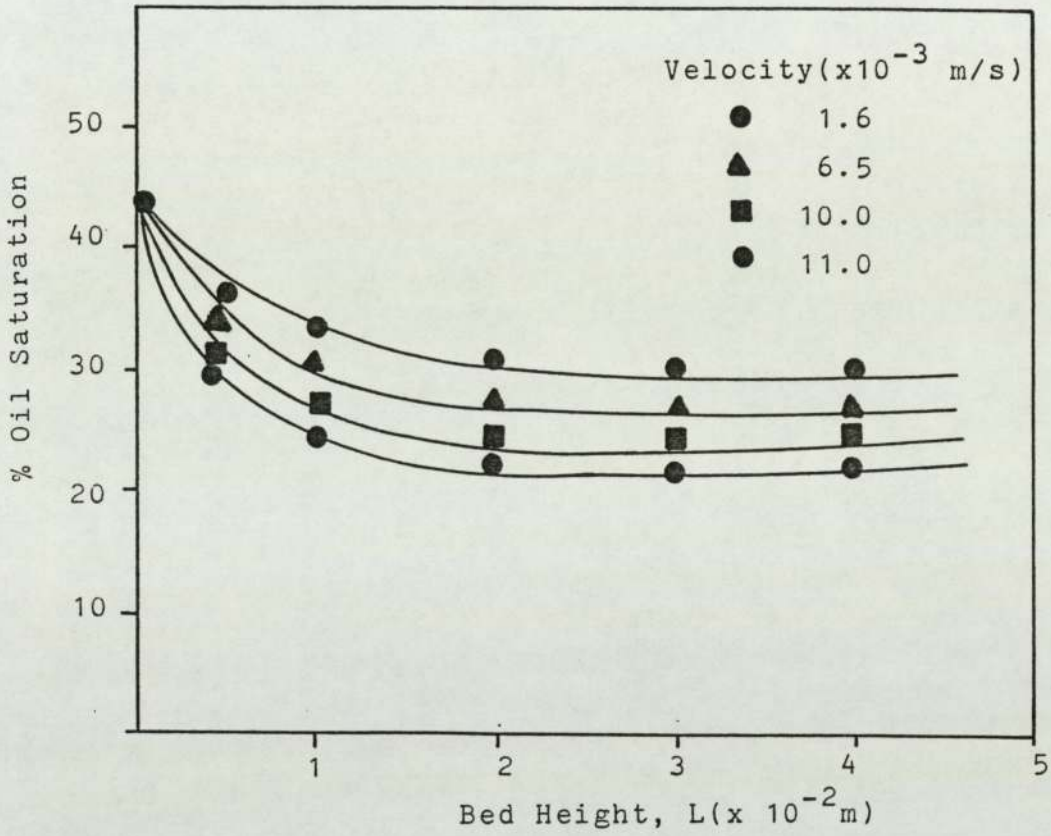
FIG. 9.14 SATURATION PROFILE PREDICTED FROM PRESSURE
DROP DATA APPROACH (d_f = 6 μm)

An alternative approach to predict the saturation profile was to use the concept of drop capture rate. The coalescer is assumed to consist of a series of layers, each of which comprises an array of cylindrical fibres. The layer thickness is also assumed to be twice the fibre diameter. By assuming no drop redispersion the number of drops entering and leaving each layer can be calculated using capture efficiencies of interception and gravity capture mechanisms. The saturation of each layer can be defined as the volume of held drops per volume of voids of that layer. This calculation procedure was repeated using a computer program given in Appendix I. The resultant saturation profile is shown in Fig. 9.15 for different velocities.

The average value of k obtained has been plotted against superficial velocity in Fig. 9.16. The value of k decreases with an increase in superficial velocity. S_E was also found to decrease with increase of superficial velocity as shown in Fig. 9.17. This confirms that increasing superficial velocity would tend to push the dispersed phase towards the exit face and hence lower the saturation.
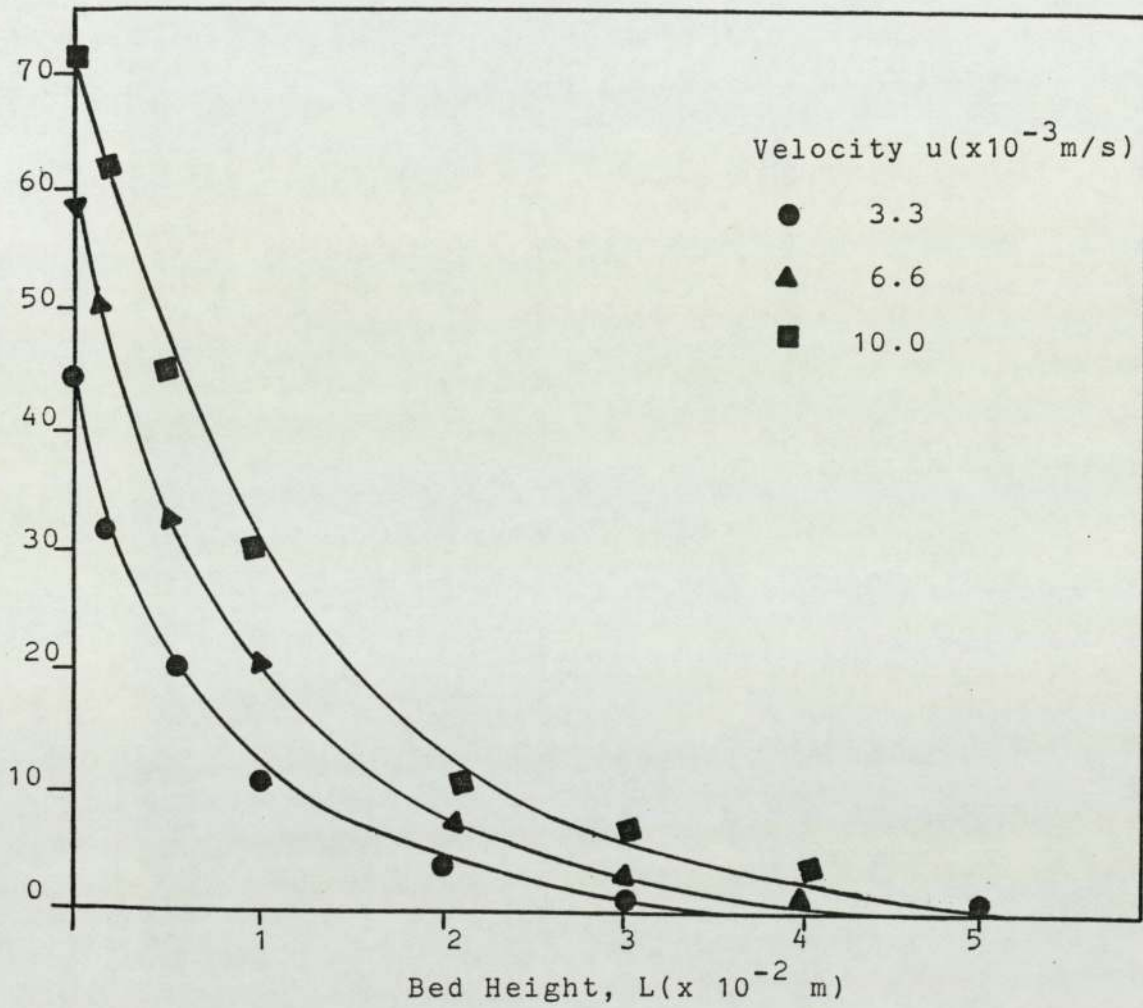
FIG.9.15 SATURATION PROFILE PREDICTED FROM CAPTURE EFFICIENCIES
APPROACH
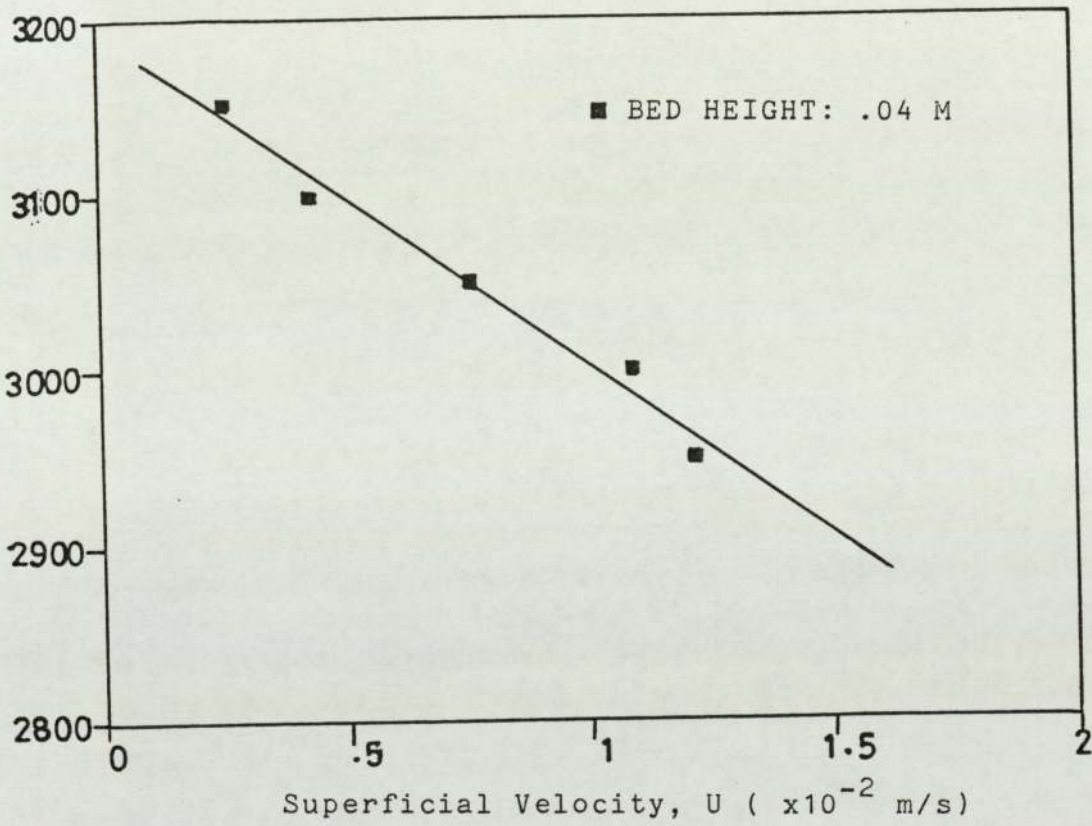
FIG. 9.16 VARIATION OF DECAY FACTOR WITH VELOCITY
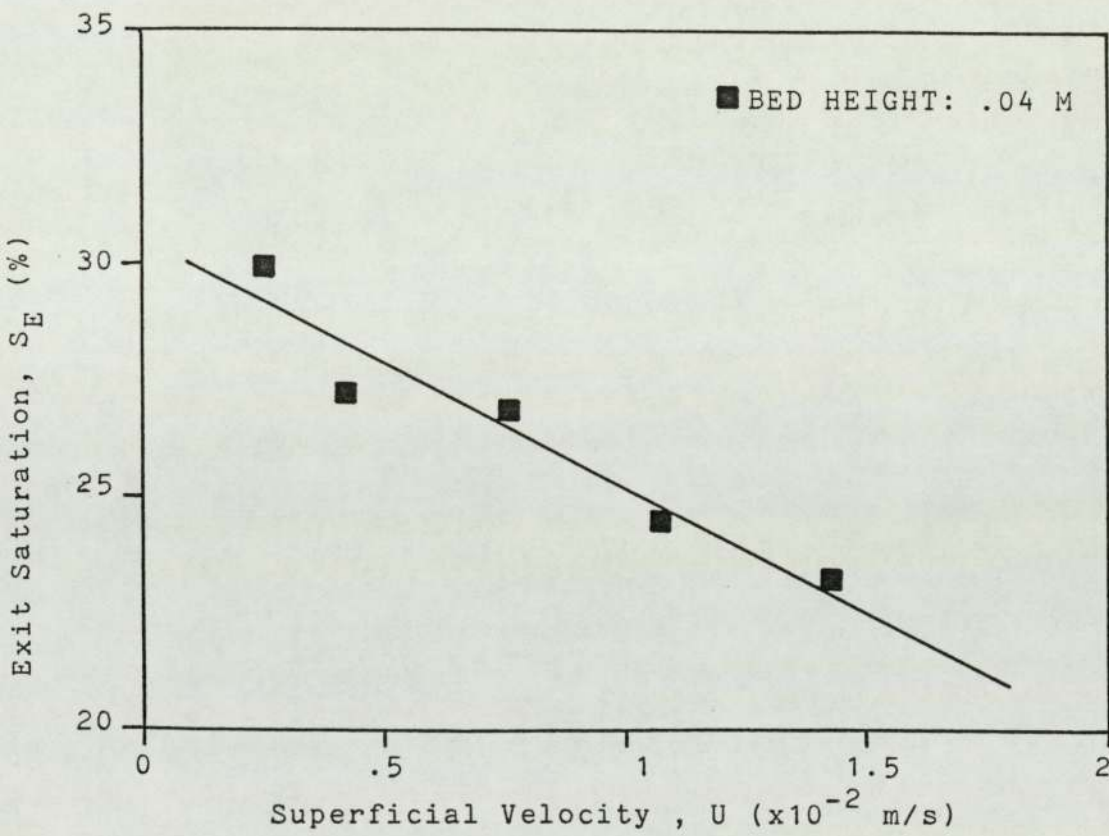
FIG. 9.17 VARIATION OF EXIT SATURATION WITH VELOCITY

CONCLUSIONS

1. Secondary dispersions of toluene in water of average
   drop size < 50 µm could be successfully coalesced
   into drops of millimeter size using beds of fibrous
   materials with operating conditions in the range 200
   to 1000 ppm phase ratio, 1.5×10^{-3} to 1.5×10^{-2} m/s
   velocity and packed heights of 0.024, 0.04 and 0.06 m.

2. Confirmation was obtained of a critical velocity,
   above which breakthrough occurred, and a critical
   bed height, above which redispersion occurred.
   For the range of operating conditions of this study,
   the critical velocity was found to be 1.5×10^{-2} m/s
   and the bed height was 6×10^{-2} m, where the separation
   efficiency was 80%.

3. Over a range of fibre diameters ,from 6 to 25 µm. the
   separation efficiency was found to increase with de-
   crease in fibre diameter. This indicates the need
   to construct a bed for a particular duty with a
   specific, monosized, fibre diameter.

4. Single phase pressure drop data were satisfactorily
   correlated by the Carman-Kozeny equation

$$\frac{\Delta P_1}{\mu_c} \frac{e_1^3 \, d_f^2}{36L(1-e_1)^2} = k \, u$$

The experimental value of Kozeny constant, k, was
found to be in good agreement with the value deduced
from theoretical considerations.

5. An expression, based on the Blake-Kozeny equation,
was derived to predict the two phase pressure drop
from a knowledge of the saturation profile:

$$\frac{\Delta P_2}{\Delta P_1} = \frac{d_f^2}{16(1-e_1)} \cdot \frac{1}{l} \int_0^L f(s)dl$$

The experimental saturation profile was found to
decay from a constant value near the inlet face to
a constant value in the downstream part of the bed.
Hence a model was postulated for determination of
average saturation.

$$S = S_I \quad , \quad 0 < l < L_I$$

$$S = (S_I - S_E)e^{-k(l-L_I)} + S_E \, , \, L_I < l < L$$

The average saturation is,

$$\bar{S} = S_E + (S_I - S_E) \frac{L_I}{L} + \frac{(S_I - S_E)}{kl} \left[1 - e^{-k(L-L_I)} \right]$$

The decay factor k was found to have a value higher
than 2000 which reduces the average saturation
equation to:

$$\bar{S} = S_E + (S_I - S_E) \frac{L_I}{L} \qquad \text{for large k}$$

6. The experimental filter coefficient gave a
    satisfactory result when compared with that
    predicted from the queueing drop model. However
    it varied over a magnitude of 800 for the other models.

7. A theoretical comparison of different drop capture
    mechanisms demonstrated that direct interception
    and sedimentation were most significant under the
    operating conditions encountered in this study,
    but that diffusion and London-Van der Waals forces
    may predominate for drops of less than 10 μm diameter.
    The drop capture efficiency may be estimated using

    $$n_{GI} = n_I + n_G + N_R N_G$$

    Application of this equation to typical operating
    conditions predicted that the drop capture rate was
    likely to be highest in the forepart of the bed.

8. Different drop release mechanisms were observed but
    drip-point was found to predominate. The exit drop
    size was found to decrease with velocity. The
    effluent entrainment increased with velocity and
    fibre diameter.

9. Based upon this theoretical and experimental study,
    a mechanism of coalescence of secondary dispersion
    is proposed as follows.

More than 95% of secondary drops entering a bed of
fibrous packing material are captured in the interstices
by interception and sedimentation mechanisms. The
drops reside in the bed, either attached to fibres or
due to interception by pores, where drop-drop coale-
scence occurs until they attain such a size that hydro-
dynamic forces exceed the restraining interfacial tension
and adhesion forces. The drops are then queued and
squeeze through the packing interstices as a dispersed
phase continuum. The dispersed phase is then conveyed
in rivulets, within fixed channels, to the exit face
where drops are formed and released by the mechanisms
of drip-point and ballooning. The drip-point drops
emerge as groups separated by constant interval times.
The number of the active channels, the number of the
primary drops and the interval times depend on the
inlet concentration of the dispersed phase.

RECOMMENDATIONS FOR FURTHER WORK

1. The fibre diameters used in this study were of a
    narrow range, i.e 6 to 25 μm. Extension of the
    experimental investigation to a wider range, i.e
    1 to 100 μm is recommended. The effects of system
    properties, i.e interfacial tension and viscosity,
    should also be investigated using other suitable dis-
    persed phases as petroleum fractions.

2. Since high drop capture efficiencies are achieved using
    small fibre diameters and large drops are formed by
    larger fibre diameters, it is recommended that beds
    should be constructed in which the fibre diameter
    increases with increase of bed height by placing the
    smaller fibres at the forepart of the bed and the larger
    fibres at the exit face.

3. A study concerning the change of drop diameter through
    the height of the bed may be worthwhile since no such
    relation has yet been established.

4. A study with two different sizes of fibres, e.g. 5 and
    50 μm, separated by free liquid to observe the release
    mechanisms of primary drops from each part of the bed,
    may help in determination of the optimum height required
    for the coalescer.

APPENDICES

APPENDIX A

PHYSICAL PROPERTIES OF LIQUID SYSTEM

APPENDIX A

PHYSICAL PROPERTIES OF LIQUID SYSTEM

I) TOLUENE

- Analar grade
- Density : 867 kg/m^3 at 20°C
- Viscosity : 0.58 x 10^{-3} kg/m.s at 20°C
- Surface tension : 27.9 x 10^{-3} N/m at 20°C
- Interfacial tension for
  toluene - water system : 29.2x10^{-3} N/m at 23°C

II) The remaining properties are presented as a
function of temperature in Figures A.1, A.2,
and A.3.

$$\frac{1}{\mu_c} = 100\{2.1482((T-8.435) + \sqrt{8078.4 + (T-8.435)^2})-120\}$$

Water, μ_c
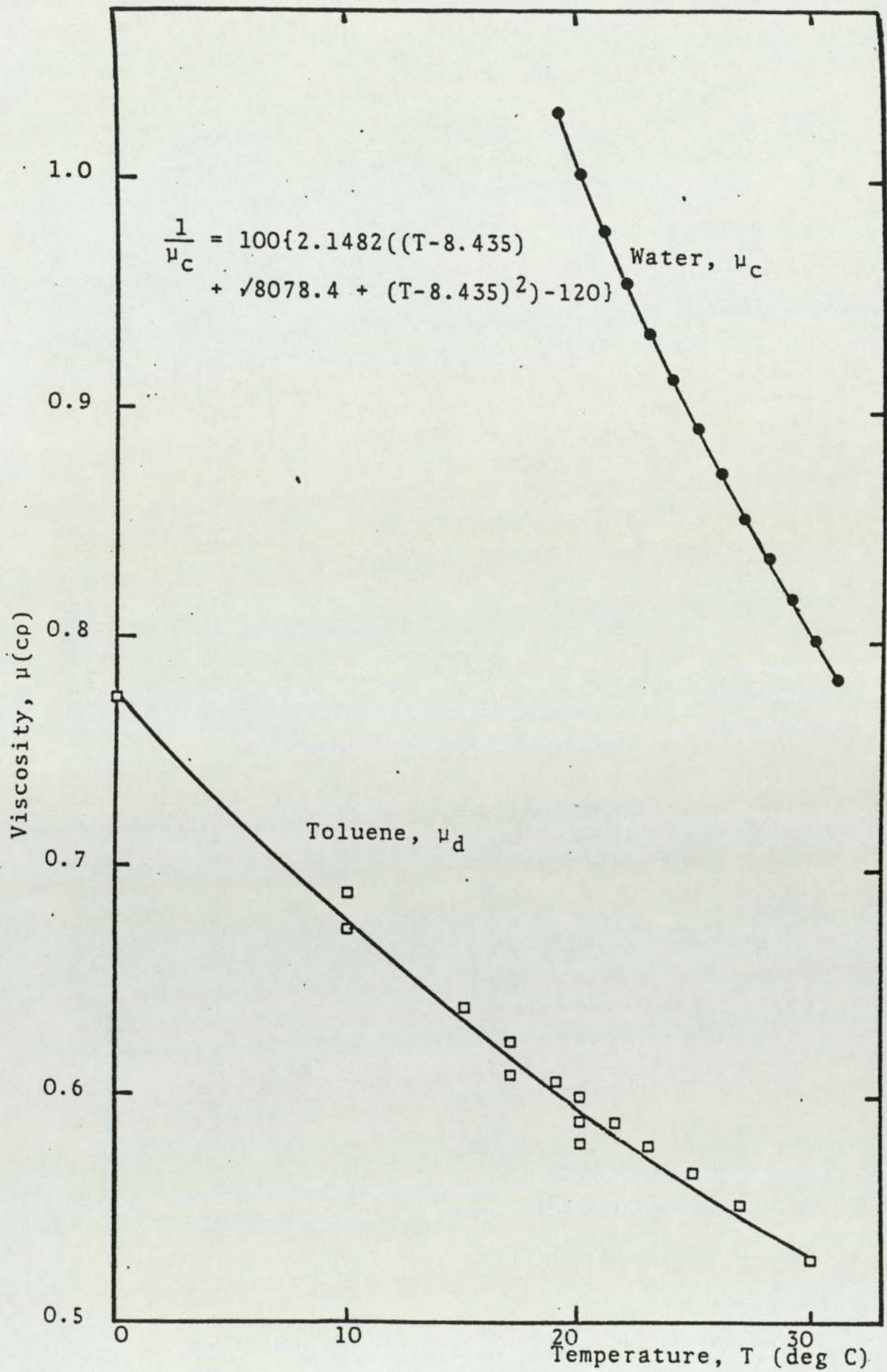
Toluene, μ_d

FIG. A.1 Phase Viscosities as a Function of Temperature
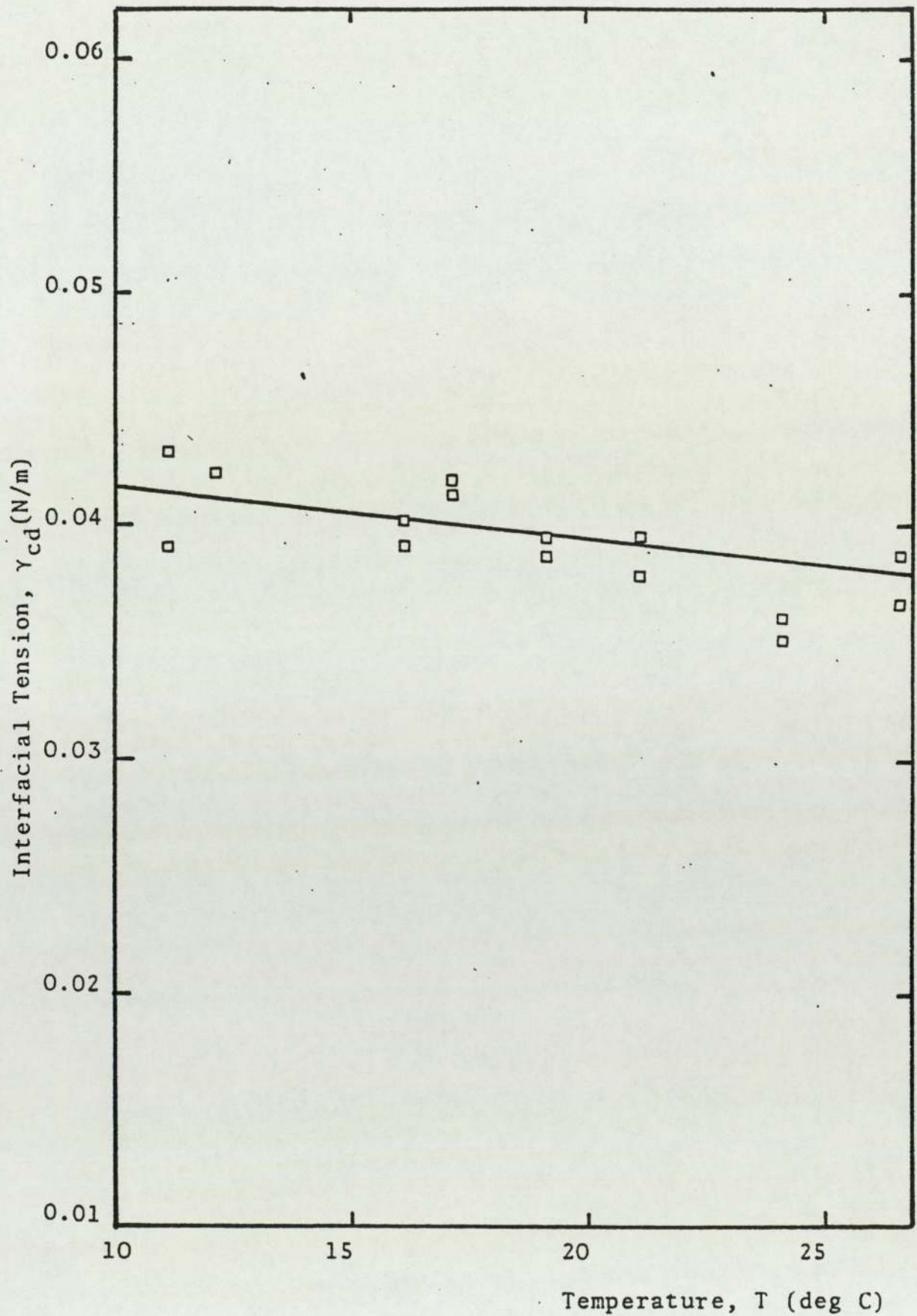
Fig. A.2 Interfacial Tension for Toluene/Water System
as a Function of Temperature
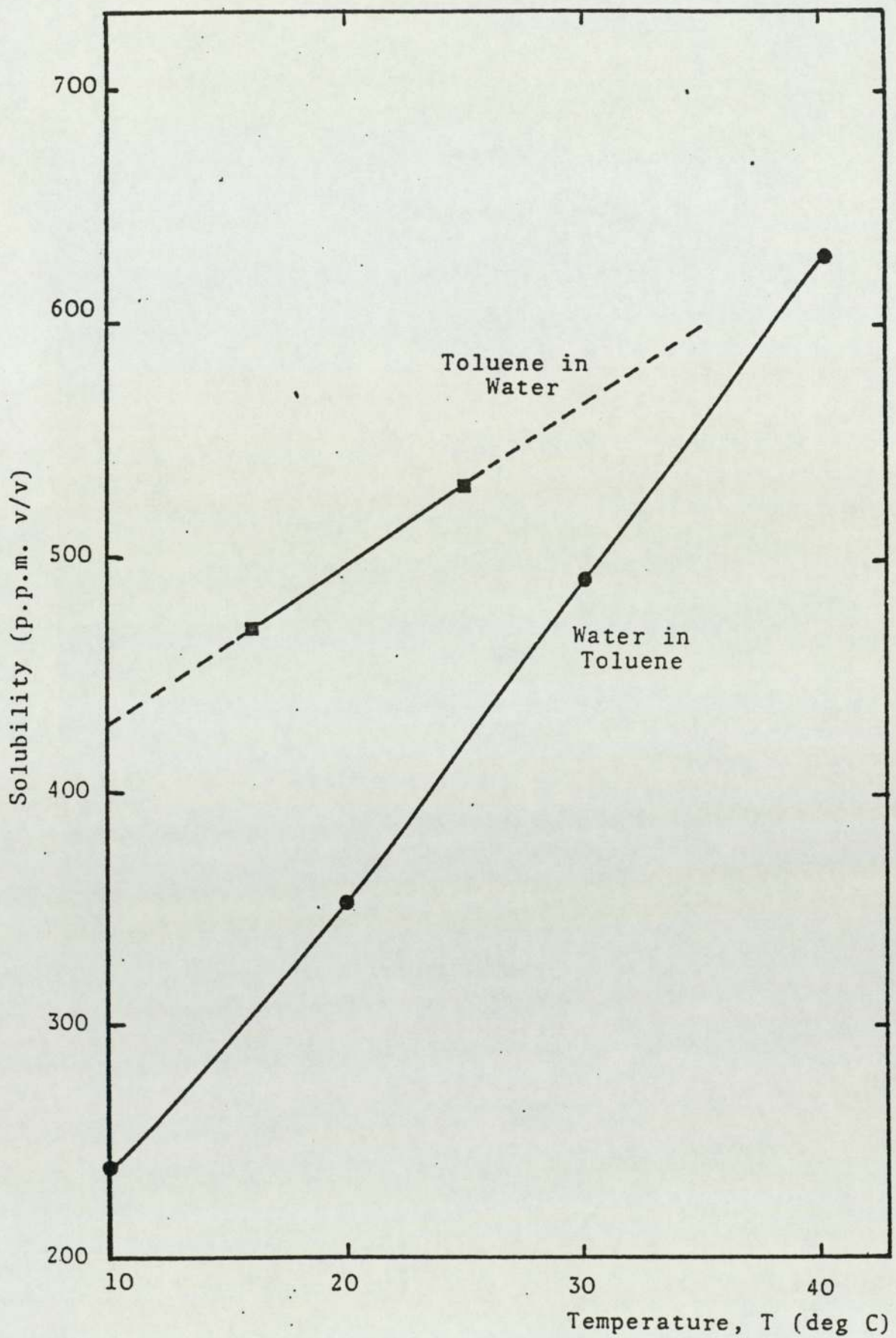
Fig. A.3 Mutual Solubility of Toluene/Water System
as Function of Temperature

APPENDIX B

DETERMINATION OF THE HAMAKER CONSTANT

APPENDIX B

DETERMINATION OF THE HAMAKER CONSTANT

An equation for calculating the London-Van der Waal's constant, which is known as Hamaker's constant was given by Sherony and Kintner (82) as

$$Q \; = \; 6\pi \; r_{22}^2 \; (\sqrt{\sigma_d^d} - \sqrt{\sigma_c^d}) \; (\sqrt{\sigma_s^d} - \sqrt{\sigma_c^d})$$

where r_{22} is the intermolecular distance, and σ_c^d, σ_d^d and σ_s^d are the London-Van der Waal's component to the surface tensions of the continuous, dispersed, and solid phase respectively.

Fowkes (83) estimates that $6\pi \; r_{22}^2$ is equal to $1.44 \times 10^{-18} \; m^2$ for water and hydrocarbon systems. Fowkes gave also, the following values for the dispersion force components (84):

$$\sigma_s^d \; = \; 0.0780 \; N/m \quad , \quad \text{for glass}$$

$$\sigma_d^d \; = \; 0.0218 \; N/m \quad , \quad \text{for water}$$

$$\sigma_c^c \; = \; 0.0285 \; N/m \quad , \quad \text{for toluene}$$

$$\therefore \quad Q = 1.44 \times 10^{-18} (\sqrt{0.0285} - \sqrt{0.0218})$$

$$(\sqrt{0.0780} - \sqrt{0.0218})$$

$$= 4.01 \times 10^{-21} \text{ J}$$

$$\therefore \quad \text{Hamaker constant, } Q = 4.01 \times 10^{-21} \text{ J}$$

APPENDIX   C

CALIBRATION OF FLOW RATE

EXAMPLE

SCALE READING

RATE-OF-FLOW - CC/MIN WATER (20°C)
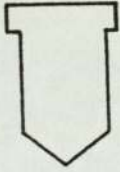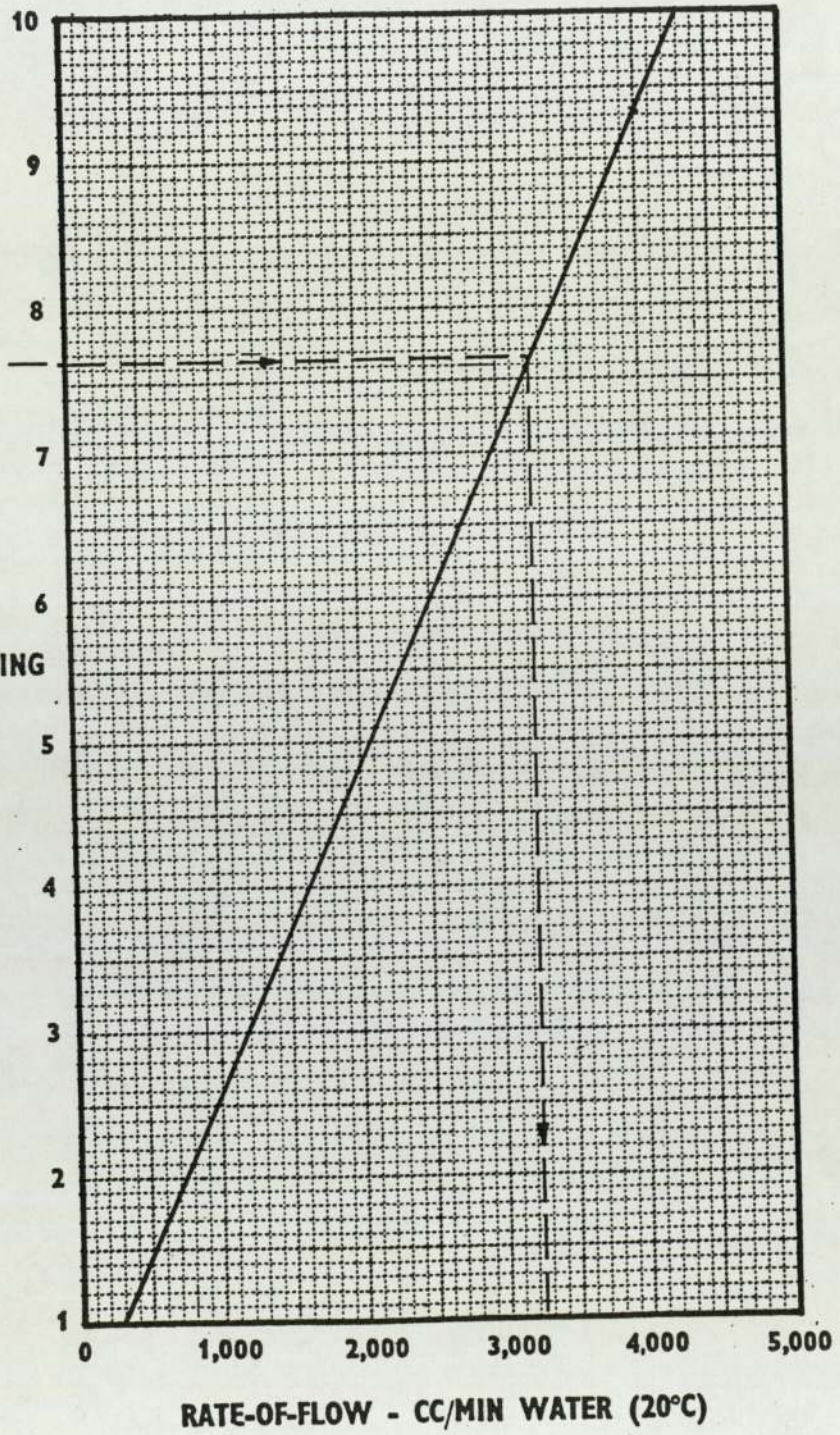
APPENDIX   D

COMPUTER PROGRAM FOR COMPARISON OF DROP CAPTURE
EFFICIENCIES

```
00100 REM         EVALUATION OF CAPTURE MECHANISM CONTRIBUTIONS
00110 REM             FOR FIBROUS BED COALESCER   TOLUENE=WATER SYSTEM
00120 DIM F(10),V(10),P(10),N(10)
00130 READ D3,E
00140 READ R3,M3,R4
00150 READ K,T,Q,G1
00160 FOR L=1 TO 10
00170 READ F(L)
00180 NEXT L
00190 FOR M=1 TO 7
00200 READ P(M)
00210 NEXT M
00220 FOR M=1 TO 6
00230 READ V
00240 PRINT 'VELOCITY=',V,'M/S'
00250 PRINT
00260 V=V/E
00270 PRINT 'DROP SIZE             TOTAL        SIGNIFICANT      %REL'
00280 PRINT '(MICRON)            EFFICIENCY      MECHANISM        CONTR'
00290 PRINT '-------------------------------------------------------------------'
00300 PRINT
00310 FOR L=1 TO 9
00320 D2=F(L)*.1E-05
00330 REM        CALCULATION OF DIMENSIONLESS GROUPS
00340 R=D2/D3
00350 R5=D3*V*R3/M3
00360 H=2-LOG(R5)
00370 S=(D2^2*R3*V)/(9*M3*D3)
00380 G=(D2^2*(R4-R3)*G1)/(18*M3*V)
00390 P5=(3*3.14159*D3*D2*V*M3)/(K*T)
00400 N1=4*Q/(9*3.14159*R^2*M3*V*D2^2)
00410 REM        CALCULATION OF CAPTURE EFFICIENCIES
00420 N(1)=(2*(1+R)*LOG(1+R)+1/(1+R)-(1+R))/(2*H)
00430 N(2)=2.16/((2*H)^.33333*P5^.66667)
00440 N(3)=-G
00450 N(4)=(R^2/H)*(((3*3.14159*H/2.0)*N1)^.33333)
00460 N6=N(1)+N(2)+N(3)+N(4)
00470 PRINT F(L),N6
00480 FOR I=1TO4
00490 C=INT(N(I)*100/N6)
00500 IF C<1 THEN 550
00510 IF I=1 THEN PRINT TAB(30),'INTERCEPTION',TAB(46),C
00520 IF I=2 THEN PRINT TAB(30),'DIFFUSION',TAB(46),C
00530 IF I=3 THEN PRINT TAB(29),'SEDIMENTATION',TAB(46),C
00540 IF I=4 THEN PRINT TAB(29),'LONDON FORCES',TAB(46),C
00550 NEXT I
00560 PRINT
00570 NEXT L
00580 FOR I=1 TO P(M)
00590 PRINT
00600 NEXT I
00610 PRINT '****************************************************************'
00620 FOR I=1 TO 8
00630 PRINT
00640 NEXT I
00650 NEXT M
00660 DATA 25.E-6,0.86
00670 DATA 1000,.1E-02,860.
00680 DATA .138048E-22,293,.401E-20,9.81
00690 DATA .1,1,5,10,15,20,25,30,50,100
00700 DATA 1,1,1,1,7,6,20
00710 DATA .001,0.331119E-2,0.662238E-2,0.993356E-2,1.32448E-2,1.655E-2
00720 END
```

VELOCITY=   .0132448   M/S

DROP SIZE (MICRON)	TOTAL EFFICIENCY	SIGNIFICANT MECHANISM	%REL CONTR
.1	6.814565E-04	DIFFUSION	87
		LONDON FORCES	11
1	1.031612E-03	INTERCEPTION	51
		DIFFUSION	12
		LONDON FORCES	35
5	1.3251207E-02	INTERCEPTION	90
		LONDON FORCES	8
10	4.5636925E-02	INTERCEPTION	95
		SEDIMENTATION	1
		LONDON FORCES	3
15	.09291799	INTERCEPTION	96
		SEDIMENTATION	1
		LONDON FORCES	2
20	.15223412	INTERCEPTION	96
		SEDIMENTATION	1
		LONDON FORCES	1
25	.22164835	INTERCEPTION	97
		SEDIMENTATION	1
		LONDON FORCES	1
30	.29977272	INTERCEPTION	97
		SEDIMENTATION	1
		LONDON FORCES	1
50	.68167851	INTERCEPTION	97
		SEDIMENTATION	1

Sample output from the program for comparison
of drop capture efficiencies (d_f = 25 μm)

Drop Diameter d_p (μm)	Superficial Velocity, u (x 10^{-2} m/s)					
	0.1	0.33	0.66	0.99	1.32	1.66
0.1	0.007	0.0037	0.0026	0.002	0.0018	0.0016
1	0.008	0.0076	0.0076	0.0077	0.008	0.0081
5	0.08	0.089	0.099	0.1	0.11	0.118
10	0.236	0.27	0.3	0.33	0.35	0.36
15	0.44	0.5	0.56	0.61	0.65	0.68
20	0.68	0.77	0.87	0.94	0.99	0.999

Table D.1 Total Caputre Efficiency for the range of velocities and drop diameter encountered in this study,

(d_f = 6μm)

Drop Diameter d_p µm	Superficial Velocity, $u (\times 10^{-2}$ m/s)					
	0.1	0.33	0.66	0.99	1.3	1.6
0.1	0.0028	0.0014	0.00097	0.00078	0.00068	0.0006
1	0.0015	0.0011	0.00103	0.001	0.00103	0.00105
5	0.0106	0.0103	0.0113	0.0123	0.0133	0.014
10	0.035	0.034	0.0385	0.0423	0.0458	0.049
15	0.0724	0.07	0.078	0.086	0.0934	0.1
20	0.12	0.115	0.128	0.141	0.153	0.165
25	0.178	0.168	0.187	0.205	0.223	0.239
30	0.245	0.228	0.253	0.278	0.301	0.324
50	0.596	0.529	0.579	0.634	0.687	0.737

Table D.2 Total capture efficiencies for the range of velocities and drop diameters encountered in this study (d_f = 25 µm)

Drop Diameter d_p (µm)	Superficial velocity, u ($\times 10^{-2}$ m/s)					
	0.1	0.33	0.66	0.99	1.3	1.66
0.1	0.0018	0.0009	0.00064	0.00052	0.00045	0.000406
1	0.00081	0.00053	0.00046	0.00044	0.000446	0.000453
5	0.0051	0.00393	0.0041	0.00447	0.00487	0.0053
10	0.0179	0.0135	0.0143	0.0157	0.017	0.0188
15	0.0383	0.0284	0.029	0.033	0.036	0.0395
20	0.066	0.0479	0.05	0.0554	0.061	0.066
25	0.1	0.072	0.075	0.0826	0.0906	0.099
30	0.141	0.0999	0.104	0.114	0.125	0.136
50	0.369	0.248	0.253	0.276	0.301	0.329

Table D.3 Total caputre efficiencies (d_f = 50 µm)

APPENDIX   E

COMPUTER PROGRAM FOR RATE OF DROP CAPTURE

```
10 DIM D(100),N(100),E(100)
20  DEF FNW(D)=113.525-3.44166*D+.0221507*D^2
40 READ D1,A2,C1,R4,R3
50 READ G1,M3,Q,BK,T,Z9,D6
55 A1=1-(.00005/(.00005+D1))^2
57 LF=.696*D6
70 FOR K=1 TO 6
80 PRINT".... ADVANCE PAPER TO TOF ....":PRINT:PRINT" PRESS ANY KEY TO CONTINU
E "
90 D$=INKEY$ : IF D$="" GOTO 90
100 CLS : READ U1 :REM U1 IN M/S
110 LPRINT:LPRINT:LPRINT" "," **    VELOCITY  :";U1;" M/S":LPRINT:LPRINT" ","
 CONCENTRATION  :";(C1*1000000!);" PPM":LPRINT :LPRINT" "," FIBRE DIAMETER  :";
D1;" micron"
150 I=1
160 D2=2
170 F1=U1*A2*C1
180 W1=FNW(D2)
190 D2=D2+2
200 W2=FNW(D2)
210 F2=.01*(W1-W2)*F1
220 D(I)=(D2-1)*.000001
230 N(I)=(6*F2)/(3.14159*D(I)^3)
250 I=I+1
260 W1=W2
270 IF D2>47 THEN 290
280 GOTO 190
290 LPRINT:LPRINT:LPRINT" "," BED HEIGHT ","    %   DROP  "
291 LPRINT                " "," "       M      "," UNCAPTURED "
292 LPRINT                " "," "  _____ "," _____ "
295 L1=.01
300 F3=0!
320 FOR J=1 TO I-1
330 R=D(J)/D1
335 R5=D1*U1*R3/M3
336 H=2!-LOG(R5)
337 V=U1/Z9
340 G=(D(J)^2*(R4-R3)*G1)/(18*M3*V)
350  P5=(3.14159*D1*D(J)*U1*M3)/(BK*T)
360 N1=(4*Q)/(9*3.14159*R^2*M3*V*D(J)^2)
370 N2=(1/H)*(2*(1+R)*LOG(1+R)+(1/(1+R))-(1+R))
380   N3=2.16/(((2*H)^.33333)*P5^.666667)
390 N4=-G
400 N5=(R^2/H)*((3*3.14159*H/2!)*N1)^.33333
410 E(J)=N2+N3+N4+N5
420 N(J)=N(J)*EXP(-(1-Z9)*E(J)*L1/(8000*D1))
425 IF N(J) < 1 THEN N(J)=0
430 F3=F3+(N(J)*3.14159*D(J)^3/6)
460 NEXT J
470 LPRINT
480 F4=F3*100/F1
490 LPRINT" ", L1,F4
500 IF L1>.2  THEN 540
510 L1=L1+.01
520 GOTO 300
540 NEXT K
550 LPRINT:LPRINT:LPRINT"    F I N I S H "
560 END
570 DATA 6.E-06,5.026548E-03,.001,860,1000.
580 DATA 9.81,1.E-03,.401E-20,1.38048E-23,293,.86,.08
585 DATA .166E-02,.33E-02,.49E-02,.66E-02,.99E-02,1.15E-02
590 REM    END OF PROGRAM
```

```
**   VELOCITY  : .00166    M/S

  CONCENTRATION  : 1000    PPM

FIBRE DIAMETER  : .000006  micron

VOIDAGE    e1    : .86
```

BED HEIGHT M	% DROP UNCAPTURED
.01	100
.02	93.32881
.03	82.15282
.04	70.54083
.05	59.76138
.06	50.45579
.07	42.75821
.08	36.51395
8.999999E-02	31.46479
9.999999E-02	27.35535
.11	23.97365
.12	21.15755
.13	18.78509
.14	16.76529
.15	15.02887
.16	13.52396
.17	12.2097
.18	11.05444
.19	10.03271
.2	9.124408

Sample output from the program for rate
of drop capture

APPENDIX F

EVALUATION OF SPECIFIC SURFACE FOR A COALESCER

APPENDIX F

EVALUATION OF SPECIFIC SURFACE FOR COALESCER CONT-
AINING DROPS OF DISPERSED PHASE.

Specific surface,

$$a = \frac{\text{(surface area of drops + surface area of fibres)}}{\text{(volume of drops + volume of fibres)}}.$$

let number of drops per unit volume of bed = N_p

then surface area $= N_p \pi\, d_p^2$

volume $= N_p \pi\, \dfrac{d_p^3}{6}$

let number of fibres per unit volume of bed = N_f

then surface area $= N_f \pi\, d_f\, 1$

volume $= N_f\, \pi\, \dfrac{d_f^2}{4}\, 1$

if void fraction of fibres $= e_1$

then $N_f = \dfrac{4(1-e_1)}{\pi d_f^2\, 1}$

if void fraction of drops $= e_p$

$$N_p = \frac{6(1-e_p)}{\pi\, d_p^3}$$

also two phase effective voidage, $e_2 = (e_p + e_1) - 1$

then $e_p = (e_2 - e_1) + 1$

but saturation, $S = 1 - \dfrac{e_2}{e_1}$

or $\quad e_2 = e_1 (1 - S)$

$\therefore \quad a = \dfrac{\dfrac{6}{d_p} (e_1 - e_2) + \dfrac{4}{d_f}(1 - e_2)}{(1 - e_2)}$

$a = \dfrac{\dfrac{6}{d_p} e_1 S + \dfrac{4}{d_f} \left[1 - e_1(1-S)\right]}{\left[1 - e_1(1-S)\right]}$

APPENDIX G

INTEGRATION OF SATURATION PROFILE

APPENDIX G

INTEGRATION OF SATURATION PROFILE

As given in Section 9.4, the saturation profile equation (9.34) is,

$$\int_{L_I}^{L} f(s)\,dl = \frac{1}{k} \int_{ge^{-k(L-L_I)}+h}^{g+h} \frac{a\,v^2+bv+c}{(v-h)(1-v)^3}\cdot dv$$

$$(G.1)$$

This integration can be solved by partial fraction:

$$\frac{av^2+bv+c}{(v-h)(1-v)^3} = \frac{A}{(1-v)} + \frac{B}{(1-v)^2} + \frac{C}{(1-v)^3} + \frac{D}{(v-h)}$$

$$av^2+bv+C = A(1-v)^2(v-h)+B(1-v)(v-h)$$

$$+ G(v-h)+D(1-v)^3$$

$$= A\left[v^3-(h+2)v^2+(2h+1)v-h\right]$$

$$+ B\left[-v^2+(h+1)v-h\right] + C\left[v-h\right]$$

$$+ D\left[-v^3 + 3v^2 - 3v + 1\right]$$

Equating Coefficients:

$$v^3 \quad : \quad o = A - D$$

$$v^2 \quad : \quad a = (h+2)\,A-B + 3D$$

$$v \quad : \quad b = (2h+1)A+(h+1)B+C - eD$$

$$v^o \quad : \quad c = -hA -hB - hC + D$$

Solution of these four simultaneous equation is:

$$A = \frac{ah^2+bh+c}{(1-h)^3} \tag{G.2}$$

$$B = \frac{h(2a+b)-a+c}{(1-h)^2} \tag{G.3}$$

$$C = \frac{a + b + c}{(1-h)} \tag{G.4}$$

$$D = \frac{ah^2 + bh + c}{(1-h)^3} = A \tag{G.5}$$

since the above expressions are independent of v,
it is possible to integrate (G.1) in its simple form.

$$\int_{ge^{-k(L-L_I)}+h}^{g+h} \frac{av^2+bv+c}{(v-h)(1-v)^3} \, dv = \int_{ge^{-(L-L_I)}+h}^{g+h}$$

$$\left[\frac{A}{(1-v)} + \frac{B}{(1-v)^2} + \frac{C}{(1-v)^3} + \frac{D}{(v-h)} \right] dv$$

$$= \left[-A \log_e(1-v) + \frac{B}{(1-v)} + \frac{C}{2(1-v)^2} + D \log_e \right.$$

$$(v-h) \left. \vphantom{\frac{C}{2}} \right]_{ge^{-k(L-L_I)}+h}^{g+h} \tag{G.6}$$

So equation (G.1) becomes:

$$\int_{L_I}^{L} f(s)dl = \frac{1}{k} \left[-A \log_e(1-v) + \frac{B}{(1-v)} + \frac{C}{2(1-v)^2} \right.$$

$$\left. + D \log_e(v-h) \right]_{ge^{-k(L-L_I)}+h}^{g+h} \qquad (G.7)$$

Since $g = (S_I - S_E)$, $h = S_E$ $\therefore$ $V_1 = g+h = (S_I-S_E)+S_E = S_I$

$$v_2 = ge^{-k(L-L_I)}+h = (S_I-S_E)e^{-k(L-L_I)} + S_E$$

$$\therefore \int_{L_I}^{L} f(s)dl = \frac{1}{k} \left[-A \log_e(1-S_I) + \frac{B}{(1-S_I)} + \frac{C}{2(1-S_I)^2} \right.$$

$$\left. + D \log_e(S_I-S_E) \right] - \left[A \log_e(1-v_2) + \frac{B}{(1-v_2)} \right.$$

$$\left. + \frac{C}{2(1-v_2)^2} + D \log_e(v_2-S_I) \right] \qquad (G.8)$$

So from equations (9.33) and (G.8)

$$\int_{o}^{L} f(s)dl = \int_{o}^{L_I} f(s)dl + \int_{L_I}^{1} f(s)dl$$

Substituting in equation (9.31) we get:

$$\frac{\Delta P_2}{\Delta P_1} = \frac{dc^2}{16(1-e_1)^2 L} \left[\left[\frac{a S_I^2 + b S_I + c}{(1-S_I)^3} \right] \cdot L_I + \right.$$

$$\frac{1}{k} \left[(-A \log_e (1-S_I) + \frac{B}{(1-S_I)} + \frac{C}{2(1-S_I)^2} \right.$$

$$+ D \log_e (S_I - S_E)) - (-A \log_e (1-v_2)$$

$$\left. + \frac{B}{(1-v_2)} + \frac{C}{2(1-v_2)^2} + D \log_e (v_2 - S_E)) \right]$$

$$(G.9)$$

where $v_2 = (S_I - S_E) e^{-k(L-L_I)} + S_E$

Equation (G.9) is the one to be used to predict pressure drop data.

APPENDIX   H

INTEGRATION OF AVERAGE SATURATION

APPENDIX   H

INTEGRATION OF AVERAGE SATURATION

The average saturation is determined by the integration of the saturation profile between O and the total height of bed L.

$$\therefore \quad \bar{S} = \frac{\int_{o}^{L} S \, dl}{\int_{o}^{L} dl}$$

$$\bar{s}L = \int_{o}^{L_I} s_I \, dL + \int_{L_I}^{L} (s_I - s_E) e^{-k(L-L_I)} \, dl + S_E \int_{L_I}^{L} dL$$

$$= s_I L_I + S_E (L-L_I)(s_I - s_E) * e^{kL_I} \int_{L_I}^{L} e^{-kL} \, dL$$

$$= s_E L + (s_I - s_E) L_I - \frac{(s_I - s_E)}{k} e^{kL_I} * (e^{-kL} - e^{-kL_I})$$

$$\therefore \quad \bar{s} = s_E + (s_I - s_E) \frac{L_I}{L} + \frac{(s_I - s_E)}{kL} \left[1 - e^{-k(L-L_I)} \right]$$

APPENDIX I

COMPUTER PROGRAM FOR PREDICTION OF SATURATION PROFILES

I.1 Program for prediction of S_E, k and the saturation profile

```
      DOUBLE PRECISION RATIO,Z1,Z2,W1,W2
     *,Z7,Z9,Z10,Z11,Z12,
     *Z13,H1,H2,H3,H4,RHS,XYZ
     *,PD2,PD1,G,DP(10),VEL(10)
      CHARACTER*60 TITLE
      REAL LI,K,LL,AVG
      READ(5,5)TITLE
5     FORMAT(A60)
      READ(5,*)E1,D,H
      READ(5,*)NP
      DC=D*1.0E-06
      LI=2*DC
      DO 800 M=1,NP
      READ(5,*)VEL(M),DP(M)
      READ(5,*)PD2,PD1
      READ*,SI,SE
10    CONTINUE
      DP(M)=DP(M)*1.0E-06
      WRITE(6,6)TITLE
6     FORMAT(1H1,10X,A60,//)
      WRITE(6,900)VEL(M)
900   FORMAT(3X,'**FOR VELOCITY =',F10.6,'CM/SEC',//)
      X1=(6*(1-E1))/DP(M)
      X2=(4/DC)+X1
      X5=(4*(1-E1))/DC
      C=(E1*((4/DC)+(6/DP(M))))**2
      D=2*E1*X2*X5
      X6=(1-E1)**2
      X7=DC**2
      F=(16*X6)/X7
150   X9=C*(SE**2)
      X10=D*SE
      X12=(1-SE)**3
      A1=(X9+X10+F)/X12
      X13=((2*C)+D)*SE
      X14=-C+F
      X15=(1-SE)**2
      B1=(X13+X14)/X15
      C1=(C+D+F)/(1-SE)
      D1=A1
      Y2=C*(SI**2)+(D*SI)
      Y3=(1-SI)**3
      Y4=((Y2+F)*LI)/Y3
      Y13=(1-SI)**2
      Y16=D1*DLOG(SI-SE)
      Y17=A1*DLOG(1-SI)
      Y18=B1/(1-SI)
      Y19=C1/(2*Y13)
      Y20=Y16-Y17+Y18+Y19
      K=10000.0
      RATIO=PD2/PD1
      G=-K*(H-LI)
130   Z1=DEXP(-K*(H-LI))
      Z2=((SI-SE)*Z1)+SE
      IF(Z2.EQ.SE) Z2=SE+0.000001
      Z7=(1-Z2)**2
```

```
      Z9=D1*DLOG(Z2-SE)
      Z10=A1*DLOG(1-Z2)
      Z11=B1/(1-Z2)
      Z12=C1/(2*Z7)
      Z13=Z9-Z10+Z11+Z12
      H1=16*((1-E1)**2)*H
      H2=(DC**2)/H1
      H3=(Y20-Z13)/K
      H4=Y4+H3
      RHS=H2*H4
      XYZ=RHS/RATIO
      IF(XYZ.GE.0.99.AND.XYZ.LE.1.02) GO TO 111
      IF(K.LT.10.0) GO TO 500
131   K=K-50.0
      GO TO 130
100   CONTINUE
500   SE=SE-0.002
      IF(SE.LT.0.005) GO TO 600
      GO TO 150
111   IF(M.EQ.1) GO TO 310
      IF(K.LT.W1) GO TO 121
      GO TO 131
121   IF(SE.LT.W2) GO TO 310
      GO TO 500
310   PRINT320,SI,SE,K
      W1=K
      W2=SE
320   FORMAT(5X,'**SI=',F6.5,/,5X,'**SE=',F12.10,/,5X,'**K=',F7.2)
      PRINT330
330   FORMAT(//,10X,50('-'),/,10X,'DEPTH',20X,'SATURATION',/,12X,
     *'MM',22X,'----',/,50('-'),/)
      LL=1.E-03
335   S=SE+((SI-SE)*(EXP(-K*(LL-LI))))
      PRINT340,(LL*1000),S
340   FORMAT(11X,F6.2,22X,F12.10)
360   IF(LL.GE.H) GO TO 600
      LL=LL+0.001
      GO TO 335
600   AVG=SE+((SI-SE)*(LI/H))+((SI-SE)/(K*H))*(1.0-EXP(-K*(H-LI)))
      PRINT20,AVG
20    FORMAT(//,5X,'***AVERAGE SATURATION=',F12.10)
      PRINT*,'------------------------------------------------------------'
800   CONTINUE
      PRINT*
      PRINT*,'****RUN COMPLETED****'
      STOP
      END
```

I.2 Program for prediction of saturation profile using the concept of drop capture rate

```
      DOUBLE PRECISION VOLOIL(100),S(100),EFFG,EFFI,EFFGI
      REAL NR,NRE,NG,N(100)
          CHARACTER*15 DATE
      PRINT*,"HOW MANY RUNS?"
      READ(5,*)K
      PRINT*,K
      DO 600 J=1,K
      PRINT*,"ENTER RUN NUMBER AND DATE !"
      READ(5,50)IJ,DATE
      PRINT*,IJ,DATE
50    FORMAT(I2,1X,A15)
      PRINT*,"HOW MANY POINTS IN THIS RUN?"
      READ(5,*)LM
      PRINT*,LM
      PRINT*,"ENTER COLLECTOR DIAMETER ,MICRON!"
      READ(5,*)D
      PRINT*,D
      DC=D*1.0E-6
      DO 500 I=1,LM
      WRITE(6,80)
80    FORMAT(1H1,2X,"ENTER VELOCITY,CM/SEC  OIL FLOW RATE,CC/MIN!")
      READ(5,*)VEL,FLOW
      PRINT*,VEL,FLOW
      PRINT*,"ENTER TIME FOR STEADY STATE ,MIN!"
      READ(5,*)TIME
      PRINT*,TIME
      PRINT*,"ENTER INLET DROP DIAMETER ,MICRON!"
      READ(5,*)DP
      PRINT*,DP
      PRINT*
      OIL=(FLOW*TIME)*1.0E-06
      DP=DP*1.0E-06
      NUM=OIL/(.523E09523*(DP**3))
      ***EFFICIENCY  CALCULATION   ***
      D=0.08
      E1=0.8655
      DDENS=866.9
      CDENS=1000.0
      CVIS=1.0E-03
      VEL1=VEL/100.0
      G=9.81
      NRE=(DC*VEL1*CDENS)/CVIS
          PRINT*," NRE= ",NRE
      NR=DP/DC
          PRINT*," NR= ",NR
      NG=((DP**2)*(DDENS-CDENS)*G)/(18.0*CVIS*VEL1)
          PRINT*," NG= ",NG
      EFFG=-NG
          PRINT*," EFFG= ",EFFG
      A=2.0-ALOG(NRE)
          PRINT*," A= ",A
```

```
      EFFI=(1.0/(2*A))*(2*(1+NR)*(ALOG(1+NR))+(1.0/(1+NR))-(1+NR))
          PRINT*, ' EFFI= ',EFFI
      EFFGI=EFFI+EFFG
          PRINT*, ' EFFGI= ',EFFGI
      WRITE(6,100)IJ,DATE
100   FORMAT(1H1,20X,'**SATURATION PROFILE**',25X,'PAGE1',
     */,5X,'RUN NUMBER:',I4,20X,'DATE:',A15)
      WRITE(6,110)VEL,EFFGI
110   FORMAT(5X,'VELOCITY:',F10.6,2X,'CM/SEC',10X,'EFFGI=',F10.6,/)
      VOLI=(7.85398163E-04)*(D**2)
      VOLII=VOLI*10.0
      VOLPP=VOLII*E1
      VOLP=VOLI*E1
      WRITE(6,150)
      DUM=NUM
      DO 400 L=1,10
      N(L)=DUM*EFFGI
      VOLOIL(L)=N(L)*0.523809523*(DP**3)
      S(L)=VOLOIL(L)/VOLP
      WRITE(6,220)L,INT(N(L)),S(L)
      DUM=DUM-N(L)
150   FORMAT(5X,80('='),/,5X,'DEPTH',17X,'NO.OF DROPS',25X,
     *'SATURATION',/,5X,80('='))
220   FORMAT(5X,I4,16X,I12,20X,E15.7)
400   CONTINUE
      DO 450 M=20,100,10
      N(M)=DUM*EFFGI
      VOLOIL(M)=N(M)*0.523809523*(DP**3)
      S(M)=VOLOIL(M)/VOLPP
      WRITE(6,220)M,INT(N(M)),S(M)
      DUM=DUM-N(M)
450   CONTINUE
      WRITE(6,420)
420   FORMAT(5X,80('='))
500   CONTINUE
      WRITE(6,520)IJ
520   FORMAT(/,5X,30('*'),'END OF RUN(',I2,')',30('*'),//)
600   CONTINUE
      STOP
      END
```

VELOCITY: .662238 CM/SEC   EFFGI=   .304112

```
=================================================================
DEPTH                    NO.OF DROPS                    SATURATION
=================================================================
      1                  429456936                    .6291288+000
      2                  298853796                    .4378030+000
      3                  207968678                    .3046617+000
      4                  144722842                    .2120103+000
      5                  100710844                    .1475354+000
      6                   70083436                    .1026681+000
      7                   48770200                    .7144544-001
      8                   33938581                    .4971800-001
      9                   23617441                    .3459814-001
     10                   16435086                    .2407642-001
     20                   11436974                    .1675449-002
     30                    7958849                    .1165924-002
     40                    5538465                    .8113522-003
     50                    3854149                    .5646100-003
     60                    2682055                    .3929051-003
     70                    1866409                    .2734179-003
     80                    1298811                    .1902681-003
     90                     903826                    .1324052-003
    100                     628961                    .9213918-004
=================================================================
```

VELOCITY: .993356 CM/SEC   EFFGI=   .356848

```
=================================================================
DEPTH                    NO.OF DROPS                    SATURATION
=================================================================
      1                  465701616                    .7751360+000
      2                  299517008                    .4985304+000
      3                  192635014                    .3206309+000
      4                  123893631                    .2062145+000
      5                   79682459                    .1326273+000
      6                   51247947                    .8529953-001
      7                   32960229                    .5486058-001
      8                   21198443                    .3528370-001
      9                   13633825                    .2269279-001
     10                    8768624                    .1459492-001
     20                    5639559                    .9386753-003
     30                    3627095                    .6037111-003
     40                    2332774                    .3882781-003
     50                    1500328                    .2497219-003
     60                     964939                    .1606092-003
     70                     620603                    .1032961-003
     80                     399142                    .6643514-004
     90                     256709                    .4272791-004
    100                     165103                    .2748055-004
=================================================================
```

I.3 Sample results for program I.3

APPENDIX J

COMPUTER PROGRAM FOR CALCULATING OF EXIT SAUTER MEAN

DIAMETER

```fortran
C           CALCULATION OF CUMULATIVE VOLUME & DROP SIZE DISTRIBUTION
C                FOR FIBROUS BED COALESCERS
C                   SAUTER MEAN DIAMETER
C
C        DM : THE MEASURED  DROP DIAMETER
C        DA : THE ACTUAL DROP DIAMETER
C        RF : THE MAGNIFICATION FACTOR
C        F  : THE NUMBER OF DROPS WITHIN THE GROUP OF DROPS
C
C
          DIMENSION DM(50),DA(50),F(50),C(50),V(50),VD(50),VV(50),
     $DD(50),FCV(50),FV(50),VC(50),S(50),RS(50),RC(50)
          SUMRS=0.
          SUMRC=0.
          WRITE(6,80)
80     FORMAT(////8X,'*** D R O P   S I Z E   D I S T R I B U T I O N'
     $,'  ***'//)
          WRITE(6,10)
10     FORMAT(7X,' DM ',9X,'DA ',7X,'F',8X,' FV ',11X, 'FCV '/
     $ 7X,' == ',9X,'== ',7X,'=',8X,' == ',11X,'==='/)
          READ(5,*)RF,K
          VSUM =0.0
          DA(1) =0.0
          VD(1) =0.0
          DO 30 I =2,K+1
          READ(5,*)DM(I),F(I)
          DA(I) =DM(I)/RF
          S(I)=DA(I)**2
          C(I) =DA(I)**3
          RS(I)=S(I)*F(I)
          RC(I)=C(I)*F(I)
          SUMRS =SUMRS+RS(I)
          SUMRC =SUMRC +RC(I)
          V(I)=(3.14/6.0)*C(I)
          VD(I) =V(I)*F(I)
          VSUM =VSUM+VD(I)
          FV(I) =VSUM
30        CONTINUE
          DO 40 I =2,K+1
          VC(I)= FV(I)/VSUM
          VV(I)=VC(I)-VC(I-1)
          DD(I)=DA(I)-DA(I-1)
          FCV(I)= VV(I)/ DD(I)
          WRITE(6,123)DM(I),DA(I),INT(F(I)),FV(I),FCV(I)
123       FORMAT(5X,F7.4,5X,F7.4,5X,I2,5X,F10.4,5X,F7.4)
40        CONTINUE
          SMD =SUMRC/SUMRS
          PRINT*,' '
          PRINT*,' '
          PRINT*,' SAUTER MEAN DIAMETER  = ',SMD
          PRINT*,' '
          PRINT*,' '
          STOP
          END
```

APPENDIX K

COMPUTER PROGRAM FOR PREDICTION OF FILTER COEFFICIENT

```
      DOUBLE PRECISION Y1,Y2,Y4,Y5,Y7,B,W(10)
      REAL MC,MD,K,LQC
      DIMENSION U(9),S(9),DI(9),DO(9),F(9),DPM(9),Z(9)
      DIMENSION DPC(9),LQC(9),YC(9),YE(9)
      DOUBLE PRECISION UI(9),X2,X3,X4,X5,H(10)
      READ(5,*)N
      DO 200 I=1,N
      READ(5,*)U(I),S(I),DI(I),DO(I),F(I)
      MC=1.0E-03
      E=.92
      HET=0.025
      K=1
      MD=.6E-03
      DC=6.E-06
      UI(I)=U(I)/(E*(1-S(I)))
      X1=3.4055174E-07
      X2=3*MC*UI(I)*K*(1+(2*MC)/(3*MD))
      X3=1+MC/MD
      X4=(X2/X3)**(-2)
      X5=X1*X4-1
      DPC(I)=DC*X5
C     THE UNIT OF ** DPC ** IS METER
      DPM(I)=DPC(I)*1000
C     THE UNIT OF ** DPM ** IS MILLIMETER
      D=.08
      LQC(I)=(3*E*D*D*S(I)*HET)/((DPC(I)**3)*2)
      A=LQC(I)
      CALL GAMMA(A,B)
      H(I)=B
      IF(H(I).GT.0.999999999) H(I)=.999999999
      Y1=HET
      Y2=2*LQC(I)
      Y3=H(I)**Y2
      Y4=ALOG(1-Y3)
      YC(I)=-Y4/Y1
      Y5=(DI(I)/DO(I))**3
      Y6=(1-F(I))*Y5
      Y7=ALOG(Y6)
      YE(I)=-Y7/Y1
      Z(I)=UI(I)
      W(I)=H(I)
 200  CONTINUE
      WRITE(6,5)
  5   FORMAT(1H1,//15X,'*** QUEUE MODEL CALCULATIONS ***',///)
      PRINT*,'                      **  TABLE ( 1 )  **'
      WRITE(6,15)
 15   FORMAT(//5X,'RUN',5X,'VELOCITY',5X,'SATURATION',5X,
     *'IN DIAM.',5X,'OUT DIAM.',5X,' EFF ')
      WRITE(6,25)
 25   FORMAT(5X,'NO.',6X,'CM/SEC',10X,'--',10X,'MICRON',
     *9X,'MM',10X,'---')
      DO 300 J=1,N
      PRINT*,'  '
      WRITE(6,35)J,(U(J)*100),S(J),(DI(J)*1.0E+06),
     *(DO(J)*1000),F(J)
 35   FORMAT(6X,I2,5X,F8.6,5X,F10.8,6X,F7.3,6X,F7.3,6X,F6.4)
      PRINT*,'  '
 300  CONTINUE
```

Computer program for prediction of filter coefficient

```fortran
      PRINT*,'---------------------------------------------------------'
      WRITE(6,45)
45    FORMAT(//,////20X,'**   TABLE ( 2 )   **')
      WRITE(6,55)
55    FORMAT(//5X,'RUN',5X,'VELOCITY',5X,'   DPC   ',6X,
     *'Q LENGTH',5X,'   GAMMA   ',5X,'CALC. F.C.',5X,'EXP.F.C.')
      WRITE(6,65)
65    FORMAT(5X,'NO.',6X,'CM/SEC',9X,'MM',12X,'--',13X,
     *'---',12X,'M-1',10X,'M-1')
      DO 400 L=1,N
      PRINT*,'  '
      WRITE(6,75)L,(Z(L)*100),DPM(L),LQC(L),W(L),YC(L),YE(L)
75    FORMAT(6X,I2,5X,F8.6,5X,F9.4,4X,E11.6,4X,F12.9,
     *4X,F9.4,5X,F9.4)
      PRINT*,'  '
400   CONTINUE
      PRINT*,'---------------------------------------------------------'
      STOP
      END
      SUBROUTINE GAMMA(A,B)
      REAL LNHC,LQ(6),GLNH(6)
      DOUBLE PRECISION B
      DATA LQ/5.9768,58.17091,167.99152,489.39,2733.8936,4963.0/
      DATA GLNH /-1.0E-02,-1.0E-04,-1.0E-05,-1.0E-06,-1.0E-07,-1.0E-08/
      IF(A.GE.5.976825.AND.A.LE.10) GO TO 20
      IF(A.GT.10.AND.A.LE.100) GO TO 30
      IF(A.GT.100.AND.A.LE.1000) GO TO 40
      IF(A.GT.1000.AND.A.LE.10000) GO TO 50
      IF(A.GT.10000.AND.A.LE.100000) GO TO 60
      IF(A.GT.100000) GO TO 70
20    Y8=(LQ(2)-LQ(1))/(GLNH(2)-GLNH(1))
      LNHC=(Y8*GLNH(2)-LQ(2)+A)/Y8
      HC=2.7182818**LNHC
      B=HC
      GO TO 90
30    Y8=(LQ(3)-LQ(2))/(GLNH(3)-GLNH(2))
      LNHC=(Y8*GLNH(3)-LQ(3)+A)/Y8
      HC=2.7182818**LNHC
      B=HC
      GO TO 90
40    Y8=(LQ(4)-LQ(3))/(GLNH(4)-GLNH(3))
      LNHC=(Y8*GLNH(4)-LQ(4)+A)/Y8
      HC=2.7182818**LNHC
      B=HC
      GO TO 90
50    Y8=(LQ(5)-LQ(4))/(GLNH(5)-GLNH(4))
      LNHC=(Y8*GLNH(5)-LQ(5)+A)/Y8
      HC=2.7182818**LNHC
      B=HC
      GO TO 90
60    Y8=(LQ(6)-LQ(5))/(GLNH(6)-GLNH(5))
      LNHC=(Y8*GLNH(6)-LQ(6)+A)/Y8
      HC=2.7182818**LNHC
      B=HC
      GO TO 90
70    PRINT*,' LQ= ',A,' O U T  O F  R A N G E '
      B=0.999999999
90    RETURN
      END
```

** TABLE (1) **

RUN NO. --	VELOCITY CM/SEC	SATURATION --	IN DIAM. MICRON	OUT DIAM MM	EFF --
1	.331119	.19854	12.6	.671	.9659
2	.662238	.16461	12.7	.546	.9333
3	.993356	.16111	12.8	.463	.8750
4	1.324480	.10534	12.9	.389	.9408

** TABLE (2) **

RUN NO. --	VELOCITY CM/SEC	DPC MM	Q LENGTH --	GAMMA --	CALC. F.C. --	EXP. F.C. --
1	.480401	7.8452	136	.999989100	145.5987	382.591
2	.921778	2.1287	5640	.999999999	284.8116	349.765
3	1.376897	.9524	61600	.999999999	225.0450	321.155
4	1.721428	.6082	154600	.999999999	202.0393	326.089

Sample results of filter coefficient calculations (d_f= 6 micron)

NOMENCLATURE

Symbols have the following meanings except where specifically indicated in the text.

a	specific surface area (m^2/m^3)
a_c	collector radius (m)
a_p	drop radius (m)
A	flow parameter (-)
A_c	surface area of container per unit volume of bed (m^2/m^3)
A_{cap}	area of capillary available for flow (m^2)
A_F	Happel's cell flow parameter for assemblage of cylinders (-)
A_S	Happel's cell flow parameter for assemblage of spheres (-)
b	width of capillary (m)
C	fractional concentration of dispersion (-)
d_a	aperture diameter (m)
d_c	collector diameter (m)
d_f	average fibre diameter (m)
d_{fe}	effective fibre diameter (m)
d_H	hydraulic radius (m)
d_p	drop diameter (m)
d_{pc}	critical drop diameter for release (m)
d_{pe}	exit drop size (m)

D_{AB}	molecular diffusion coefficient (m^2/s)
D	diameter of coalescing bed (m)
e	voidage fraction (-)
f_p	friction factor (-)
f_w	correction factor for wall effect (-)
F_{AD}	adhesion force (N)
F_{DL}	double layer force (N)
g	acceleration due to gravity = 9.81 (m/s^2)
h	drop/collector separation (m)
	film thickness for capillary flow (m)
H	dimensionless separation between drop and collector = h/a_p (-)
H^*	dimensionless separation at reaf stagnation
I	point mass capture rate (m^2/s)
j	rate of particle capture per unit sphere length ($n_o/m\ s$)
k	relative permeability (-)
κ	saturation profile parameter characterizing rate of decay (-)
k'	Boltzman constant
K	Kozeny constant (-)
K_o	shape factor (-)
l	distance into coalescing bed from inlet face (m)
L	bed height (m)
L_e	effective path length (m)

L_E length of bed near exit face having constant saturation value (m)

L_I Length of bed near inlet face having constant saturation value (m)

n number of drops (-)

n_o number of drops entering interval 1 from inlet face (-)

n_1 number of drops leaving interval 1 from inlet face (-)

N_{AD} adhesion number $= \dfrac{4Q}{9\pi R^2 A} \cdot \dfrac{1}{\mu_c u d_p^2}$ (-)

N_G gravity number $= \dfrac{d_p^2 (\rho_d - \rho_c) g}{18 \mu_c u}$ (-)

N_{Pe} Peclet number $= \dfrac{d_f u}{D_{AB}}$ (-)

N_R interception number $= \dfrac{d_p}{d_f}$ (-)

N_{RD} direct interception number $= \dfrac{d_p}{d_a}$ (-)

N_{Re} Reynolds number $= \dfrac{d_f u \rho_c}{\mu_c}$ (-)

N'_{Re} Reynolds number $= \dfrac{d_p u \rho_c}{\mu_c}$ (-)

N_{Stk} Stoke's number $= \dfrac{d_p^2 \rho_c u}{9 \mu_c d_f}$ (-)

ΔP pressure drop (N/m^2)

q_i flowrate of phase i (m^3/s)

Q Hamaker constant (J)

Q Total volumetric flowrate (m^3/s)

r distance from centre of cylinder or sphere (m)

r_{22} intermolecular distance (m)

S	local saturation of dispersed phase (-)
$\bar{S}$	average saturation of dispersed phase (-)
S_c	local saturation of continuous phase (-)
S_d	local saturation of dispersed phase when used in conjunction with S_c (-)
S_E	saturation near exit face of bed (-)
S_I	saturation near inlet face of bed (-)
t	time (s)
T	temperature (^{O}K)
T	tortuosity factor (-)
u	superficial velocity (m/s)
u_1	aqueous superficial velocity for single phase (m/s)
u_2	aqueous superficial velocity for two phase flow (m/s)
u_{cap}	interstitial velocity (m/s)
X	cross sectional area (m^2)

Greek Letters

α	volume of solids in the bed = $1-e_1$ (-)
γ	interfacial tension (N/m) ; Degree of balking in Eqn. 9.6.B
ε	dielectric constant of continuous phase
σ	surface tension (N/m)
η	drop capture efficiency (-)
η_c	coalescence efficiency (-)
μ	viscosity (Ns/m^2)
ρ	density (kg/m^3)
λc	calculated filter coefficient (m^{-1})

λe experimental filter coefficient (m^{-1})

ν kinematic viscosity (m^2/s)

ψ streamline function for drop/collector system (-)

θ polar coordinate for drop/collector system (rad)

Subscripts

1   single phase flow

2   two phase flow

c   continuous phase

d   dispersed phase

f   bed of fibres

s   bed of spheres

D   diffusion

D   direct interception

G   gravity sedimentation

I   interception

II   inertial impaction

L   London forces

T   total

REFERENCES

REFERENCES

1. Austin, D.G., Ph.D. Thesis, University of Aston (1979).

2. Jeffreys, G.V., and Davies, G.A., "Recent Advances in Liquid-Liquid Extraction", Ch. 14, Editor Hanson, C., Pergamon Press (1971).

3. Cantrell, A., "Annual Refining Survey", The Oil and Gas Journal, PP. 82-106, April 1, (1974).

4. Chieu, J., Gloyna, E.F., et.al., Proceedings of the Industrial Waste Conference, 30, PP. 611-620, (1977).

5. Waterman, L.C., Chem. Eng. Prog., 10, 61, Oct, (1965).

6. Sadek, S.E., Hendricks, C.D., Ind. Eng. Chem. Fund., 13(2), 139, (1974).

7. Thomas, R.J., Mumford, C.J., Int. Solvent Extraction Conf., Hague, Vol.1, 400, (1971).

8. Hayes, J., G., et.al, Chem. Eng. Prog., 45, 235, (1949).

9. Tuerk, H., Dechma-Monogr., 74, 205-219, (1974).

10. Robertson, D., J. Appl. Phys., 44,(9), 3924, (1973).

11. Shalhoub, N.G., Private communication, (1981).

12. Fahim, M.A., and Akbar, A.M., J. Environ. Sci. Health, A19(3), 299-319 (1984).

13. Abdel-Ghani, M.S., and Davies, G.A., Chem. Eng. Sci., 40(1), 1985.

14. Poleo, S.B., Ph.D. Thesis, University of Aston in Birmingham (1983).

15. Al-Meshan, M.A.F., Ph.D. Thesis, University of Aston in Birmingham (1985).

16. Ibrahim, S.Y., M.Sc Thesis, University of Aston in Birmingham (1981).

17. Jeater, P., Rushton E., and Davies, G.A., Filtration and Separation, 129, March (1980).

18. Jaisinghani, R.A., Filtration and Separation, 367, July (1977).

19. Spielman, L.A., and Su, Y.P., Ind. Eng. Chem. Fund., 16(2), 272 (1977).

20. Wilkinson, D., Mumford, C.J., Jeffreys, G.V., AIChE Journal, 910, Sep. (1975).

21. Shah B., Langdon, W., and Wasan, D., Env. Science and Technology, Vol.11, No.2, 167, Feb. (1977).

22. Bitten J.F., J. of Colloid and Interface Science, 33,(2), 265, June (1970).

23. Davies, G.A., and Jeffreys,G.V., Ind. Eng. Chem. Fundam., Vol.9, No.3, 519 (1970).

24. Hazlett, R.N., I&EC Fundam. Vol. 8, No. 4, 625, Nov. (1969).

25. Hazlett, R.N., I&EC Fundam, Vol.8, No.4, 633, Nov.

(1969).

26. Sareen, S.S., Rose P.M., Gudesen, R.C. and Kintner, R.C., AIChE Journal, 12(6), 1045, (1966).

27. Spielman, L.A., and Goren, S.L., Ind. Eng. Chem. Fund., 11(1), 73, (1972).

28. Rosenfeld, J.I. and Wasan, D.T., Can. J. Chem. Eng. 52, 3, (1974).

29. Johnnesson, M., M.Sc. Thesis, UMIST, (1974).

30. Jeater, J.P., M.Sc. Thesis, UMIST, (1978).

31. Sherony, D.F., and Kintner, R.C., Can. J. Chem. Eng. 49, 314 (1971).

32. Spielman, L.A.,Goren S.L., Ind. Eng. Chem. 62(10), (1970).

33. Hazlett, R.N., and Robert, N., Presentation to Filtration Society, July 6, (1971).

34. Osterman, J.W., Filt. 8 Sep., March 1, April, 127 (1966).

35. Rumscheidt, F.D., and Manson, S.G., J. Colloid Sci., 16, 238, (1961).

36. Carool, B.J., Lucassen, J., "Theory and Practice of Emulsion Technology" Symp. Soc. Chem. Ind, Brunel Univ., pp 29-41, (1974).

37. Taylor, G.I., Proc. Roy. Soc., (London), A138, 47(1932).

38. Timotika, S., Proc. Roy. Soc., (London), A153, 302 (1936).

39. Selker, A.H., Sleicher, C.A., Can. J. Chem. Eng., 43, PP 298-301, (1965).

40. Becher, P.J., Coll. Interface Sci., 24, pp 91-96 (1967).

41. Nara Singa, E.V.L., Kumar, R., Kuloor, N.R., Chem. Eng. Sci., 21, pp 867-880, (1966).

42. Polichronakis, C., M.Sc. Thesis, University of Aston, Birmingham, October (1972).

43. Shalhoub, N.G., Ph.D. Thesis, University of Aston, Brinmingham, (1975).

44. Elgar, C., B.Sc. Project Report, University of Aston, Birmingham, (1977).

45. Sherman, P., "Emulsion Science", Academic Press, London, (1968).

46. Meissner, H.P., Chertaw, B. Ind. Eng. Chem., 38(8), (1946).

47. Wilkinson, M.J., B.Sc., Project Report, University of Aston, January (1974).

48. Hermanie, P.H.J., Van der Waarden, M.J., Coll. Interface Sci., 21, pp 513-521 (1966).

49. Langdon, W.M., Naik, P.P., and Wasan, D.T., Environ. Sci. & Technol., 6, 905, (1972).

50. Davies G.A., and Jeffreys, G.V., Filtration and Separation, July, August, 349, (1969).

51. Spielman, L.A., and Goren, S.L., Ind. Eng. Chem. Fund., 11 (1), 66, (1972).

52. Burtis, T.A., and Kirkbride, C.G., Trans. AIChE. 42(3), 413, (1946).

53. Voyutskii, S.S., et.al., Dokl. Akad. Nouk, SSR, 91, 1155, (1953),(C.A. 49, 12053d (1955).

54. Gudsen, R.C., M.Sc. Thesis, IIT, Chicago (1964).

55. Vinson C.G., Churchill, S.W., The Chem. Eng. J., 1, 110, (1970).

56. Bartle, J.W., Filtration and Separation, Sept/Oct, 1, (1966).

57. Lindenhofen, H.E., Filtration and Separation, July/Aug, 317, (1968).

58. Lindenhofen, H.E., Filtration and Separation, Sept/Oct., 567, (1969).

59. Hazlett, R.N., Carhart, H.W., Filtration and Separations, July/Aug, 456, (1972).

60. Allak, A.M., and Jeffreys, G.V., AIChE J., 564, May, (1974).

61. Rose, P.R., M.Sc. Thesis, Illinois Institute of Technology, Chicago, (1961).

62. Leverett, M.C., Trans.,A.I.M.E., $\underline{132}$, 149 (1939).

63. Jones, P.J., World Oil, $\underline{129}$, (2) 170 (1949).

64. Carpenter, C.W. Jr., Bail, P.T., Bobek, J.E., Soc. Petrol. Eng. Jrl.,March 9 (1962).

65. Davies, R., Ind. Eng. Chem., $\underline{62}$ (12), 87 (1970).

66. Lloyd, N.E., J. Coll. Sci, $\underline{14}$, 441 (1959).

67. Weissberger, A., "Techniques of Chemistry", Vol. 1, part IIIA, Wiley Interscience (1972).

68. Attarzadeh, G.R., Ph.D. Thesis, University of Aston in Birmingham (1979).

69. Zinky, W.R., Ann. N.Y. Acad. Sci., $\underline{158}$, 741 (1969).

70. Malvern Electronics, "Malvern Particle Sizer 2200 Instruction Manual", Malvern, England (1981).

71. Coulter Electronics, Ltd., "Coulter Counter Model TA II Instruction Manual, Harpenden, England (1981).

72. Irani, R.R., Callis, C.F., "Particle Size: Measurement, Interpretation and Application", John Wiley (1963).

73. Kahn, A., Lewis, D.R., J. Phys. Chem., $\underline{58}$, 801 (1954).

74. Beroit, H., Ann. Phys., $\underline{6}$, 561 (1951).

75. O'konski, C.I., Zimm, 8, Science, $\underline{11}$, 113 (1950).

76. Smith, T.N., Chem. Eng. Sci., $\underline{29}$, 583 (1974).

77. Thompson, B.J., et.al, Applied Optics, $\underline{6}$ (3), 519 (1967).

78. Grauke, A., Applied Optics, $\underline{13,}$ No. 12, Dec. (1974).

79. Bexon, R., J. of physics E. Scientific Instruments, $\underline{6}$, (1973).

80. Pavitt, K.W., Jackson, M.C., Adams, R.J., and Bartlett, J.T., J. of physics E. Scientific Instruments, $\underline{3}$, (1970).

81. Coulter Counter Training Course, Coulter Electronics Ltd, Harpenden, Aug. (1981).

82. Sherony, D.F., Kintner, R.C., AIChE 8, $\underline{17}$, (2), 291, (1971).

83. Fowkes, F.M., Ind. Eng. Chem., $\underline{56}$, (12), 40, (1964).

84. Fowkes, F.M., in "Chemistry and Physics of Interfaces", pp 1-12, American Chemical Society, Washington D.C., (1965).

85. Coulson, J.M., and Richardson, J.F., "Chemical Engineering", Vol.2, Pergamon Press, Oxford (1968).

86. Ergun, S., Chem. Eng. Prog., $\underline{48}$, 98 (1952).

87. Macdonald, I.F., et.al., Ind. Eng. Chem. Fundam., $\underline{18}$, 199, (1979).

88. Carman, P.C., Trans. Inst. Chem. Eng., $\underline{15}$, 150 (1937).

89. Haring, R.E., and Greenkom, R.A., AIChE J., $\underline{16}$, 477 (1970).

90. Azzam, M.I.S., and Dullien, F.A.L., I.E.C. Fundam., $\underline{15}$, 281 (1976).

91. Wyllie, M.R., Greygory, A.R., Ind. Eng. Chem., $\underline{41}$, 1379 (1955).

92. Johnson, M.F.L., Stewart, W.E., J. Catal., $\underline{4}$, 248 (1965).

93. Dullien, F.A.L., AIChE J., $\underline{21}$, 299 (1975).

94. Coulson, J.M., Trans. Inst. Chem. Eng., $\underline{27}$, 237 (1949).

95. Brown and Associates, "Unit Operations", John Wiley, (1951).

96. Langdon, W.M., et.al., Environ. Sci. and Tech.,
    $\underline{6}$ (10), 905 (1972).

97. G.H. Bloore Ltd., Birmingham, U.K.

98. Bitten, J.F., Fochtman, E.G., J. of Colloid
    and Interface Science, $\underline{37}$, 2, October (1971).

99. Spielman, L., Goren, S.L., Environ. Sci and Technol,
    $\underline{2}$, 4, April (1968).

100. Singhal, A.K., Dranchulk, P.M., Can. J. Che.
    Eng., 53, 3, (1975).

101. Hitit, H.A., Ph.D. Thesis, University of
    Aston, Birmingham, (1972).

102. Prieve, D.C., Ruckenstein, J.A., J. Coll. and
    Interfac. Sci., $\underline{42}$ (3), 607 (1973).

103. Emi, H., Okuyama, K., Yoshioka, N., J. Ch. Eng.
    Japan, $\underline{6}$ (4) 349 (1973).

104. Pich, J., Aerosol Science, $\underline{4}$, 217, (1973).

105. Rosenfeld, J.I., Wasan, D.T., Proc. I.S.E.C.,
    74, 319, (1974).

106. Spielman, L.A., Goren, S.L., Environmental
    Science and Technology, $\underline{4}$ (2), 135, (1970).

107. Landahl, H., Hermann, K., J. Colloid Sci., 4, 103
    (1949).

108. Langmuir, I., OSRD Rept, 865, Sept., 1942.

109. Rajagopalan, R., Tien, C., Can. J. Ch.E., $\underline{55}$,
    246 (1977).

110. Hamaker, H.C., Physica, $\underline{4}$, 1058 (1937).

111. Rosenfeld, J.I., Ph.D. Thesis, Illinois
    Institute of Technology, Chicago (1973).

112. Davies, G.A., Jeffreys, G.V., Filt, and Sep.,
    July/Aug, 349 (1965).

113. Wilkinson, D., Ph.D. Thesis, University of
    Aston in Birmingham (1974).

114. Beatty, H.A., Ethyl Corp., Ferndale, Mich.,
    Interim Tech. Rept. GR-66-30, July (1966).

115. Perry J.H., Ed., "Chemical Engineer's Handbook",
     4th ed., Sec. 5, p. 59, McGraw-Hill, New York
     (1963).

116. Gosh, M.M., Brown, W.P., Jl. Water Pollution
     Control. Fed; 47 (8), 2101 (1975).

117. Tonna, J.A., B.Sc Project Report, University
     of Aston in Birmingham, (1977).

118. Austin, D.G., Mumford, C.J., Jeffreys, G.V.,
     Solvent Extraction Meeting, Newcastle upon
     Tyne, Sep. (1976).

119. Wilkinson; D, Mumford, C.J., Jeffreys, G.V.,
     AIChE, 21, 5, Sep. (1975).

120. Gasmelseed, G.A., Ph.D. Thesis, University of
     Aston, (1985).

121. Othman, F.M.S., Unpublished Report, University
     of Aston, Dec. (1983).

122. Bizzari, N., B.Sc. Project Report, Kuwait
     University (1984).

123. Al-Watan Daily Newspaper, No. 2937, Mon. 25th April,
     page 1, Kuwait, 1983.

124. Dullein, F.A.L., 'Porous Media', Academic Press,
     London (1979).